ELTON EDUARDO NOVAIS ALVES

SOIL AND TREE X-RAY SPECTROSCOPY ANALYSIS OF BRAZILIAN TROPICAL MANGROVE ECOSYSTEM

Thesis submitted to the Soil Science and Plant Nutrition Graduate Program of the Universidade Federal de Viçosa as partial fulfillment of the requirements for the degree of *Doctor Scientiae*.

VIÇOSA
MINAS GERAIS – BRAZIL
2018

Ficha catalográfica preparada pela Biblioteca Central da Universidade Federal de Viçosa - Câmpus Viçosa

T
A474s
2018

Alves, Elton Eduardo Novais, 1989-
Soil and tree X-ray spectroscopy analysis of Brazilian tropical mangrove ecosystem / Elton Eduardo Novais Alves. – Viçosa, MG, 2018.
xii, 91f. : il. (algumas color.) ; 29 cm.

Orientador: Liovando Marciano da Costa.
Tese (doutorado) - Universidade Federal de Viçosa.
Inclui bibliografia.

1. Química do solo. 2. Biogeoquímica. 3. Mangues. 4. Solos - Análise. 5. Árvores - Análise. 6. Ecologia dos manguezais. I. Universidade Federal de Viçosa. Departamento de Solos. Programa de Pós-graduação em Solos e Nutrição de Plantas. II. Título.

CDD 22 ed. 631.4

ELTON EDUARDO NOVAIS ALVES

SOIL AND TREE X-RAY SPECTROSCOPY ANALYSIS OF BRAZILIAN TROPICAL MANGROVE ECOSYSTEM

Thesis submitted to the Soil Science and Plant Nutrition Graduate Program of the Universidade Federal de Viçosa as partial fulfillment of the requirements for the degree of *Doctor Scientiae*.

APPROVED: February 23, 2018.

Pablo de Azevedo Rocha

Flávio César Vicentin

Luiz Carlos Ruiz Pessenda

Leonardus Vergütz
(Co-adviser)

Liovando Marciano da Costa
(Adviser)

To my beloved parents Ana Maria and José Cézar

To my siblings, family and friends,

To my beloved Mariana Reis,

To all teachers and professors.

“Nothing in life is to be feared, it is only to be understood. Now is the time to understand more, so that we may fear less.”

Marie Skłodowska Curie

ACKNOWLEDGMENTS

Antes de tudo, agradeço aos meus pais Ana Maria e José Cézar e toda a minha família (irmãos, irmãs, primos e tios) por tudo e por sempre confiar em mim e em minhas escolhas.

À Universidade Federal de Viçosa (UFV), por ter me acolhido desde 2007, por me dar muitas oportunidades para desenvolver minhas ideias, conhecer pessoas fantásticas, realizar amizades e por ser uma universidade de excelência, a qual me orgulho de fazer parte.

Ao Programa de Pós-Graduação em Solos e Nutrição de Plantas e para todos os colegas, estudantes de pós-graduação, técnicos, professores e funcionários do Departamento de Ciências do Solo por fornecer todas as condições necessárias para desenvolvimento deste trabalho.

Agradeço à CAPES e ao Programa Ciência sem Fronteiras pela bolsa de doutorado *Sanduíche* na Carolina do Norte, EUA (projeto A105/13). Foi um privilégio ter participado dessa experiência que foi de extrema importância para minha formação. E ao CNPq pela bolsa de doutorado no Brasil.

To North Carolina State University and all colleagues graduate students, technicians, faculty and staff of Soil and Crop Sciences Department. In special to professors Jot Smith, Wayne P. Robarge, and Terrence G. Gardner and graduate students for moments spent together.

To the Synchrotron laboratories: National Synchrotron Light Source II (NSLS-II), Stanford Synchrotron Radiation Lightsource (SSRL), and the Brazilian Synchrotron Light Laboratory (LNLS). Where I had experienced fantastic moments, where I improved my knowledge in the X-ray spectroscopy, and also generated valuable scientific data. A special thank by valuable help of the beamline scientists Samuel Webb and Courtney Roach (SSRL); Juergen Thieme, Chen-Wiegart, Ryan Tappero and Lili (NSLS-II); Flávio Vicentin and Simone Betim (LNLS)

Agradeço ao meu professor Ph.D. Liovando Marciano da Costa, um exemplo de profissional e cidadão brasileiro. Por incontáveis discussões

produtivas em seu escritório, por sempre me apoiar e pelo valioso conhecimento compartilhado.

Agradeço ao meu coorientador professor D.Sc. Leonardus Vergütz pelo conhecimento compartilhado, pela ter me dado a oportunidade de realizar o doutorado *sanduíche* nos EUA e por todas as sugestões feitas durante minha pós graduação.

Thank my co-adviser Ph.D. Dean Hesterberg, for the shared knowledge, for the valuable moments spent at USA, and for all suggestions made during my Doctorate. Also thank to his family for hosted me in the US.

Ao D.Sc. Pablo de Azevedo Rocha pela amizade, pela valiosa ajuda durante todas as etapas do meu Doutorado, desde o treinamento da XRF, até o planejamento, coleta, análise e discussão dos dados. Você é um grande amigo!

Agradeço ao professor D.Sc. Luis Henrique Silva e D.Sc. Flávio Vicentin por sugestões valiosas durante o meu doutorado, especialmente em meu exame de qualificação.

Aos membros da banca de defesa da tese pelas sugestões na melhoria do trabalho: Professor Liovando Costa, Professor Luiz Pessenda, Professor Leonardus Vergütz, D.Sc. Flávio Vicentin, D.Sc Pablo Rocha.

Agradeço aos meus amigos que conheci em Raleigh, Carolina do Norte. Um agradecimento especial ao Vinicius, Tássia, Zezé, Marcelo, Aline, Danilo, Aelton, Natalia, Patrícia e Jorge. Sou muito grato pelos momentos que passamos juntos nos EUA. Esses momentos incríveis me ajudaram a lidar com a saudade de casa.

À Taislaine Rocha e Fabiane Ballotin por sua ajuda durante a amostragem do solo e a análise XANES, respectivamente. Ao professor André Faria e Saymon Bittencourt pela ajuda durante a coleta de amostras. Ao Martin Meier na ajuda com a elaboração dos mapas da tese. Ao professor Mario Tomazello e Daigard Ricardo (ESALQ-USP) pelo auxílio na preparação das amostras de madeira.

À minha melhor amiga, colega de trabalho e amada Mariana Reis, que me ajudou nos últimos seis anos a suportar tempos difíceis e a proporcionar-me momentos de alegria.

Agradeço aos amigos de república/alojamento, desde que eu deixei a casa dos meus pais, aos 14 anos de idade. Aos amigos do alojamento da Escola Agrotécnica de São João Evangelista, MG, do alojamento Novíssimo da UFV, e das repúblicas que morei em Viçosa.

Para todos os que contribuíram de alguma forma, direta ou indiretamente, obrigado pelos momentos de ajuda, descontração e crescimento pessoal.

Thank you all!

BIOGRAPHY

ELTON EDUARDO NOVAIS ALVES, son of José Cézar de Novais Alves and Ana Maria Gonçalves Alves, was born in Santa Bárbara, MG, Brazil, on June 25th, 1989.

He joined the high school and technical course at Escola Agrotécnica Federal de São João Evangelista-MG (2014), graduating as Agricultural Technician in 2006.

In 2007, he joined the Universidade Federal de Viçosa, in Agronomy course, obtaining a Bachelor of Science degree in January of 2012. In this date started the Master's degree course in the Soil Science Department of Universidade Federal de Viçosa, concentrating his studies in Soil Chemistry and Soil Fertility area, obtained a *Magiter Scientae* degree in Soil Science and Plant Nutrition in February of 2014.

In March of 2014 he started the Doctorate course in Biogeochemistry and Soil Chemistry area at Soil Science Department. Between September of 2015 and September of 2016, he was Visiting Scholar at North Carolina State University, USA, where part of his research was developed. The thesis has been submitted to the committee in February of 2017, to obtain the *Doctor Scientiae* degree in Soil Science and Plant Nutrition.

CONTENTS

ABBREVIATION LIST ..... **viii**

ABSTRACT ..... **ix**

RESUMO ..... **xi**

GENERAL INTRODUCTION **1**

CHAPTER I: Mangrove Ecosystem, Tree-Ring Analysis, And Spectroscopy Techiniques: A Short Review **2**

1.1. Mangrove Ecosystem 2
1.2. Tree-Rings Analysis 4
1.3. Spectroscopy Techniques 6
1.3.1. X-ray Fluorescence Spectroscopy (XRF) 7
1.3.2. X-ray Absorption Spectroscopy (XAS) 13
1.4. References 18

CHAPTER II: Biogeochemistry Of Contaminated And Non-Contaminated Tropical Mangrove Soils **23**

2.1. Abstract 23
2.2. Introduction 23
2.3. Materials and Methods 25
2.4. Results 31
2.5. Discussion 34
2.6. Conclusions 39
2.7. References 40
2.8. Supporting Information for Chapter II 44

CHAPTER III: TENDER X-RAY SYNCHROTRON RADIATION DAMAGE IN ENVIRONMENTAL SAMPLES DURING SULFUR SPECIATION **49**

3.1. Abstract 49
3.2. Introduction 49
3.3. Materials and Methods 51
3.4. Results 54
3.5. Discussion 59
3.6. Conclusions 60
3.7. References 61
3.8. Supporting Information for Chapter III 64

CHAPTER IV: X-RAY ABSORPTION AND FLUORESCENCE MICROSCOPY APPLIED TO TREE-RING CHEMICAL STUDY OF TROPICAL MANGROVE **66**

4.1. Abstract 66
4.2. Introduction 67
4.3. Materials and Methods 68
4.4. Results and Discussion 73
4.5. Conclusions 82
4.6. References 83
4.7. Supporting Information for Chapter IV 87

GENERAL CONCLUSIONS **91**

ABBREVIATION LIST

µSXRF:	Synchrotron X-ray fluorescence microscopy
µXANES:	X-ray absorption near edge structure microscopy
µXRF:	X-ray fluorescence microscopy
BG:	Background (spectrum baseline)
CDSDR:	Concha D'Ostras Sustainable Development Reserve
CNPEM:	Brazilian Center for Research in Energy and Materials
LCF:	Linear combination fitting
LNLS:	Brazilian Synchrotron Light Laboratory
PCA:	Principal components analysis
S_8:	Elemental sulfur
SDD:	Silicon drifted detector
SSRL:	Stanford Synchrotron Radiation Lightsource
SXRF:	Synchrotron X-ray fluorescence spectroscopy
XANES:	X-ray absorption near edge structure spectroscopy
XAS:	X-ray absorption spectroscopy
XRF:	X-ray fluorescence spectroscopy
λ:	Wavelength

ABSTRACT

ALVES, Elton Eduardo Novais, D.Sc., Universidade Federal de Viçosa, February, 2018. **Soil and tree X-ray spectroscopy analysis of Brazilian tropical mangrove ecosystem**. Adviser: Liovando Marciano da Costa. Co-Advisers: Leonardus Vergütz and Dean Hesterberg.

The present research has been performed in Concha D'Ostras Sustainable Development Reserve (CDSDR), Guarapari, Espírito Santo state, Southeast Brazil. We assess the mangrove soil and tree chemical composition and speciation by X-ray fluorescence (XRF) and absorption (XANES) spectroscopy techniques, collected in synchrotron radiation laboratories at Stanford University, California (SSRL), and CNPEM, Campinas-SP (LNLS). The present thesis was structured in four chapters, being three chapters have been wrote as scientific manuscripts. The **Chapter I** contains basic informations about the main research topics: 1) Mangrove ecosystems; 2) Spectroscopy techniques; and 3) Dendrochemistry studies. In the **Chapter II**, we compared the biogeochemistry of better preserved (P1) and contaminated (P2) tropical Brazilian mangrove soils in terms of elemental composition, pH and reduction-oxidation (redox) potential (Eh), and S speciation. XRF analysis showed unique depth-distributions of S, Fe, Cl, Ca, K, Ti, Cr, Br, Sr, and Zr in each area. Sulfur K-edge XANES spectroscopy showed that the mangrove location and conservation state influenced the soil S speciation. Pyrite (FeS_2) was the dominant S mineral (~50% of S) found in both soil profiles, and more abundant organic and elemental S (S-org and S^0) in profile P1 indicated greater microbiological activity in the better preserved mangrove site. A decrease in the proportion of SO_4^{2-} with depth in P1 following a decrease on Eh. However, in profile P2 we verified an increase in the SO_4^{2-} in deeper soil layers, indicating greater influx of from seawater. In essence, S speciation was directly influenced by seawater encroachment. In the **Chapter III** we evaluated the effect of tender X-ray radiation (2.4-2.6 keV) in the sulfur species present in environmental samples under cryo-temperature (115±5 K) to minimize the radiation-damage during S K-edge XANES analysis. We performed six sequential S K-edge XANES (2.4 to 2.6 keV) in pure standards (S_8 and $FeSO_4.7H_2O$), environmental samples (Pyrite, Frozen and Lyophilized Mangrove Soil), and a mixture of S_8 +

Starch. Tender X-ray synchrotron radiation-damage resulted in the reduction of sulfur only in the carbon rich sample (S_8 + Starch). The cold finger at 115 K was effective in minimize the radiation-damage. Thus, it is recommended to use the cold finger during the S K-edge XANES data for those samples that are rich in organic carbon for environmental studies. Powder samples are recommended (as lyophilized soil) because they are simpler to mount, in order to obtain more homogenous sample, and avoid the analysis of gaseous sulfur species, which is important when the objective is to study only the solid state phases in the sample. In the **Chapter IV** we aimed to assess the Ca distribution and speciation into *Avicennia* mangrove tree, using μXRF and Ca K-edge μXANES analysis (5 μm beam size) combined with multivariate analysis during data process. Increment cores were extracted from the *Avicennia* mangrove at CDSDR and were analyzed by XRF and XANES techniques at SSRL. The Ca content was greater in internal part of wood (heartwood) than in the external part (sapwood) and showed a systematic distribution into tree-rings, being possible to use this data to identify “chemical-rings” in the sample. The PCA and cluster multivariate analysis showed that Ca species are distinct in the sapwood (more calcium oxalate and carbonate) and heartwood (more calcium sulfate), which can be related to a Ca role in the plant, as structural (heartwood) or a labile form (sapwood). This study showed that multivariate analysis of Ca speciation data and the Ca distribution in the tree-ring, using a microprobe X-ray spectroscopy, provide valuable information about chemical records in the mangrove tropical tree-rings.

RESUMO

ALVES, Elton Eduardo Novais, D.Sc., Universidade Federal de Viçosa, fevereiro de 2018. **Análises espectroscópicas de raios X do solo e árvore do manguezal brasileiro**. Orientador: Liovando Marciano da Costa. Coorientadores: Leonardus Vergütz e Dean Hesterberg.

A presente pesquisa foi realizada na Reserva de Desenvolvimento Sustentável da Concha D'Ostras (RDSCO), Guarapari, Espírito Santo. Foram avaliadas a composição e a especiação química do solo e da árvore de mangue a partir das técnicas de espectroscopia de fluorescência de raios X (XRF) e absorção (XANES). A maioria dos dados apresentados foi coletada em laboratórios de radiação síncrotron na Universidade de Stanford, Califórnia (SSRL) e CNPEM, Campinas-SP (LNLS). A presente tese foi estruturada em quatro capítulos, sendo três capítulos escritos como manuscritos científicos. O **Capítulo I** contém informações básicas sobre os principais tópicos da pesquisa: 1) Ecossistemas de manguezais; 2) Técnicas de espectroscopia; e 3) Estudos da dendroquímica. No **Capítulo II**, comparou-se a biogeoquímica dos solos de dois manguezais, um mais preservado (P1) e outro contaminado (P2), em termos de composição elementar, pH e potencial de redução-oxidação (redox) (Eh) e especiação do S. Verificou-se na análise de XRF, as distribuições específicas de S, Fe, Cl, Ca, K, Ti, Cr, Br, Sr e Zr nos perfis dos solos P1 e P2. Verificou-se com a análise de XANES que a localização e o estado de conservação do mangue influenciaram a especiação do S no solo. A pirita (FeS_2) foi o mineral de enxofre mais abundante (~ 50% de S) encontrado em ambos os perfis de solo, e o as formas orgânicas e elementar (S-org e S^0) foram mais abundantes no perfil P1, indicando maior atividade biológica no manguezal mais preservado. Uma diminuição na proporção de SO_4^{2-} com profundidade em P1 após uma diminuição em Eh. No entanto, no perfil P2 verificou-se o aumento do SO_4^{2-} em camadas de solo mais profundas, indicando maior influxo da água do mar. Assim, a especiação S foi diretamente influenciada pela entrada da água do mar. No **Capítulo III**, foi avaliado o efeito da radiação X (2,4-2,6 keV) nas espécies de enxofre presentes em amostras ambientais sob criotemperatura (115 ± 5 K) para minimizar os danos causados pela radiação durante os de análise XANES da borda K do enxofre. Seis

espectros XANES sequenciais (borda K do S, 2.4 a 2.6 keV) foram realizados em cada uma das seguintes amostras: padrões puros (S_8 e $FeSO_4.7H_2O$), amostras ambientais (pirita, solo de manguezal congelado e liofilizado) e uma mistura de amido com S_8. A radiação síncrotron resultou na redução de enxofre apenas na amostra rica em carbono (S_8 + amido). O dedo frio em 115 K foi efetivo para minimizar os danos causados pela radiação. Assim, recomenda-se usar o dedo frio durante os dados XANES da borda S para aquelas amostras que são ricas em carbono orgânico para estudos ambientais. As amostras de pó são recomendadas (como solo liofilizado) pela maior facilidade de preparo, montagem e homogeneidade, além de evitar a análise de espécies de enxofre gasoso, o que é importante quando o objetivo é estudar apenas as fases de estado sólido na amostra. No **Capítulo IV**, objetivou-se avaliar a distribuição e a especiação de Ca na madeira da *Avicennia* (mangue), utilizando as técnicas de μXRF e μXANES (tamanho de feixe de 5 μm), combinada com análise multivariada durante o processamento dos dados. Amostra da madeira da *Avicennia* do mangue da RDSCO foi analisada pelas técnicas XRF e XANES no laboratório de luz síncrotron SSRL. O conteúdo de Ca foi maior na parte interna da madeira (cerne) do que na parte externa (alburno) e verificou-se a distribuição sistemática nos anéis das árvores, sendo possível usar esses dados para identificar "anéis químicos" na amostra. Verificou-se na análise multivariada de PCA e de agrupamento que as espécies de Ca são distintas no alburno (mais oxalato de cálcio e carbonato) e cerne (mais sulfato de cálcio), o que pode estar relacionado ao papel de Ca na planta, como estrutural (cerne) ou forma lábil (alburno). Este estudo mostrou que a análise multivariada dos dados de especiação do Ca e a distribuição do Ca no anel da árvore, usando uma espectroscopia de raios X de microfeixe, fornecem informações valiosas sobre os registros químicos nos anéis das árvores tropicais dos manguezais.

GENERAL INTRODUCTION

Climate change is a challenge that humanity must face in the coming decades. Coastlines will be affected due to the rise in sea level. Thus, basic information about estuarine environments (e.g., mangrove ecosystems) biogeochemistry is very important to better understand which impacts can occur due to natural or anthropogenic changes (CHURCH et al., 2008; LEMONTE et al., 2017).

The present research has been performed in Concha D'Ostras Sustainable Development Reserve (CDSDR), Guarapari, Espírito Santo state, Southeast Brazil. A biogeochemical study was performed to assess the chemical composition and speciation of mangrove soil and tree by X-ray fluorescence (XRF) and absorption (XANES) spectroscopy techniques. Most of data presented were collected in synchrotron radiation laboratories at Stanford University, California (SSRL), and at Brazilian Center for Research in Energy and Materials, Campinas-SP (LNLS).

The general goal of the present thesis was to show how spectroscopy analysis can provide valuable and unique geochemistry informations about Tropical mangrove ecosystem, such as in tropical tree-ring studies. Here, we aimed to assess the influences of sea water and preservation status in: 1) Chemical composition in two mangrove soil profiles by XRF analysis; and 2) Sulfur speciation in both soil profiles by S K-edge XANES analysis. Also, we assessed mangrove tree-rings chemical composition by XRF and Ca K-edge XANES analysis to identify patterns of Ca distribution and speciation into mangrove tree-rings.

This thesis was structured in four chapters, being three chapters have been wrote as scientific manuscripts. The first chapter contains basic informations about the main research topics: 1) Mangrove ecosystems; 2) Tree-ring analysis; and 3) Spectroscopy techniques.

CHAPTER I

MANGROVE ECOSYSTEM, TREE-RING ANALYSIS, AND SPECTROSCOPY TECHINIQUES: A SHORT REVIEW

1.1. Mangrove Ecosystem

Mangrove is a non-taxonomic term used to describe an assemblage of tropical and subtropical trees and shrubs. These plants are adapted to a wet and saline habitat in the intertidal zone, with 16 families and 40 to 50 species. Mangrove ecosystem is a term used to describe the entire mangrove community and its environment (SHARITZ & PENNINGS, 2006; WOODROFFE & DAVIES, 2009; REY et al., 2012).

Mangrove ecosystems are estuarine environments of low energy, located in transition zone between continent and ocean, in coastline regions. These environments are influenced by both seawater (tides) and fresh water (from the river). These continental and oceanic influences provide nutrients and sediments to mangrove ecosystems, which contribute to a very rich biologically environment (ROBERTSON & ALONGI, 1992; DIEGUES, 2002; SAINT-PAUL & SCHNEIDER, 2010). They are geologically recent, formed during the Quaternary (WOODROFFE & GRINDROD, 1991; GOMES et al., 2016), and cover approximately 16 million hectares of coastline worldwide (HOSSAIN & NURUDDIN, 2016). In Brazil, they are found in almost entire coastline, with the total area of 1.4 million hectares (KJERFVE & LACERDA, 1993; ARRIVABENE, 2011).

Important roles are played by mangrove ecosystems. They are responsible for soil formation and stabilization of coastline; they filter upland runoff; they are habitat for a diverse group of marine organisms (fish, crabs, oysters) and wildlife such as birds and reptiles. Mangroves produce large amounts of detritus that may contribute to productivity in offshore waters. And for humans they are shield for coastal population against storms; and allow promoting commercial and sport activities, as fishing and ecotourism (SCHAEFFER-NOVELLI, 1995; VANNUCCI, 2001; REY et al., 2012).

However, mangroves areas are threatened by sea level rising due to climate change (CHURCH et al., 2008; LEMONTE et al., 2017) and especially by anthropogenic impacts, such as improper disposal of domestic sewage and stormwater runoff from encroaching urban areas. These impacts have resulted in major losses of mangrove ecosystems for residential and industrial occupancy, agriculture and charcoal production and salt extraction, besides the anthropogenic pollution generated by these activities (REY et al., 2012).

Mangroves occupy an area around 7000 hectares of Espírito Santo state, and the most extensive forests are found in the Vitória Bay and estuaries of Piraqueaçu and São Mateus rivers (VALE & FERREIRA, 1998). The floristic composition consists basically of four species: *Avicennia schaueriana*, *Avicennia germinans*, *Laguncularia racemosa*, and *Rhizophora mangle*. *Rizophora mangle* bark contains tannin used to waterproof and give a characteristic color to a clay pot from Goiabeiras, a cultural heritage of the Espírito Santo state (ARRIVABENE, 2011; IPHAN, 2018).

Concha D'Ostras Sustainable Development Reserve (CDSDR) is located in Guarapari city (Figure 1.1). The CDSDR was initially created as an ecologic park in 2003 and in 2007 was decreed as Sustainable Development Reserve aiming to maintain this ecosystem and protect its biodiversity by sustainable use of local population (IEMA, 2005). The total area of this reserve is 953 ha, and its perimeter is 38.7 km. The main economic activities of population near to CDSDR is related to tourism, fishing, extractivism, commercialization of products obtained with solid waste collection, and agricultural activities (IEMA, 2004). Guarapari city is a touristic city which has a total population of 119,802 (IBGE, 2014). However, in the summer season over 1 million of tourist visit Guarapari, which increases the anthropogenic impacts in the mangrove ecosystem close to this area.

The initial soil biogeochemistry study performed in the CDSDR was made by Rocha (2016). This study contains very important basic and preliminary information about CDSDR, which was very useful to develop the present thesis. Thus, the reading of Rocha (2016) study is recommended for further biogeochemical information about Concha D'Ostras SDR. And both theses have important information, which contribute for a better characterization

and basic information about biogeochemical process, which occurs in this mangrove ecosystem.

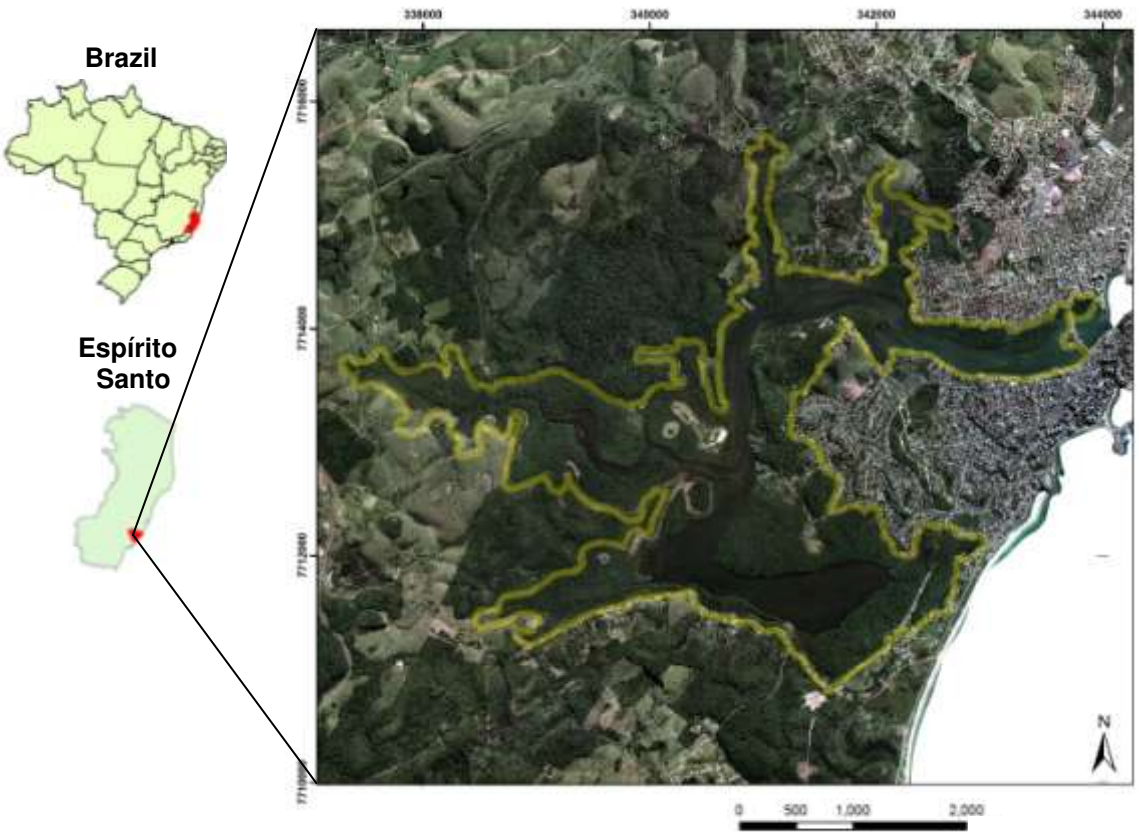

Figure 1.1. Concha D'Ostras Sustainable Development Reserve located in Guarapari city, Espírito Santo State, Southeast Brazil coastline.

1.2. Tree-Rings Analysis

Tree-rings are formed due to seasonality of environmental condition (e.g., rainfall, temperature, sunshine duration, flooding, salinity) during the tree growth. These stress factors induce a cambial dormancy, resulting in growth zones in the wood (DUNWIDDIE & LAMARCHE, 1980; WORBES, 1995). Annual tree-rings are very common in species growing in temperate zones (e.g, conifers). In this species, the rings are easily identified, because there is a contrast between the light-coloured, large and thin-walled cells produced early in the growing season (earlywood), and the smaller, thicker-walled cells produced later in the season (latewood). Thus, during a year, the wood produce two rings, namely as earlywood and latewood (DUNWIDDIE & LAMARCHE,

1980). Besides trees of temperate zones, tropical tree species also can produce tree-rings due to season seasonality (WORBES, 1995). The tree-rings formation in mangrove species have been demonstrated by several researches (WORBES, 2002; MENEZES et al., 2003; VERHEYDEN et al., 2004a; VERHEYDEN et al., 2004b; VERHEYDEN et al., 2005; SOUZA et al., 2016).

Briefly, dendrochronology is a science which extracts information from dated tree-rings, and matching these information with past environment conditions. Dendrochronology has several branches (subdisciplines), such as dendroecology, dendroarcheology, dendroclimatology and the dendrochemistry. Dendrochemistry consists in the chemical analysis of tree-rings (FRITTS, 1976; BALOUET et al., 2009). Dendrochemistry studies enable the prediction of preterit chemical environmental conditions related to soil, water, and air chemical quality (BALOUET et al., 2009; SMITH et al., 2014). Natural and anthropogenic events as volcanic eruption or toxic chemical elements release, respectively, can be registered as chemical information inside tree-ring, being possible to access this information by dendrochemistry methodologies (SMITH & HOUSTON, 1994; SHEPPARD et al., 2007; SHEPPARD et al., 2008; SMITH et al., 2008; BALOUET et al., 2009; SMITH et al., 2014).

The correct application of dendrochronology and dendrochemistry consists of knowledge in wood function, formation, structure, and plant metabolism and physiology role of chemical elements. Such as the understanding the structure and function of xylem, phloem, vessels elements, heartwood, sapwood, and others specific topics of wood anatomy and tree physiology (SMITH et al., 2014).

The pioneer researches about inorganic chemical composition of wood have been made by chemical analysis of wood ash as a potential potassium fertilizer source (FOREST PRODUCTS LABORATORY, 1919). However, this work had not measured the wood variation chemical composition. With the detection limit improvement of analytical techniques have been possible to analyze few sample amounts, which allowed assessing the spatial variation of wood chemical composition (SAFFORD et al., 1974; SMITH & HOUSTON, 1994; SMITH et al., 2014)

Currently improvements in the detection limits and spatial resolution of spectroscopy techniques allow performing microchemical maps from micro until nanometric scales of several chemical elements. Some of these new techniques are non-destructive, being possible to perform several different complementary analyses in the same sample. For dendrochemistry studies, spectroscopy analysis enable assess inter or intra-annual chemical composition variations of several chemical elements (MAJUMDAR et al., 2012; SMITH et al., 2014).

Different kind of spectroscopy techniques are utilized in dendrochemistry studies, such as Particle or Proton-Induced X-ray Emission (PIXE); Scanning X-ray Fluorescence Microscopy (SXFM); Laser Ablation Inductively Coupled Plasma Mass Spectrometry (LA-ICP-MS); and the X-ray Fluorescence Spectrometry (XRF). In the following sections, there are fundamental information about two spectroscopy techniques: the X-ray Fluorescence (XRF) and X-ray Absorption Spectroscopy (XAS). Several dendrochemistry studies have utilized XRF analysis (725 results found in ScienceDirect website for "XRF and tree-ring" terms); however, tree-ring studies with XAS analysis are scant.

1.3. Spectroscopy Techniques

Currently knowledge says that the universe consists of two entities: Matter and Energy, where they can be interrelated through the Einstein´s equation $E = m.c^2$. Matter (e. g., electrons) and energy (e. g., electromagnetic energy) can be originated from different sources and can move in the space through particles or waves until they get absorbed by or annihilated in some material. This mass and energy transportation phenomena is called radiation (EISBERG & RESNICK, 1985; AHMED, 2015).

Electromagnetic radiation refers to propagation of waves of magnetic and electric fields through the space-time. The electric and magnetic field vectors of the wave are perpendicular to each other and to the direction of propagation. The electromagnetic waves consist of several photons, which carry energy (E), linear momentum (p), and angular momentum (ω) (BUNKER, 2010). Basic characteristics of the electromagnetic radiation are its frequency (ν) and

wavelength (λ) that are related by $\lambda = \frac{c}{\nu}$, where c is the light speed (wave traveling through the vacuum). Thus, the electromagnetic waves can propagate with several different frequency or wavelength.

The set of multiple electromagnetic wavelengths is denominated spectrum, and the electromagnetic spectrum regions are classified by wavelength or frequency into radio ($\lambda > 0.3$ m), microwave (1 mm $< \lambda <$ 0.3 m), infrared (0.76 μm $< \lambda <$ 1 mm), visible (0.4 $< \lambda <$ 0.76 μm), ultraviolet (8 $< \lambda <$ 400 nm), X-rays (0.01 $< \lambda <$ 10 nm) and gamma rays (λ<0.01 nm). The electromagnetic waves interact with matter, but its behavior changes qualitatively with different wavelengths (AHMED, 2015).

The X-ray radiation is the region of electromagnetic spectrum and its energy (0.124 to 124 keV) and wavelength (0.01 $< \lambda <$ 10 nm) will interact with electrons of atoms leading its ionization. Others interaction between radiation and matter occurs, e.g. scattering, diffraction, and absorption. Those interactions are used to study different matters composition and structure. Thus, when we use the part of electromagnetic spectrum interaction with some material, we call this as spectroscopy technique (BUNKER, 2010; AHMED, 2015).

Several spectroscopy techniques were developed due to better understanding of electromagnetic interactions with the matter, with the development of atom models, and the quantum physics advances. Currently, several new equipments (spectrometers) have been developed, and are applied in different knowledge areas (EISBERG & RESNICK, 1985; KELLY et al., 2008; BUNKER, 2010; AHMED, 2015). As in this present thesis have been used the X-ray Fluorescence and X-ray Absorption spectroscopy, the following topics have more details about how they work.

1.3.1. X-ray Fluorescence Spectroscopy (XRF)

The XRF is a technique which studies a specific interaction between X-ray radiation and the atoms of the sample. The main objective of XRF application is to identify which chemical elements are present in the specimen (qualitative analysis) and its content (quantitative analysis). As the chemical elements, or the atoms, are the main components to be studied by XRF, it is

important to have a basic understanding of the atom model (BERTIN, 1978; GRIEKEN & MARKOWICZ, 2002; BECKHOFF et al., 2006).

The atom model of quantum mechanics is based in mathematics equations: the Schrödinger's wave equation. Mathematical restriction had to be adopted to solve Schrödinger's equation for the hydrogen atom. These restrictions were named quantum numbers, and they are sets of numerical integer (quantized or discrete) values which give acceptable solutions to the Schrödinger wave equation. Initially three restrictions were made and corresponded to the quantum numbers: principal (*n*), azimuthal (*l*), and magnetic (*m*). A fourth quantum number spin (*s*) came after and, currently, there are four quantum numbers. What is very interesting in the quantum atomic model is the quantization of the energy of electrons. Bohr proposed this quantization in his model. However, Bohr could not explain why they were quantized. In the Schrödinger wave equation the quantization is naturally presented (EISBERG & RESNICK, 1985; BUNKER, 2010).

There are some physics concepts by the quantum numbers, besides them be only a mathematical strategy to solve the Schrödinger wave equation. The quantum numbers can have the following values: 1) $n = 1, 2, 3, \ldots$ and physically it represents the atoms shells or energy level of an electron (K, L, M…); 2) the *l* assumes values equal to $n-1$, and physically it represents the atoms subshells or angular momentum (s, p, d, f); 3) the *m* can have values equal to $-l < n < l$ and physically it represents the projection of the angular momentum, and the *s* has the values equal to $-½, +½$, physically it represents a intrinsic angular momentum of electron (EISBERG & RESNICK, 1985; BUNKER, 2010).

The combination of the quantum numbers enables to determine the total energy of electrons in the atoms (Table 1). The quantized energy levels (K, L_I, L_{II},...) presented in the Table 1 are also named binding energy or absorption edge. These basic informations are crucial for better understanding the XRF and XAS spectroscopy.

Table 1. Electron distribution into the fulfilled K, L, and M shells of atom. This represents the electron distrubution based in the quantum numbers. Which explains the energy levels (or absorption edge or binding energy) K, L_I, L_{II}, L_{III},M_I, M_{II}, M_{III}, M_{IV}, M_V.

Quantic N°	**Electron**									
	K Shell		**L Shell**							
Principal *(n)*	1	1	2	2	2	2	2	2	2	2
Azimuthal *(l)*	0	0	0	0	1	1	1	1	1	1
Magnetic *(m)*	0	0	0	0	-1	-1	0	0	1	1
Spin *(s)*	-1/2	+1/2	-1/2	+1/2	-1/2	+1/2	-1/2	+1/2	-1/2	+1/2
$j = l + s$	-1/2	+1/2	-1/2	+1/2	+1/2	+3/2	+1/2	+3/2	+1/2	+3/2
Electron Symbol	1s	1s	2s	2s	$2p_{1/2}$	$2p_{3/2}$	$2p_{1/2}$	$2p_{3/2}$	$2p_{1/2}$	$2p_{3/2}$
Energy Level	K = 1s		$L_I = 2s$				$L_{II} = 2p_{1/2}$	$L_{III} = 2p_{3/2}$		

N°	M Shell																	
n	3	3	3	3	3	3	3	3	3	3	3	3	3	3	3	3	3	3
l	0	0	1	1	1	1	1	1	2	2	2	2	2	2	2	2	2	2
m	0	0	-1	-1	0	0	1	1	-2	-2	-1	-1	0	0	1	1	2	2
s	-1/2	+1/2	-1/2	+1/2	-1/2	+1/2	-1/2	+1/2	-1/2	+1/2	-1/2	+1/2	-1/2	+1/2	-1/2	+1/2	-1/2	+1/2
j	-1/2	+1/2	+1/2	+3/2	+1/2	+3/2	+1/2	+3/2	+3/2	+5/2	+3/2	+5/2	+3/2	+5/2	+3/2	+5/2	+3/2	+5/2
ES	3s	3s	$3p_{1/2}$	$3p_{3/2}$	$3p_{1/2}$	$3p_{3/2}$	$3p_{1/2}$	$3p_{3/2}$	$3d_{3/2}$	$3d_{5/2}$	$3d_{3/2}$	$3d_{5/2}$	$3d_{3/2}$	$3d_{5/2}$	$3d_{3/2}$	$3d_{5/2}$	$3d_{3/2}$	$3d_{5/2}$
EL	$M_I = 3s$		$M_{II} = 3p_{1/2}$		$M_{III} = 3p_{3/2}$		$M_{IV} = 3d_{3/2}$		$M_V = 3d_{5/2}$									

All XRF spectrometer have at least the three components (Figure 1.2): 1) Radiation source; 2) Sample holder, were characteristics lines or fluorescence are produced; and 3) Detection and data process system (spectrum generation). The excitation source can be electrons beam (e.g, electron microscopes), protons, alpha particles or electromagnetic radiation. Electromagnetic radiation can be generated by accelerating charged particle (synchrotron source) or by breaking accelerated charges particles (*bremsstrahlung* spectrum). The *bremsstrahlung* spectrum can be generated in X-ray tubes (also it generates anode characteristics lines, e.g., Rh Kα, by electrons-anode interaction), which are very common in benchtop spectrometers. The *bremsstrahlung* radiation has a continuum spectrum from zero to max tube energy (e. g., 50 keV), and those photons are targeted to sample and interact with the atoms (BERTIN, 1978; GRIEKEN & MARKOWICZ, 2002; BECKHOFF et al., 2006).

The schematic steps for X-ray fluorescence generation are in (Figure 1.3). When the income photon (e.g., produced in the X-ray tube) has energy equal or greater than binding energy of the electron in inner shells (K, L, M) of the atom, this photon is absorbed and transfer energy to this electron. The

ejected electron can go to a vacant shell or can be ejected from the atom as a photoelectron with kinetic energy equals to $E_{kinetic} = E_{Income} - E_{bind}$. This phenomenon is named photoelectric effect. The inner shell is now vacant and the atom is in excited state. The following event is the electron transition from a higher energy level (external shell) to a lower energy level orbital (internal shell) (BERTIN, 1978; GRIEKEN & MARKOWICZ, 2002; BECKHOFF et al., 2006). This step is very fast (femtoseconds) and the electron transition occurs in quantized way (quantum jump) (Figure 1.3).

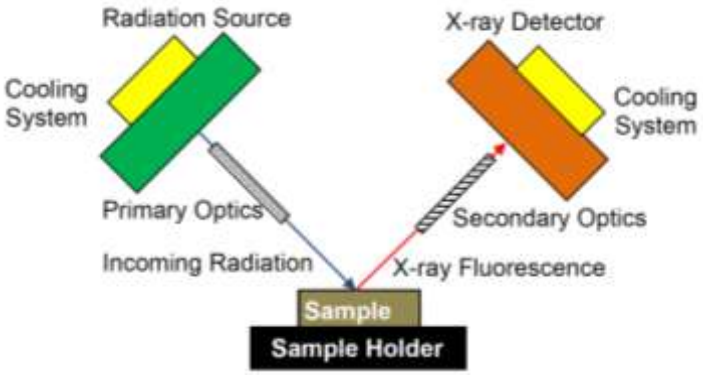

Figure 1.2. Basics components of benchtop X-ray fluorescence spectrometers

The difference between the binding energy of the electron after (higher binding energy) and before (lower binding energy) quantum jump, results in the emission of an X-ray photon, due to the energy conservation law. This X-ray fluorescence photon has a specific energy which is equal to the difference of binding energy of electron after and before the transition, e.g., $E_{K\alpha_1} = E_K - E_{L_{III}}$. The notation $K\alpha$ was proposed for Siegbahn and it refers to a characteristic line that was emitted from an electron transitions between L_{III} and K absorption edges. Others characteristic lines for electric dipole transitions (selection rule; $\Delta n \neq 0, \Delta l = \pm 1, \Delta j = \pm 1 \; ou \; 0$) and notation are in Figure 1.4.

The energy magnitude of the characteristic lines is related to the chemical element. Different chemical elements have different numbers of protons, thus different electromagnetic attraction force between proton and the electron (Coulomb forces). This means that the electron of K shell of Ca atoms (20 protons) has greater binding energy than the electron of K shell of P atoms (15 protons). Thus, the $Ca\,K\alpha$ energy (3.69 keV) is greater than $P\,K\alpha$ (2.01

keV). The fluorescence or characteristic line enable identify which elements are presents in the sample (qualitative analysis).

The fluorescence photons are detected by detection system which determines the energy and intensity of each photon, providing the XRF spectrum (Figure 1.5). The photon intensity of specific characteristic line is related to the chemical element concentration. Thus after data process, it is possible to create calibration curves for each chemical element and estimates their concentration in the unknown sample (quantitative analysis) (GRIEKEN & MARKOWICZ, 2002; SITKO & ZAWISZA, 2012).

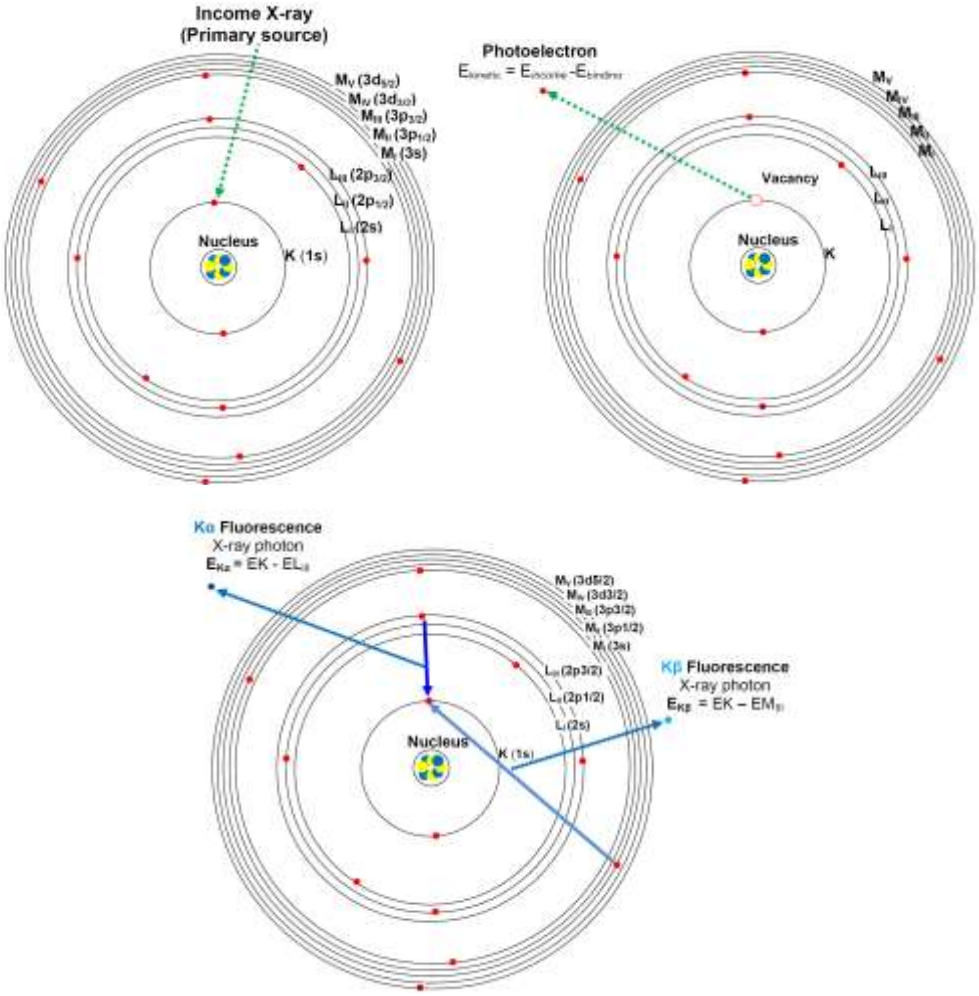

Figure 1.3. Schematic model for the X-ray fluorescence generation using the Bohr´s atom model (quantized shells). The steps are: Atom excitation; Vacancy generation; Electronic transition; and Emission of characteristic radiation.

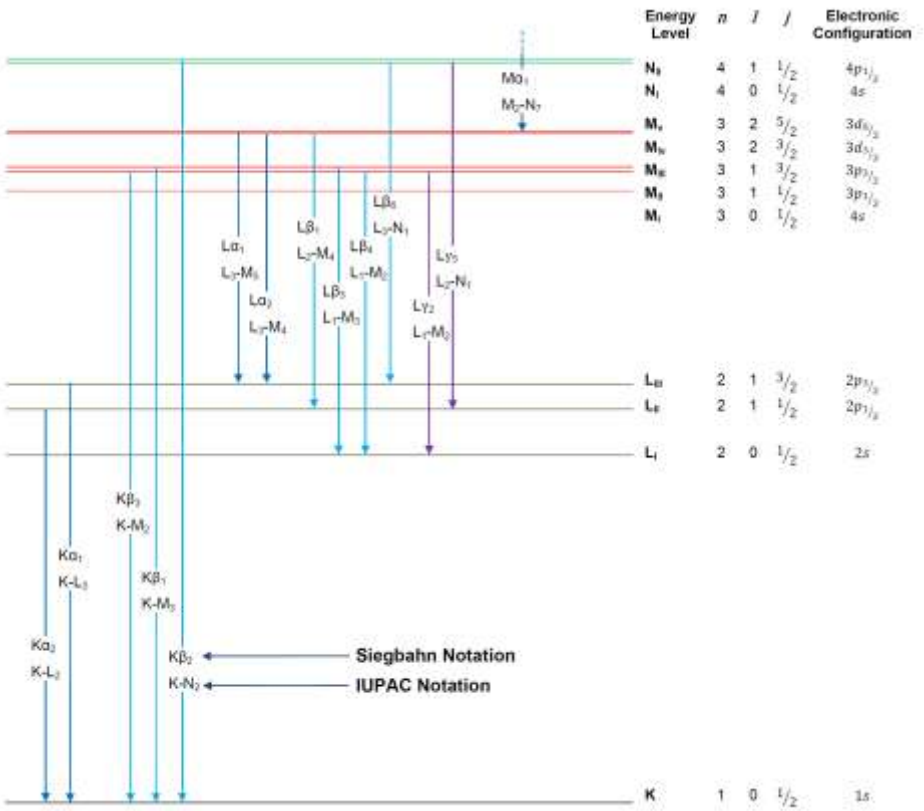

Figure 1.4. X-ray fluorescence characteristic lines for electric dipole transitions.

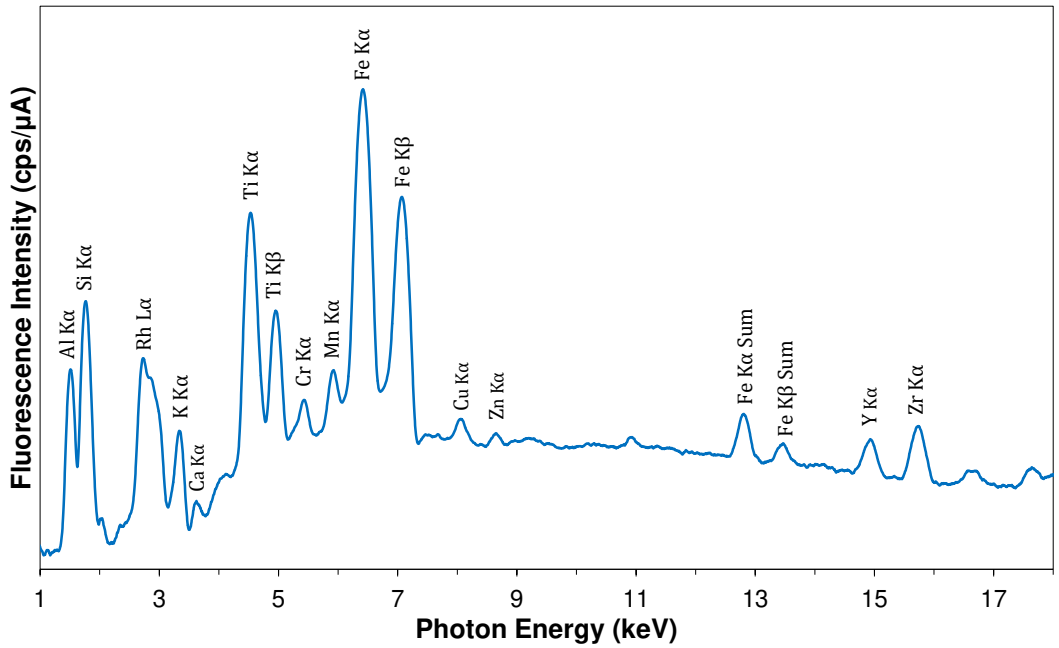

Figure 1.5. X-ray fluorescence spectrum. The continuum spectrum (base line) and Rh Lα are resulted from the backscattering of *bremsstrahlung* spectrum and Rh lines, respectively, produced from the X-ray tube. The peaks are the characteristic fluorescence lines of chemical elements present on sample.

1.3.2. X-ray Absorption Spectroscopy (XAS)

X-ray absorption spectroscopy (XAS) also is used to study the interaction between X-ray radiation and the atoms present in the sample. However, unlike XRF, the XAS is used to identify specific features of a target chemical element. The XAS has been used for several propose in environmental sciences. One of main XAS studies in environmental sciences is to identify chemical species or structural characterization of an element presents in the sample (KELLY et al., 2008; BUNKER, 2010; CALVIN, 2013). Thus, the XRF and XAS are complementary techniques, and together provide information about the chemical elemental content (e.g. Ca content) and chemical speciation of crystalline or non-crystalline materials (e.g., $CaCO_3$, $CaSO_4$, Ca-EDTA complex). Others information can be obtained from XAS, as the oxidation state, coordination number, molecular orbital hybridization, density of unoccupied states (KELLY et al., 2008; BUNKER, 2010; CALVIN, 2013).

To perform XAS analysis the radiation beam must be very well collimated, with high photon flux, and also is required a high resolution monochromator, able to produce a monochromatic light with ~0.1 eV energy resolution scale. This kind of radiation can be generated in the synchrotron laboratories. Synchrotron radiation is produced when relativistic charged particles (e. g., accelerated electrons close to light velocity), are forced to move along curved trajectories by applied magnetic fields. In general, synchrotron radiation facilities produce electromagnetic spectrum from infrared to hard X-rays (KELLY et al., 2008; BUNKER, 2010; CALVIN, 2013; JOLY & GRENIER, 2016; KAS et al., 2016).

Synchrotron radiation is directed for specific places named beamlines which are located at tangent position of storage ring of synchrotron storage ring (Figure 1.6). The beamlines are the place where the experiments are performed and XAS data are collected. The schematic beam line setup and data collection process are in Figure 1.7.

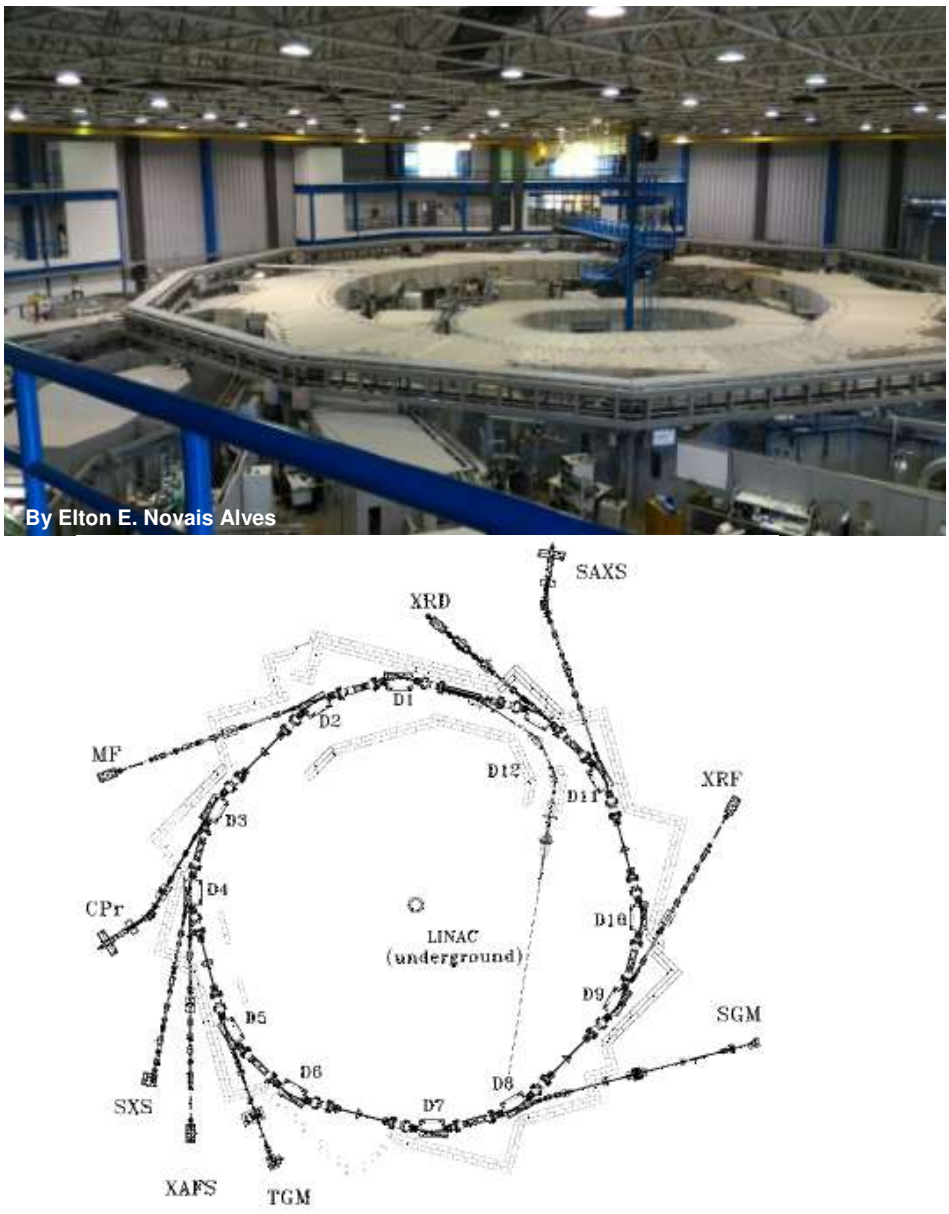

Figure 1.6. Photography of UVX at Brazilian Synchrotron Light Laboratory and schematic representation of beamlines (CRAIEVICH & RODRIGUES, 1997)

XAS spectrum contains the X-ray absorption intensity by a given incident energy ($\mu_x(E)$) (Figure 1.8). Before the absorption edge (Pre-edge region) the absorption is minimal, because incident energy has lower energy that the binding energy of target electron (e.g., electron of K shell of Zr), thus minimal interaction occurs between incident photon and binding electron. When the monochromator keeps moving (each few eV) and increasing the incident photon energy and reaches the same value than electron binding energy occurs a sharp increasing in the absorption, which can be found by the maximum of first

derivate of this spectra. The higher peak observed close to absorption edge in the spectrum is named white line. When the incident energy keeps increasing, it is observed some features in the XAS spectrum, which is named fine structure and contains more information about neighborhood of atoms (Figure 1.8) (KELLY et al., 2008; BUNKER, 2010; CALVIN, 2013; JOLY & GRENIER, 2016; KAS et al., 2016)..

Several acronyms are used in the X-ray Absorption spectroscopy. The most comprehensive name is XAS, which refers the measurements of the exponential decay (Beer's law) of photons beam of a given energy through a sample. The XANES is the acronym for X-ray Absorption Near Edge Structure spectroscopy and it comprises part of the XAS spectrum, in general refers to energy range from -10 to 50 eV relative to E_0 (edge), in other words, it is the spectrum near the absorption edge. EXAFS is the acronym for Extended X-ray Absorption Fine Structure spectroscopy, comprises the XAS spectra region which begins at + 50 eV and stretches several hundreds of electron-volts (e.g., +1000 eV) from the absorption edge (Figure 1.8).

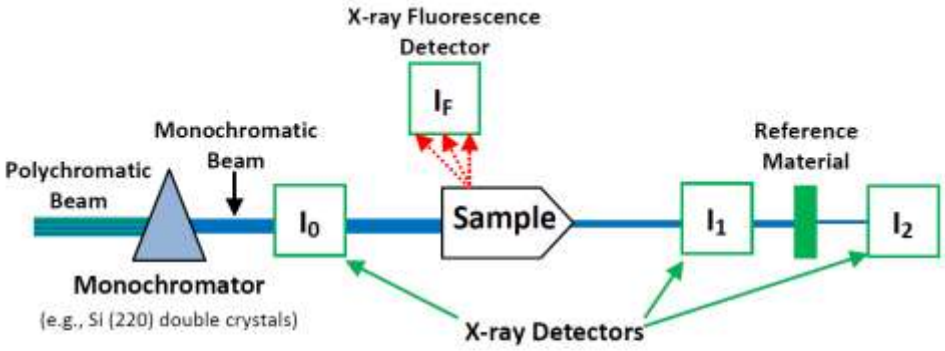

- Sample Absorption in **Transmission** mode: $\mu_x(E) = \ln\left(\frac{I_0}{I_1}\right)$
- Sample Absorption in **Fluorescence** mode: $\mu_x(E) \propto \ln\left(\frac{I_F}{I_0}\right)$
- Reference Material Absorption for calibration: $\mu_x(E) = \ln\left(\frac{I_1}{I_2}\right)$

Figure 1.7. Schematic setup of data collection at synchrotron radiation laboratories. When possible, XAS data are collected in both transmission and fluorescence mode. The polychromatic synchrotron radiation passes through a monochromator, and the intensity is measured by a X-ray detector (I_0). Now, the monochromatic beam reaches the sample, producing X-ray fluorescence which is measured by an energy dispersive detector (I_F). The remaining beam passes through a second detector (I_1), a reference material (e.g, Fe foil) for calibration,

and a third detector (I_2) before termination. X-ray absorption is calculated depending of detector data used, as described in the figure.

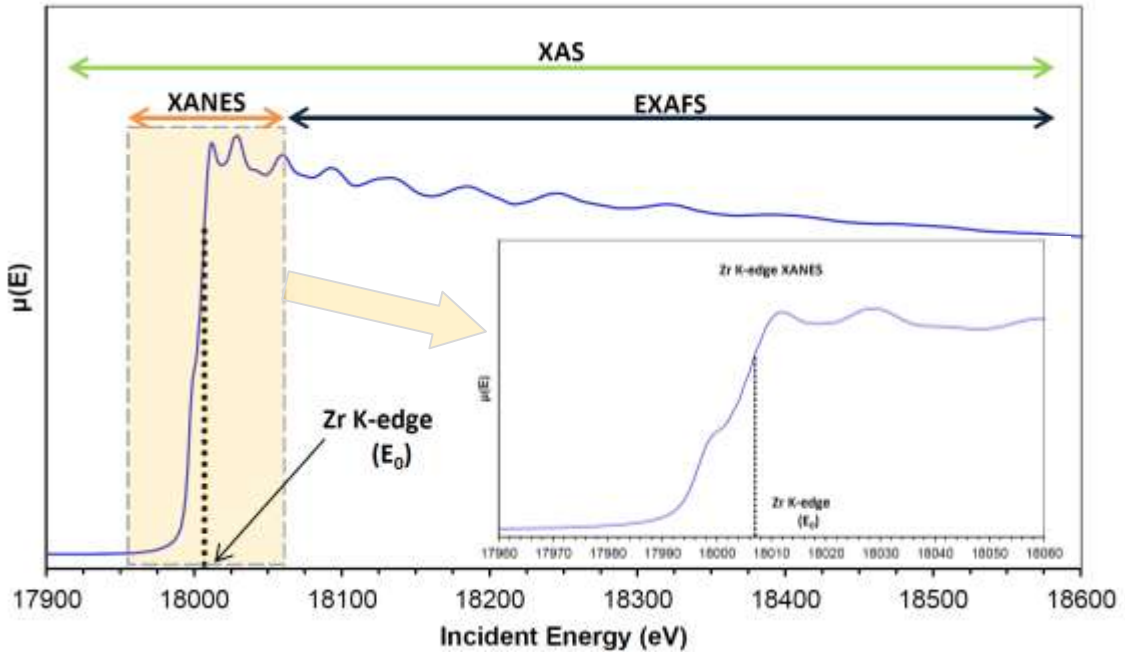

Figure 1.8. X-ray absorption (XAS) spectrum of metallic zirconium K-edge. XANES and EXAFS regions area highlighted. This spectrum contains several chemical information about Zr, as oxidation state, densities of unoccupied states, and neighborhood atoms. Spectrum data extracted from Hephaestus software (RAVEL & NEWVILLE, 2005).

XANES region shows distinct features that relate to the specific photoelectron transitions within the absorbing atom (as Zr, in Figure 1.8). These spectral features provide information about: chemical element oxidation state; coordination chemistry (tetrahedral, octahedral, etc.); molecular orbitals – orbital hybridization. The oxidation state can be determined observing an E_0 shift in the spectra (e.g. for sulfur in Figure 2.4, Chapter II).

The XAS data process consists in convert raw data to μ(E) (Figure 1.7), energy calibration (reference material), find absorption edge (E_0 = maximum of first derivate of spectrum or second derivate equal to zero), pre- and post-edge fitting, and finally, normalization of the signal to a value of edge-step equal to 1.

XANES data are often used for a semi-quantitative analysis of unknown spectra by using knowing pure standards (fingerprints) in linear combination fitting tools. A common technique used for assessing the valence state and phases present in a sample is linear combination fitting (LCF). The LCF consists in a set of pure standards measured spectra which are used to obtain an optimal fit of an unknown sample spectrum by non-linear least square minimization, by an iterative method. Thus, it is possible estimates the proportion (semi-quatitative) of chemical species of the target element in the unknown sample.

1.4. References

AHMED, S. N. Properties and sources of radiation. In: (Ed.). **Physics and Engineering of Radiation Detection**. Waltham: Elsevier, 2015, p.1-64.

ARRIVABENE, H. P. **Morfoanatomia, histoquímica e teor de ferro foliar em *Avicennia schaueriana* Stapft & Leechm, *Laguncularia racemosa* (L.) Gaertn. e *Rhizophora mangle* L. ocorrentes em cinco áreas de manguezal do Estado do Espírito Santo**. (Dissertation). Biologia Vegetal, Universidade Federal do Espírito Santo, Vitória, 2011. 130 p.

BALOUET, J. C.; SMITH, K. T.; VROBLESKY, D.; OUDIJK, G. Use of Dendrochronology and Dendrochemistry in Environmental Forensics: Does It Meet the Daubert Criteria? **Environmental Forensics**, v. 10, n. 4, p. 268-276, 2009.

BECKHOFF, B.; KANNGIEßER, B.; LANGHOFF, N.; WEDELL, R.; WOLFF, H. **Handbook of Practical X-Ray Fluorescence Analysis**. Berlin: Springer-Verlag, 2006. XXIV, 863 p.

BERTIN, E. P. **Introduction to X-Ray Spectrometric Analysis**. New York: Springer US, 1978

BUNKER, G. **Introduction to XAFS: A Practical Guide to X-ray Absorption Fine Structure Spectroscopy**. Cambridge: Cambridge University Press, 2010

CALVIN, S. **XAFS for Everyone**. Boca Raton, FL: CRC Press, 2013. 475 p.

CHURCH, J. A.; WHITE, N. J.; AARUP, T.; WILSON, W. S.; WOODWORTH, P. L.; DOMINGUES, C. M.; HUNTER, J. R.; LAMBECK, K. Understanding global sea levels: past, present and future. **Sustainability Science**, v. 3, n. 1, p. 9-22, 2008.

CRAIEVICH, A. F.; RODRIGUES, A. R. LNLS Synchrotron Source and Beamlines: Status, First Experiments and User Access. **Brazilian Journal of Physics**, v. 27, n. 4, p. 417-424, 1997.

DIEGUES, A. C. S. A. **Povos e Águas: inventário de áreas úmidas brasileiras**. São Paulo: NUPAUB-USP, 2002

DUNWIDDIE, P. W.; LAMARCHE, V. C. Dendrochronological characteristics of some native Australian trees. **Australian Forestry**, v. 43, n. 2, p. 124-135, 1980.

EISBERG, R.; RESNICK, R. **Quantum Physics of Atoms, Molecules, Solids, Nuclei and Particles** New York: John Wiley and Sons, 1985. 864 p.

FOREST PRODUCTS LABORATORY, F. **Potash from wood ashes.** Madison: US Forest Service 1919, p.1. (Technical Note E2)

FRITTS, H. C. Dendrochronology and Dendroclimatology. In: (Ed.). **Tree Rings and Climate**: Academic Press, 1976, p.1-54.

GOMES, F. H.; KER, J. C.; FERREIRA, T. O.; MOREAU, A. M. S. S.; MOREAU, M. S. Characterization and pedogenesis of mangrove soils from Ilhéus-BA, Brazil. **Revista Ciência Agronômica**, v. 47, p. 599-608, 2016.

GRIEKEN, R. E. V.; MARKOWICZ, A. A. **Handbook of X-ray spectrometry**. New York: Marcel Dekker, 2002. 985 p.

HOSSAIN, M. D.; NURUDDIN, A. A. Soil and Mangrove: A Review. **Journal of Environmental Science and Technology**, v. 9, n. 2, p. 198-207, 2016.

IBGE, INSTITUTO BRASILEIRO DE GEOGRAFIA E ESTATÍSTICA. Censo Demográfico 2014. v. 2014. Available in: <http://www.ibge.gov.br/home/estatistica/populacao/censo2010/default_atlas.shtm>. Accessed in: 01/12/2018.

IEMA. **Concha D'Ostra (2) - Levantamento Das Informações Básicas. Relatório Parcial** Vitória, ES: Instituto Estadual de Meio Ambiente, 2004

IEMA. **Reavaliação da Categoria de Unidade de Conservação Estabelecida pela Lei no 7.658/04, Estação Ecológica Estadual Concha D'Ostra Município de Guarapari – ES.** Vitória, ES: Instituto Estadual de Meio Ambiente, 2005

IPHAN. INSTITUTO DO PATRIMÔNIO HISTÓRICO E ARTÍSTICO NACIONAL. 2018. Available in: <http://www.iphan.gov.br/>. Accessed in: 01/16/2018.

JOLY, Y.; GRENIER, S. Theory of X-Ray Absorption Near Edge Structure. In: Bokhoven, J. A. V. e Lamberti, C. (Ed.). **X-Ray Absorption and X-Ray Emission Spectroscopy**. Chichester, UK: John Wiley & Sons, 2016, p.73-97.

KAS, J. J.; JORISSEN, K.; REHR, J. J. Real-Space Multiple-Scattering Theory of X-Ray Spectra. In: Bokhoven, J. A. V. e Lamberti, C. (Ed.). **X-Ray Absorption and X-Ray Emission Spectroscopy**. Chichester, UK: John Wiley & Sons, 2016, p.51-72.

KELLY, S. D.; HESTERBERG, D.; RAVEL, B. Analysis of Soils and Minerals Using X-ray Absorption Spectroscopy. In: Ulery, A. L. e Richard Drees, L. (Ed.). **Methods of Soil Analysis Part 5 - Mineralogical Methods**. Madison, WI: Soil Science Society of America, 2008, p.387-463. (SSSA Book Series)

KJERFVE, B.; LACERDA, L. D. **Mangroves of Brazil.** Okinawa: International Society for mangrove ecosystems, p.245-272, 1993.

LEMONTE, J. J.; STUCKEY, J. W.; SANCHEZ, J. Z.; TAPPERO, R.; RINKLEBE, J. R.; SPARKS, D. L. Sea Level Rise Induced Arsenic Release from Historically Contaminated Coastal Soils. **Environmental Science & Technology**, v. 51, n. 11, p. 5913-5922, 2017.

MAJUMDAR, S.; PERALTA-VIDEA, J. R.; CASTILLO-MICHEL, H.; HONG, J.; RICO, C. M.; GARDEA-TORRESDEY, J. L. Applications of synchrotron μ-XRF to study the distribution of biologically important elements in different environmental matrices: A review. **Analytica Chimica Acta**, v. 755, p. 1-16, 2012.

MENEZES, M.; BERGER, U.; WORBES, M. Annual growth rings and long-term growth patterns of mangrove trees from the Bragança peninsula, North Brazil. **Wetlands Ecology and Management**, v. 11, p. 233–242, 2003.

RAVEL, B.; NEWVILLE, M. ATHENA, ARTEMIS, HEPHAESTUS: data analysis for X-ray absorption spectroscopy using IFEFFIT. **Journal of Synchrotron Radiation**, v. 12, n. 4, p. 537-541, 2005.

REY, J. R.; WALTON, W. E.; WOLFE, R. J.; CONNELLY, R.; O'CONNELL, S. M.; BERG, J.; SAKOLSKY-HOOPES, G. E.; LADERMAN, A. D. North American Wetlands and Mosquito Control. **International Journal of Environmental Research and Public Health**, v. 9, n. 12, p. 4537-4605, 2012.

ROBERTSON, A. I.; ALONGI, D. M. **Tropical Mangrove Ecosystems**. Washington: American Geophysical Union, 1992, v.41 (Coastal and Estuarine Studies)

ROCHA, P. A. **Solos do manguezal da Baía de Guarapari – ES: mineralogia e fósforo como indicador de contaminação por esgoto doméstico**. Departamento de Solos, Universidade Federal de Viçosa, Viçosa, 2016. xi, 90 p.

SAFFORD, L. O.; SHIGO, A. L.; ASHLEY, M. Gradients of Cation Concentration in Discolored and Decayed Wood of Red Maple. **Canadian Journal of Forest Research**, v. 4, n. 4, p. 435-440, 1974.

SAINT-PAUL, U.; SCHNEIDER, H. **Mangrove Dynamics and Management in North Brazil**. Berlin: Springer-Verlag Berlin Heidelberg, 2010, v.211 (Ecological Studies, Analysis and Synthesis)

SCHAEFFER-NOVELLI, Y. **Manguezal: Ecossistema Entre a Terra e o Mar**. São Paulo: Caribbean Ecological Research, 1995. 64 p.

SHARITZ, R. R.; PENNINGS, S. C. Development of Wetland and Plant Communities. . In: Batzer, D. P. e Sharitz, R. R. (Ed.). **Ecology of Freshwater and Estuarine Wetlands**. Berkeley, CA, US: University of California Press, 2006, p.177–241.

SHEPPARD, P. R.; SPEAKMAN, R. J.; RIDENOUR, G.; GLASCOCK, M. D.; FARRIS, C.; WITTEN, M. L. Spatial patterns of tungsten and cobalt in surface dust of Fallon, Nevada. **Environmental Geochemistry and Health**, v. 29, n. 5, p. 405–412, 2007.

SHEPPARD, P. R.; ORT, M. H.; ANDERSON, K. C.; ELSON, M. D.; VA´ZQUEZ-SELEM, L.; CLEMENS, A. W.; LITTLE, N. C.; SPEAKMAN, R. J.

Multiple dendrochronological signals indicate the eruption of Parícutin volcano, Michoacán, Mexico. **Tree-Ring Research**, v. 64, n. 2, p. 97-108, 2008.

SITKO, R.; ZAWISZA, B. Quantification in X-Ray Fluorescence Spectrometry. In: Sharma, S. K. (Ed.). **X-Ray Spectroscopy**. Rijeka, Croatia: InTech, 2012, p.280.

SMITH, K. T.; HOUSTON, D. R. Metal concentrations in wood of sugar maple infected with sapstreak disease. **Canadian Journal of Forest Research**, v. 24, n. 1, p. 185–188, 1994.

SMITH, K. T.; BALOUET, J. C.; OUDIJK, G. Elemental scanning of an increment core using EDXRF: from fundamental research to environmental forensics applications **Dendrochronologia**, v. 26, p. 157–163, 2008.

SMITH, K. T.; BALOUET, J. C.; SHORTLE, W. C.; CHALOT, M.; BEAUJARD, F.; GRUDD, H.; VROBLESKY, D. A.; BURKEN, J. G. Dendrochemical patterns of calcium, zinc, and potassium related to internal factors detected by energy dispersive X-ray fluorescence (EDXRF). **Chemosphere**, v. 95, p. 58–62, 2014.

SOUZA, B. T.; ESTRADA, G. C. D.; SOARES, M. L. G.; CALLADO, C. H. Occurrence of annual growth rings in Rhizophora mangle in a region with low climate seasonality. **Anais da Academia Brasileira de Ciências**, v. 88, n. 1, p. 517-525, 2016.

VALE, C. C.; FERREIRA, R. D. Os manguezais do litoral do Estado do Espírito Santo. In: Simpósio de Ecossistemas da Costa Brasileira, 1998, São Paulo:ACIESP, p. 88-94.

VANNUCCI, M. What is so special about mangroves? **Brazilian Journal of Biology**, v. 61, n. 4, p. 599-603, 2001.

VERHEYDEN, A.; HELLE, G.; SCHLESER, G. H.; DEHAIRS, F.; BEECKMAN, H.; KOEDAM, N. Annual cyclicity in high-resolution stable carbon and oxygen isotope ratios in the wood of the mangrove tree Rhizophora mucronata. **Plant, Cell & Environment**, v. 27, n. 12, p. 1525-1536, 2004a.

VERHEYDEN, A.; KAIRO, J. G.; BEECKMAN, H.; KOEDAM, N. Growth Rings, Growth Ring Formation and Age Determination in the Mangrove Rhizophora mucronata. **Annals of Botany**, v. 94, n. 1, p. 59-66, 2004b.

VERHEYDEN, A.; ROGGEMAN, M.; BOUILLON, S.; ELSKENS, M.; BEECKMAN, H.; KOEDAM, N. Comparison between $\delta^{13}C$ of α-cellulose and bulk wood in the mangrove tree *Rhizophora mucronata*: Implications for dendrochemistry. **Chemical Geology**, v. 219, n. 1, p. 275-282, 2005.

WOODROFFE, C. D.; GRINDROD, J. Mangrove Biogeography: The Role of Quaternary Environmental and Sea-Level Change. **Journal of Biogeography**, v. 18, n. 5, p. 479-492, 1991.

WOODROFFE, C. D.; DAVIES, G. The morphology and development of tropical coastal wetlands In: Perillo, G. M. E., Wolanski, E.*, et al* (Ed.). **Coastal Wetlands: An Integrated Ecosystem Approach** Amsterdam, Netherlands: Elsevier, 2009, p. 65-88.

WORBES, M. How to Measure Growth Dynamics in Tropical Trees a Review. **IAWA Journal**, v. 16, n. 4, p. 337-351, 1995.

WORBES, M. One hundred years of tree-ring research in the tropics: a brief history and an outlook to future challenges. **Dendrochronologia**, v. 20, n. 1, p. 217-231, 2002.

CHAPTER II

BIOGEOCHEMISTRY OF CONTAMINATED AND NON-CONTAMINATED TROPICAL MANGROVE SOILS

2.1. Abstract

Mangrove ecosystems are dynamically influenced by seawater. Here we compared the biogeochemistry of better preserved and contaminated tropical mangrove soils in terms of elemental composition, pH and reduction-oxidation (redox) potential (Eh), and S speciation. Soils from two distinct areas located in a Tropical Brazilian mangrove ecosystem were sampled: P1 – a better preserved and more inland area, and P2 – an area closer to the beach that has been contaminated by domestic sludge disposal. Ten soil-profile samples were collected from each area at 5 or 10 cm intervals and preserved for analysis. X-ray fluorescence (XRF) analysis showed unique depth-distributions of S, Fe, Cl, Ca, K, Ti, Cr, Br, Sr, and Zr in each area. Sulfur K-edge XANES spectroscopy showed that the mangrove location and conservation state influenced the soil S speciation. Pyrite (FeS_2) was the dominant S mineral (~50% of S) found in both soil profiles, and more abundant organic and elemental S (S-org and S^0) in profile P1 indicated greater microbiological activity in the better preserved mangrove site. A decrease in the proportion of SO_4^{2-} with depth in P1 following a decrease on Eh. Although Eh also decreased with depth in profile P2, a corresponding increase in the proportion of SO_4^{2-} was indicative of greater influx from seawater. In essence, S speciation was directly influenced by seawater encroachment with the latter being affected by human impacts.

2.2. Introduction

The chemical composition and speciation of elements in soils provides valuable informations about soil formation, biological influences, and anthropogenic impacts on natural ecosystems. Analyses such as X-ray fluorescence (XRF) spectrometry and X-ray absorption spectroscopy (XAS)

have greatly impacted environmental sciences, allowing scientists to discover processes and mechanisms occurring at multiple scales ranging from the field to the nanoscale (HESTERBERG et al., 2011; WERNER, 2017). These techniques should be especially useful for exploring the biogeochemistry of poorly understood estuarine ecosystems like mangroves.

Mangrove ecosystems are located in subtropical and tropical areas in estuarine environments, and they have characteristic trees and shrubs (namely mangrove) that are adapted to the nonconsolidated, tidal-influenced, and saline soils (ROBERTSON & ALONGI, 1992; DIEGUES, 2002; SAINT-PAUL & SCHNEIDER, 2010). These environments are geologically recent, formed during the Quaternary (WOODROFFE & GRINDROD, 1991; GOMES et al., 2016), and cover approximately 16 million hectares of coastlines worldwide (HOSSAIN & NURUDDIN, 2016). Improper management of mangrove areas leads to their degradation, resulting in negative socioeconomic and environmental impacts. Mangroves are especially threatened by anthropogenic impacts such as improper disposal of domestic wastes and stormwater runoff from encroaching urban areas.

Sulfur is a key element that can provide insights into chemical and biological states of mangroves. Sulfur occurs in the environment mainly in six different oxidation states [S(-II), S(-I), S(0), S(II), S(IV), and S(VI)]. The combination of oxidation states in intermittently flooded mangrove ecosystems should be affected by forms of S originally in sedimentary deposits along with dynamic influxes of S from seawater and freshwaters (riverine and runoff waters), and soil redox reactions that are mainly governed by biotic processes (FERREIRA et al., 2007). Seawater, which contains an average of 28 mmol L^{-1} SO_4^{2-}, is the main source of S in mangrove soils (MORRIS, 1995). Biogeochemical processes catalyzed by microorganisms under low O_2 contents of water-saturated soils reduce SO_4^{2-}-S (NEUBAUER et al., 2005). Factors such as distance from the open ocean, altitude, and tide height can influence these processes (FERREIRA et al., 2007). In some cases, rates of SO_4^{2-} influx can be greater than its reduction rates in soils (MORRIS, 1995). Biological reduction of S is usually coupled to oxidation of organic C compounds, and generating organic S forms and sulfide (e.g., H_2S, HS^-) that can complex with Fe and

chalcophilic trace elements to form iron monosulfide, pyrite, and trace-element sulfides and organic forms (NEUBAUER et al., 2005). In general, biological sulfate reduction produces (RICKARD, 2012) over 97% of the sulfide at the Earth's surface, whereas abiotic processes such as volcanoes and hydrothermal vents are responsible for only 3%.

Studies about S speciation and its dynamics in tropical mangrove soils are scarce. The destructive nature of conventional chemical-extraction techniques for evaluating forms of S in soils can alter S speciation during the extraction. Moreover, field sampling and sample handling are very critical for minimizing chemical alterations from the natural condition. Our preliminary tests (Figure S2.2) suggested that short time (15 min) exposure of soil samples to air, can promote detectable sulfur oxidation. Thus, care must be taken to avoid changes in oxidation states of S (and other elements) between sampling and speciation analysis. In this study, we used liquid nitrogen during the field sampling to immediately freeze the soil samples to preserve their properties, and S speciation was performed in lyophilized samples, using X-ray absorption near edge structure spectroscopy (XANES) (see Methods).

Our aim was to assess S chemical speciation along with elemental composition, pH and Eh in soils from two Tropical Brazilian mangroves that are more or less influenced by anthropogenic impacts and seawater. We hypothesize that S species in these mangrove ecosystems are directly influenced by anthropogenic influence (preservation state), distance to the ocean, and in the soil depth. We expected more oxidized S in the upper soil layers that have more influx of atmospheric O_2, and more reduced S in deeper layers with higher organic C contents.

2.3. Materials and Methods

Study Area Characterization: The mangrove ecosystem studied is located in the Concha D'Ostras Sustainable Development Reserve, Guarapari city, Espírito Santo state, Brazil (Figure 2.1). The climate according to Köppen classification is Aw, tropical hot and wet, characterized by a short dry season in the winter and a rainy summer (ALVARES et al., 2013). Two soil profiles were

sampled from extreme borders of the Reserve area. The first soil profile site, P1 (20° 40' 17.4" S, 40° 33' 02.0" W, and 3 m a.s.l), was situated at 7.6 km from the river mouth. The P1 site is distant from the urban area, being considerate well preserved and less contaminated that P2, with a clayey soil (hand texturing), more rich in organic matter (dark color), and has dense mangrove vegetation. The second soil profile site, P2 (20° 39' 54.1" S, 40° 29' 56.5" W, sea level), is situated near to the urban area and few meters from the open sea, the soil is sandy (hand texturing), and it is highly contaminated by domestic sludge disposal coming from the urban center (Figure 2.1).

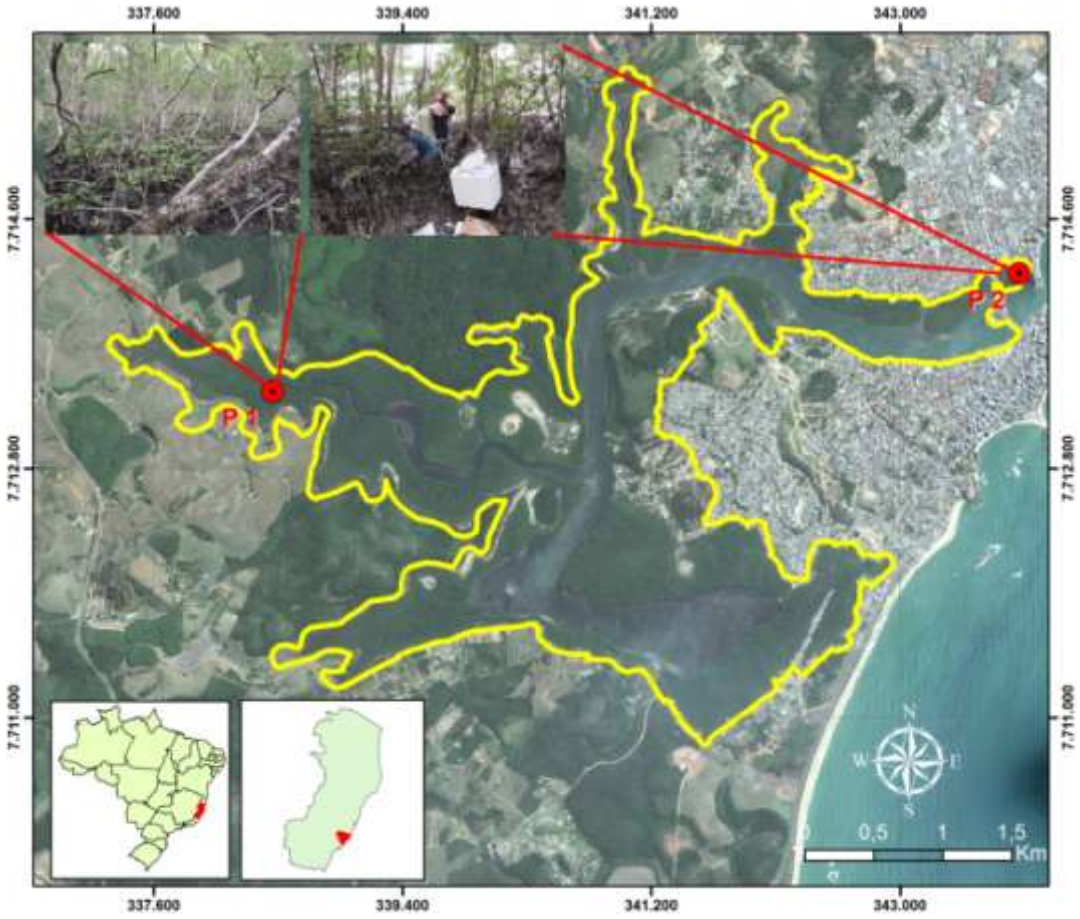

Figure 2.1. Tropical Brazilian mangrove located in the Concha D'Ostras Sustainable Development Reserve (area inside yellow line), Guarapari city, Espírito Santo state, Brazil. Sampled sites P1 (preserved and 7 km from the sea) and P2 (more degraded, few meters from the sea) are indicated.

Soil Sampling and Preparation: Both soil sampling and soil storage were a critical part of this study because our preliminary test showed that significant microbiological oxidation of reduced S species occurs within as 15 min of contact between a soil sample and air (Figure S2.2). Thus, the following procedures were designed to avoid S oxidation. Two soil profiles (P1 and P2) were sampled with a semi-opened, 7 cm wide, and 90 cm long stainless steel soil core sampler (model Napoleão, Sondaterra®, Piracicaba-SP, Brazil). Sampling was done manually up to a soil depth (65 cm in P1 and 50 cm in P2) at which impedance prevented further boring.

Soil samples were collected in duplicate at 5 cm depth intervals, using plastic pots of 33 cm^3 and 3 cm wide. First, we marked the soil profile each 5 cm using a plastic ruler and stainless knife (Figure 2.2-A); then we inserted two of the plastic pots into the 5 cm marked soil profile (Figure 2.2-B); we removed the plastic cups and we filled with the maximum soil amount present in that 5 cm layer. After soil-filled, the plastic cups were closed, labeled, and immediately immersed in liquid nitrogen (-196 ºC) (Figure 2.2-C). During the soil sampling we observed a higher density of mangrove roots in three layers (10-20, 25-35, 40-50) of the P1 soil profile. These layers showed low soil amount because of root predominance, and we combined two soil layers of 5 cm wide into one with 10 cm wide to obtain enough soil volume. Thus, the depth sampled were: P1) 0-5, 5-10, 10-20, 20-25, 25-35, 35-40, 40-50, 50-55, 55-60, 60-65; and P2) 0 to 50 each 5 cm (10 layers). Ten layers from each soil profile and two replicates from each soil layer were obtained, resulting in 40 soil samples.

All soil samples were kept frozen during transport and were lyophilized in a FreeZone Bulk Tray Dryer (model 7806031, Labconco, Kansas-MO, USA) at our laboratory.

Figure 2.2. Soil sampling. **A)** Soil profile removed from the mangrove site and marked each 5 cm. **B)** Two plastic cups into the 5 cm wide soil layer to soil sampling. **C)** Closed and filled with soil samples plastic cups were placed in the box filled with liquid nitrogen immediately after collected.

XRF Analysis: The lyophilized soil samples were ground, sieved (100 mesh), pressed into a pellet (6 t cm^{-2}, by 1 min dwell time) and analyzed in a Microprobe X-ray Fluorescence Energy Dispersive Spectrometer (µEDX 1300, Shimadzu, Kyoto, Japan). This XRF device is able to detect only chemical elements with atomic number greater than 10 (Mg to U). The total elemental quantification was performed using the Fundamental Parameters (FP) Method, using oxygen to mass balance elements in FP quantitative method calculation (ALVES et al., 2015). We used the five following certified soil reference materials to determine the sensitivity coefficients of FP method: SS1 and SS2 from SCP Science and 2709a, 2710a, and 2711a from NIST. The µEDX has a small beam, the elemental quantification represents an average of 400 points (1 s for each point) distributed into a rectangle area of the surface of the soil pellets. The Rh tube parameters were 50 keV of voltage and 100 µA of current. The dead time of Si(Li) detector varied from 20 to 25 % and the fluorescence intensities were normalized by real time and current (cps μA^{-1}) before transformation into concentration units using the FP method. The detectable elements were considered those with a net peak intensity that was seven times the root square of the background ($Net\ Peak > 7 \times \sqrt{BG}$), as determined by the µEDX software.

S K-Edge XANES Spectroscopy: The lyophilized soil samples were analyzed on the SXS beamline at the Brazilian Synchrotron Light Laboratory (LNLS), Campinas, São Paulo state, Brazil (ABBATE et al., 1999). All XANES spectra were acquired in fluorescence mode using a silicon drift detector (SuperFast SDD, AMPTEK, Bedford-MA, USA). The incident photon energy was selected by a Si(111) double-crystal monochromator with a 0.6 x 1.2 mm (FWHM) beam size. The monochromator energy calibration was performed using metallic Mo (Mo L_3-edge, 2520 eV) and calibration was checked each 12 h with a pyrite standard calibrated against Mo. All samples and standards were spread onto S-free, double-sided carbon tape and mounted onto a stainless steel sample holder. The sample was aligned at 45° incident angle to the incoming beam with the detector placed within the horizontal plane at 90° from the incoming beam to reduce the elastic scattering background (horizontal polarization from bending magnet). The measurements were performed under low vacuum (~$5x10^{-7}$ mbar). Each XANES spectrum comprised 233 points collected at the following energy steps: 1) Pre-Edge = 2440 to 2467 eV, 1 eV step; 2) Edge = 2468 to 2486 eV, 0.2 eV step; 3) Post- Edge = 2487 to 2600 eV, 1 eV step. The dwell time at each point (energy) was 1 s (8 min for the whole spectra), and at least three spectra were collected by each sample or standard.

XANES Spectra Processing: The collected spectra were initially processed with the program Athena of the Demeter software package (RAVEL & NEWVILLE, 2005). In the Athena software, we determined the E_0 (2471 eV for reduced S species) of all raw spectra by the zero crossing of the second derivative. All spectra of the same sample/standard were examined visually to remove any glitches, and to check for general quality before merging to diminish noise. The merged spectra were exported as ".xmu" from Athena and further processing was performed using statistical software R 3.3.2 (CORE, 2017) with the "LCF v. 1.6-6" package (WERNER, 2017).

We utilized the "LCF" package in the R software according to the protocol described by Werner & Prietzel (2015) to perform the linear combination fitting of spectra of standards and samples spectra. The merged soil-sample spectra were initially linearly baseline-corrected from −30 to −15 eV and normalized and

flattened to an absorption (edge-step) of 1 from 28 to 128 eV with respect to E_0. The combination of all possible baseline correction and edge-step normalization parameters using R code resulted in 10,044 baseline corrected and edge-step-normalized sample spectra. The parameter "param.float" in the LCF package was configured as: 1) First range of Pre-edge = -25 to -22, each 1 eV; 2) Second range of Pre-edge = -16 to -14, each 1 eV; 3) First range of Post-edge = 15 to 60, each 1.5 eV; 4) Second range of Post-edge = 60 to 100, each 1.5 eV.

Part of the standards used was analyzed in the SXS beamline at LNLS and part was downloaded from the ESRF database (FACILITY, 2017). The best-chosen fit from the LCF analysis was the one showing the lowest R factor (from 0.9 to 5.6 x 10^{-3}). All graphs were generated in the R 3.3.2 (CORE, 2017), using the "Graphics" v. 3.4.1 (CORE, 2017) package.

Eh, pH, and EC Measurements: A 10 cm^3 subsample of lyophilized soil material was mixed for 1 min in a plastic cup with 25 mL distilled water. After 1 h of equilibrium time between soil and water, they were mixed to form a homogeneous suspension. Eh and pH were measured simultaneously with combination electrodes of Ag/AgCl with glass for pH and Ag/AgCl with Pt-ring electrode for Eh (model HI98121, Hanna Instruments, Rhode Island, EUA). The soil solution electrical conductivity (EC) was measured by a benchtop conductivity meter (model CD12, BEL Engineering®, Monza, Italy) in the same soil suspensions used for Eh and pH measurements.

2.4. Results

XRF Spectrometry: The chemical elements that were detected by XRF analysis in each layer of the soil sample are indicated in Figure S2.1. We selected 10 chemical elements to assess their distribution in the soil depth (Figure 2.3). The total profile average of S content was greater in P1 (3.4 ± 0.8%) than in P2 (2.3 ± 0.5%). In P2, the highest S content was in the 20-25 cm layer (3.2%), and in P1 the highest S content was found in the 40-50 cm layer (5%). In both profiles, deeper layers showed lower S contents (23 g kg^{-1} in P1 and 17 g kg^{-1} in P2). Although Fe and S contents in P1 and P2 followed similar trends with depth (Figure 2.3, Table S2.1), Pearson correlations between S and Fe were not significant ($r = 0.21$, $p = 0.4$, Table S2.1).

The Br and Cl contents in the profiles are directly related to seawater influence in soil (ALCALÁ & CUSTODIO, 2008), and we found a high and significant linear correlation between both elements ($r = 0.92$, $p < 0.01$; Table S2.1). The Br and Cl contents at both sites decreased in deeper layers (Figure 2.3).

Site P2 had a greater content of K than site P1 (means of 6.5 ± 0.7 and 5 ± 0.7, respectively), and K content increased with soil depth in both profiles. Both Ca and Sr contents increased sharply with depth below 25 cm in P2, and these chemical elements were correlated in both profiles ($r = 0.99$ $p < 0.01$, Table S2.1). Trace amounts of As and Zn were found by XRF analysis, but their values were below the detection limit and were not presented. The chemical elements Ti (2 to 8 g kg^{-1}) and Zr (0.37 to 2.4g kg^{-1}) showed a large range of contents in both of the soil profiles, and both were positively correlated with Si content ($r > 0.6$, Table S2.1). Both Zr and Ti typically occur in sparingly soluble minerals in soils (e. g., zircon and rutile/anatase) and are often used as references for assessing gains and losses of other elements at different depths in a soil profile (JACKSON et al., 1953; STILES et al., 2003). In our case, the variations with depth might indicate variations in the mineralogical composition of the sediments deposited in the mangroves over time.

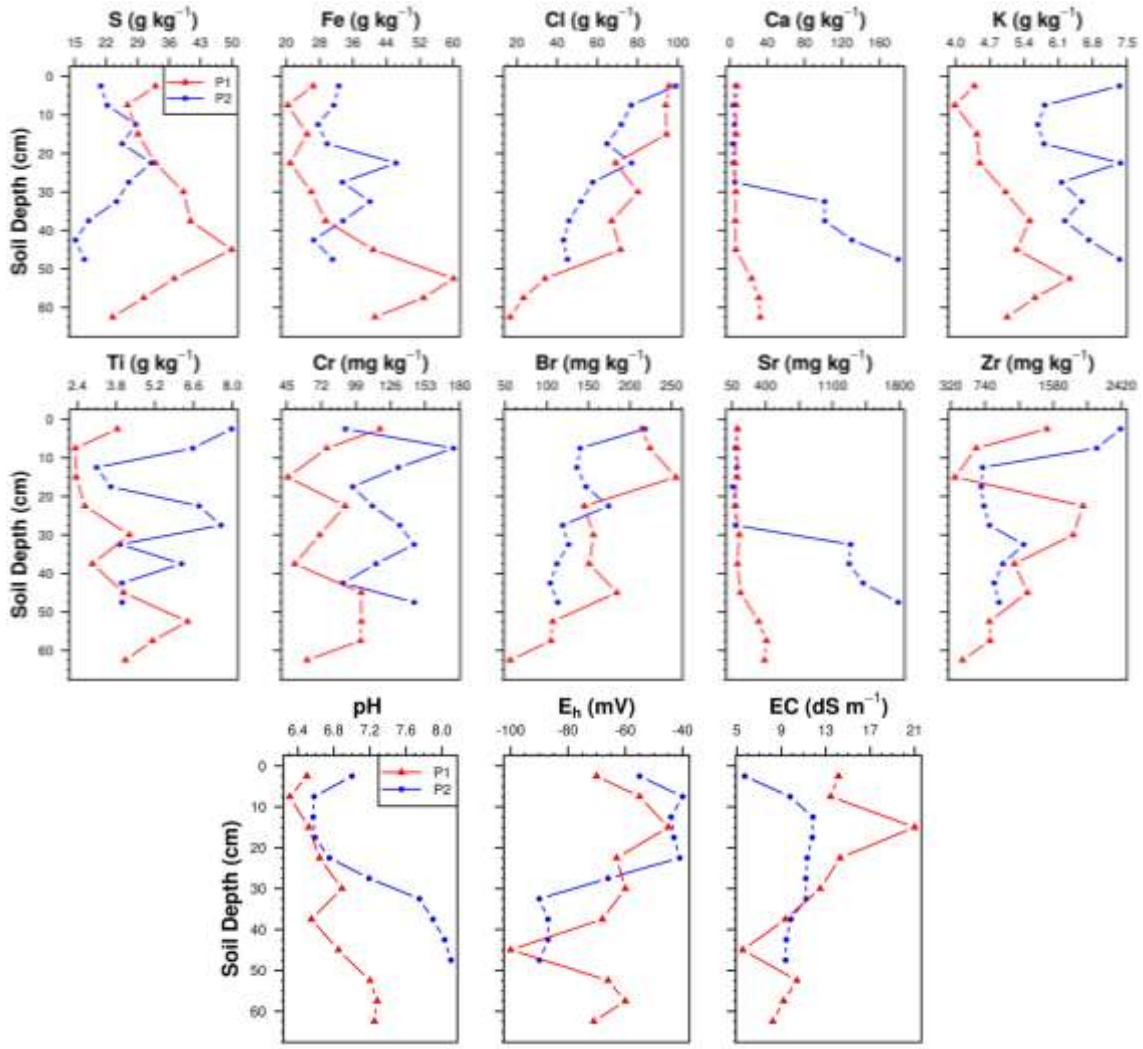

Figure 2.3. Chemical elemental content determined by XRF analysis with semi-quantitative method (based in Fundamental Parameters methods); and electrochemical values (pH, Eh and EC) of P1 (red) and P2 (blue) soil profiles in Tropical Brazilian mangrove.

S K-Edge XANES Spectrometry: Sulfur K-Edge XANES analysis showed the presence of both oxidized (S^{+6} at 2482 eV) and reduced (S^{-1}, and, S^{-0} at 2472 eV) S species in both mangrove sites, P1 and P2 (Figure 2.4). On average, spectra for the soil from the site near to the sea (P2) showed higher absorption intensity (higher peak) at 2482 eV than those of P1, indicating a greater SO_4^{2-} abundance in P2.

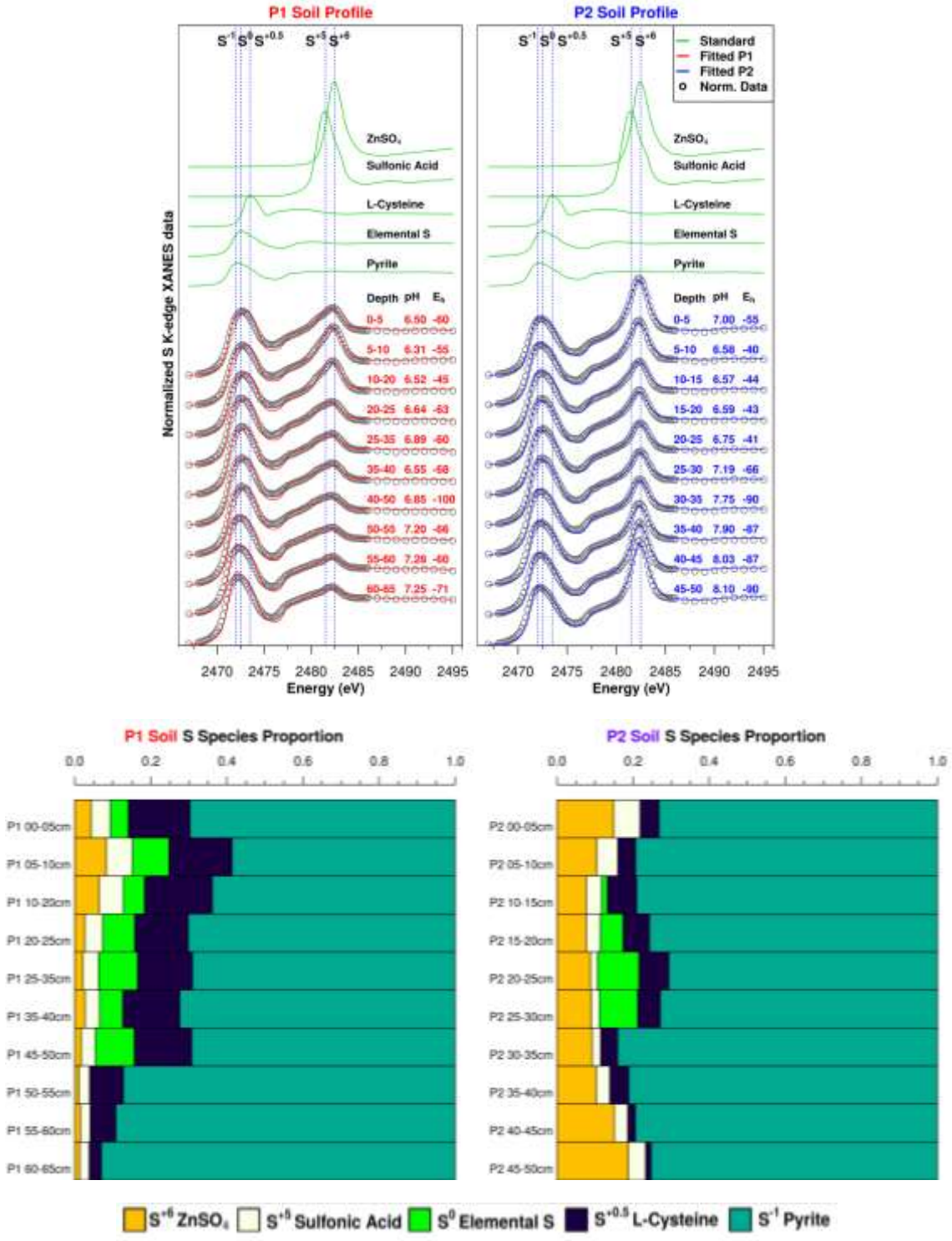

Figure 2.4. Combinations of five sulfur standards of different oxidation states yielding the best linear-combination fits to S K-edge XANES spectra of soil samples collected from Tropical Brazilian mangrove soil profiles in more degraded site near the ocean (P2); and in a better preserved and distant from the sea (P1).

Linear combination fitting (LCF) analysis indicated that SO_4^{2-} content decreased from 15% to 9% from 0 to 30 cm soil depth in P2, but increased again from 9 to 19% in deeper layers (30 to 50 cm). In P1, this effect was not observed, and the sulfate decreased from 4 to 1% from 0 to 65 cm of soil profile. LCF analysis also indicated that sulfide species, modeled as pyrite, composed on average 74 ± 11% and 77 ± 4% of total S across all depths in P1 and P2, respectively (Figure 2.4). Moreover, fits indicated that SO_4^{2-} species were more dominant in P2 (11 ± 4%) than in P1 (3 ± 2%). Elemental S (S^0) and organic S (S-org) were most abundant in the undisturbed mangrove site (P1). However, we did not identify S^0 in soil layers deeper than 50 cm in P1 and deeper than 35 cm in P2 (Figure 2.4). On average, the P1 S-org content was 13 ± 5% (0 to 65 cm) and the S^0 content was 8 ± 2% (0 to 50 cm). In P2 the average S-org content was 5 ± 2% (0 to 50 cm) and the S^0 content 4 ± 5% (0 to 35 cm).

2.5. Discussion

The higher Br and Cl content in upper soil layers can be related to organic chemical species (organohalogens compounds), naturally produced by microorganisms, algae and sponges presents in the estuarine environments (FAULKNER, 1980). The greater K content in P2 indicates the seawater influence. The increasing of Ca and Sr content in deeper layers is related to significant presences of shells fragments in these soil layers that were evident during field sampling and laboratory handling.

The S-org accumulation in P1 seems to be related to the more conservative state of P1 site or because the greater clay content of this soil favors preservation of organic matter compared to the sandy texture of P2 (SIX et al., 2002; BARRETO et al., 2016). The mangrove in which we sampled P1 also are had more exuberant vegetation (visually), which provides greater organic carbon inputs compare to a more degraded site (P2). Organic carbon inputs are directly linked to sulfur redox states, because the organic C is the main electron donor for SO_4^{2-} reduction to sulfides by microorganisms presents

in the mangrove soil at low Eh conditions (NEUBAUER et al., 2005; HAUSMANN et al., 2016).

Sulfide forms have a very important environmental in generating sparingly soluble solid-phase species (of low Ks) that immobilize toxics elements such as As, Cd, Co, Cu, Hg, Ni, Pb, and Zn, thereby diminishing bioaccumulation (ANKLEY, 1996; LUOMA & RAINBOW, 2005; CLAYDEN et al., 2017). LeMonte et al. (2017) verified that sea level rise potentially impacts As release from contaminated coastal soils by decreasing Eh, but they highlighted the importance of S in decreasing As mobilization into the water. Thus, the Eh increasing in estuarine environments can be more dangerous, because sulfide oxidation will decreases the soil pH and can release toxic trace elements to the system, and increasing the C emission by the microorganism's respiration (BURTON et al., 2011).

The predominance of pyrite formation, determined by XANES analysis (Figure 2.4), showed coupling of the biogeochemistry of S and Fe in these estuarine mangroves (TOBIAS & NEUBAUER, 2009). Pyrite formation is well known in diverse natural systems (MADIGAN et al., 2015; FIKE et al., 2016). We indentified framboidal pyrite in the silt fraction of our mangrove soil samples (ROCHA, 2016) by scanning electron microscopy (Figure 2.5). The formation of framboidal pyrite in mangrove soils is related to biotic process (RICKARD, 1975; ZHANG et al., 2014). For example, Rickard (1970) proposed biogenic models suggesting that framboid pyrite results from the replacement of an organic spherical globule or from a gaseous vacuole. However, it is important to mention that abiotic process can, also, forms framboidal pyrite (SAWLOWICZ, 1993; WILKIN & BARNES, 1997).

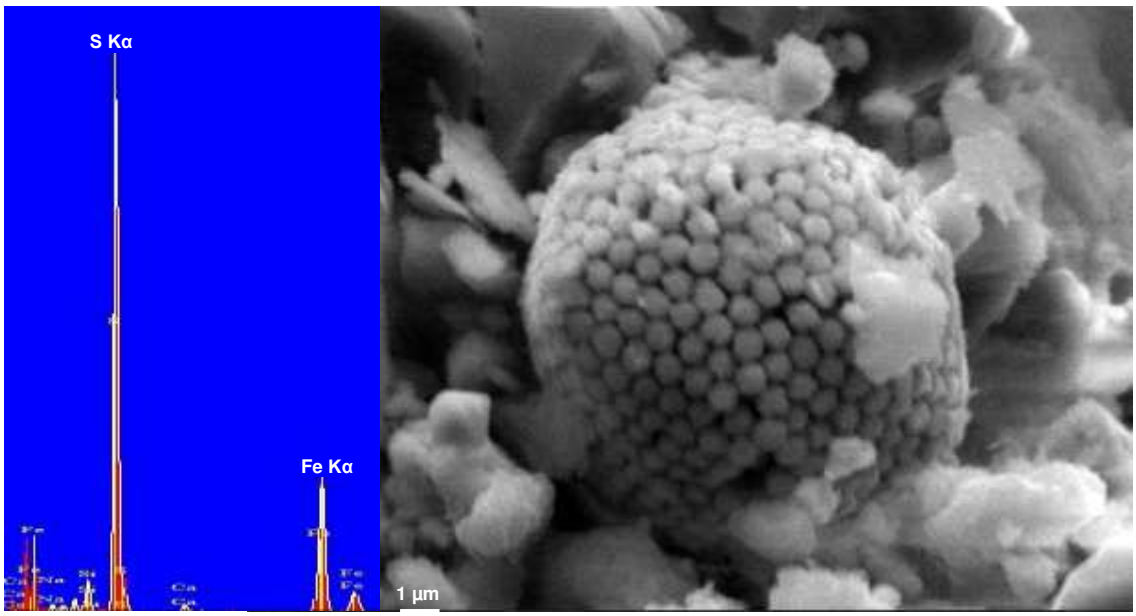

Figure 2.5. Scanning electron microscopy (SEM) image of framboidal pyrite found in the silt fraction of Tropical Brazilian mangrove soil, including energy-dispersive spectroscopy (EDS) results showing strong Fe Kα and S Kα fluorescence peaks that are characteristic of pyrite (ROCHA, 2016).

It is generally expected to find more reduced S species in deeper mangrove soil layers because of sulfate reduction under lower Eh conditions. Although both of our soil profiles showed ≥70% of S as reduced species (fitted as pyrite or L-cysteine) at all depths (Figure 2.4), the greater sulfate content throughout the P2 profile, which is within few meters from the sea, is hypothesized to be due to tidal-driven influxes of sulfate at rates exceeding that of sulfate reduction to sulfide rate (MORRIS, 1995). In P1, the greater accumulation of reduced S species (pyrite) in the deeper layers might be due to greater sulfate reduction rates forming insoluble sulfide species such as pyrite.

Insights on redox-driven S speciation can be gained from thermodynamic Eh-pH diagrams, although is unlikely that equilibrium is achieved in dynamic natural environments such as in mangrove soils (BROOKINS, 1988). The Eh and pH conditions measured in our field samples overlap with equilibrium conditions favoring formation of pyrite, HS^- and H_2S (Figure 2.6). Elemental sulfur, which was suggested by our XANES fitting analysis to constitute 5 – 10% of total S in profiles P1 and P2, is thermodynamically stable at lower pH (<5)

and greater Eh (50 to 300 mV) than was found in our soil samples (blue rectangle in Figure 2.6). But, conditions that are favorable for S^0 formation might be achieve during low tide by processes such as O_2 inputs from tree roots and bioturbation by crabs (FERREIRA et al., 2007) coupled with localized, acidic conditions generated by partial oxidation of H_2S or Fe(II).

Elemental S can be formed by abiotic process, where the H_2S oxidation generates unstable products as S^0, polisulfanes, sulfite and tiosulfates (MISHANINA et al., 2015). But, in mangrove soils the biotic process is predominant, as described by Behera et al. (2014), where they highlight the role of mangrove soil microorganisms in sulfides partial oxidation to S^0. Diverse groups of microorganisms act in this process, such as archaea, bacteria, fungi, and actinomycetes (RICKARD, 2012; MADIGAN et al., 2015; FIKE et al., 2016). Photoautotrophic microorganisms, as green and purples sulfur bacteria (*Chlorobium* and *Chromatium*), produce S^0 by CO_2 reduction under light (equation (1)). Heterotrophic and chemolithotrophic microorganisms, such as fungi *Aspergillus*, bacteria *Bacillus*, and actinomycetes, also oxidize sulfide species to S^0 (equation (2)). Other anaerobic chemolithotrophic microorganisms generate S^0 during the denitrification process, using NO_3^- as the final electron acceptor (equation (3)) (BEHERA et al., 2014; FIKE et al., 2016).

Thus, sulfide oxidation is coupled with biotic reduction of O_2, CO_2, or NO_3^- as energy source for chemolithotrophs or for autotrophic fixation of CO_2, and also for H_2S detoxification. In this process, S^0 can be accumulated as granules, inside or outside of microorganisms cells. The S^0 is stable when sulfides species are not limited in the system, and the S^0 can be oxidized to sulfate in low sulfides availability (MADIGAN et al., 2015; FIKE et al., 2016).

Therefore, the S^0 and S-org species found in our mangrove soil samples are directly linked with microbiology metabolisms of specific groups that are more abundant or activity in better preserved mangrove site, due to more organic carbon inputs and bioturbation process as root and crabs activities.

$$2H_2S + CO_2 \xrightarrow{\text{Light}} 2S^0 + CH_2O_{(carbohydrate)} + H_2O \quad (1)$$

$$H_2S + 0.5O_2 \rightarrow S^0 + H_2O \quad (2)$$

$$S^{2-} + 0.4NO_3^- + 2.4H^+ \rightarrow S^0 + 0.2N_2 + 1.2H_2O \quad (3)$$

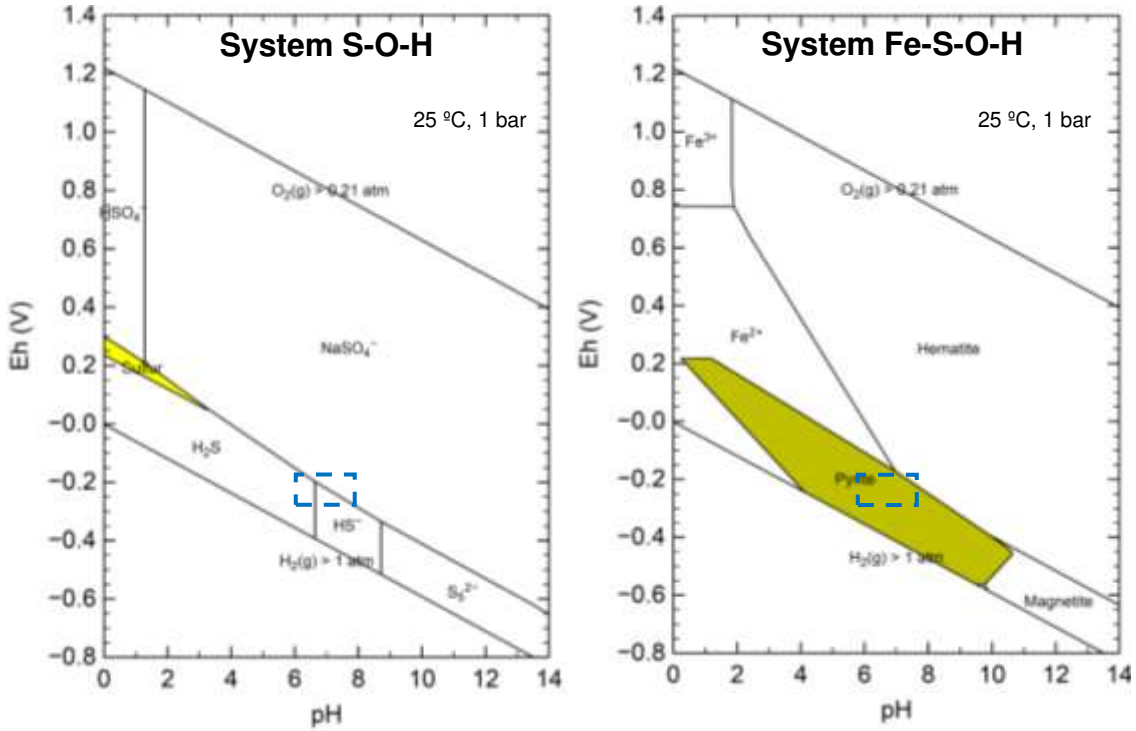

Figure 2.6. A) Eh-pH diagram of S in the system S-O-H, with S activity in solution of 1 mmol L^{-1}. B) Eh-pH diagram of Fe in the system Fe-S-O-H, with Fe activity in solution of 1 µmol L^{-1} and S activity of 1 mmol L^{-1}. Blue rectangle is the maximum and minimum pH and Eh values encountered in the mangrove soil samples. The stability field of elemental S and Pyrite are highlighted. These diagrams were made in the PhreePlot software (KINNIBURGH & COOPER, 2011; PARKHURST & APPELO, 2013).

2.6. Conclusions

A combination of XRF and S K-edge XANES spectroscopy of Tropical Brazilian mangrove soil profiles revealed basic information about chemical dynamics in mangrove ecosystems. We determined different chemical elements (Al, Br, Ca, Cl, Fe, K, S, Si, Sr, Ti, and Zr) content in soil profiles that are influenced by site preservation state and seawater. Our results demonstrated that sulfur chemical species depend on mangrove position, condition, and soil depth, which influence the Eh-pH, carbon input, and microbiological activity. The success of sulfur speciation in flooded environments was based on sampling and analysis protocols that were intended to avoid sample oxidation. The SO_4^{2-} occurrence in deeper mangrove soil layers is related the seawater influence, the main S source to this ecosystem. The higher content of organic forms of S and elemental S indicated by XANES fitting could be related to greater microbial activity in this finer-textured, more organic-mattter rich mangrove profile. Here, we demonstrated that the S K-edge XANES spectroscopy assessments is a powerful tool to better understanding of environmental quality and dynamics of tropical estuarine environments.

2.7. References

ABBATE, M.; VICENTIN, F. C.; COMPAGNON-CAILHOL, V.; ROCHA, M. C.; TOLENTINO, H. The soft X-ray spectroscopy beamline at the LNLS: technical description and commissioning results. **Journal of Synchrotron Radiation**, v. 6, n. 5, p. 964-972, 1999.

ALCALÁ, F. J.; CUSTODIO, E. Using the Cl/Br ratio as a tracer to identify the origin of salinity in aquifers in Spain and Portugal. **Journal of Hydrology**, v. 359, n. 1, p. 189-207, 2008.

ALVARES, C. A.; STAPE, J. L.; SENTELHAS, P. C.; GONÇALVES, J. L. M.; SPAROVEK, G. Köppen's climate classification map for Brazil. **Meteorologische Zeitschrift**, v. 22, n. 6, p. 711-728, 2013.

ALVES, E. E. N.; COSTA, L. M.; ROCHA, P. A.; BITTENCOURT, S. F. E.; FARIA, A. L. L. D.; SCHAEFER, C. E. G. R. Utilização do μ-EDX para determinação de elementos químicos marcadores de metamorfismo em saprolitos de contato. In: III Simpósio Mineiro de Ciência do Solo, 2015, Viçosa: Grupo de Estudos de Fertilizantes da Universidade Federal de Viçosa, p. 31-33.

ANKLEY, G. T. Evaluation of metal/acid-volatile sulfide relationships in the prediction of metal bioaccumulation by benthic macroinvertebrates. **Environmental Toxicology and Chemistry**, v. 15, n. 12, p. 2138-2146, 1996.

BARRETO, M. B.; LO MONACO, S.; DIAZ, R.; BARRETO-PITTOL, E.; LOPEZ, L.; PERALBA, M. D. C. R. Soil organic carbon of mangrove forests (Rhizophora and Avicennia) of the Venezuelan Caribbean coast. **Organic Geochemistry**, v. 100, n. Supplement C, p. 51-61, 2016.

BEHERA, B.; MISHRA, R.; DUTTA, S.; THATOI, H. Sulphur oxidising bacteria in mangrove ecosystem: A review. **African Journal of Biotechnology**, v. 13, n. 29, p. 2897-2907, 2014.

BROOKINS, D. G. **Eh-pH Diagrams for Geochemistry**. Berlin: Springer-Verlag Berlin Heidelberg, 1988

BURTON, E. D.; BUSH, R. T.; JOHNSTON, S. G.; SULLIVAN, L. A.; KEENE, A. F. Sulfur biogeochemical cycling and novel Fe-S mineralization pathways in a tidally re-flooded wetland. **Geochimica et Cosmochimica Acta**, v. 75, n. 12, p. 3434-3451, 2011.

CLAYDEN, M. G.; LESCORD, G. L.; KIDD, K. A.; WANG, X.; MUIR, D. C. G.; O'DRISCOLL, N. J. Using sulfur stable isotopes to assess mercury bioaccumulation and biomagnification in temperate lake food webs. **Environmental Toxicology and Chemistry**, v. 36, n. 3, p. 661-670, 2017.

CORE, R. T. R: A Language and Environment for Statistical Computing. **R Foundation for Statistical Computing,** v. 3.4.2, 2017. Available in: <https://www.R-project.org/>. Accessed in: 10/10/2017.

DIEGUES, A. C. S. A. **Povos e Águas: inventário de áreas úmidas brasileiras**. São Paulo: NUPAUB-USP, 2002

FACILITY, E. S. R. **European Synchrotron Radiation Facility**, 2017. 2017.

FAULKNER, D. J. Natural Organohalogen Compounds. In: Hutzinger, O. (Ed.). **The Natural Environment and the Biogeochemical Cycles**. Berlin: Springer-Verlag Berlin Heidelberg, 1980, p.229-254. (The Handbook of Environmental Chemistry)

FERREIRA, T. O.; OTERO, X. L.; VIDAL-TORRADO, P.; MACIAS, F. Redox Processes in Mangrove Soils under Rhizophora mangle in Relation to Different Environmental Conditions. **Soil Science Society of America Journal**, v. 71, n. 2, p. 484-491, 2007.

FIKE, D. A.; BRADLEY, A. S.; LEAVITT, W. D. Geomicrobiology of Sulfur. In: Ehrlich, H. L., Newman, D. K.*, et al* (Ed.). **Ehrlich's Geomicrobiology**. Boca Raton: CRC Press 2016, p.479-515.

GOMES, F. H.; KER, J. C.; FERREIRA, T. O.; MOREAU, A. M. S. S.; MOREAU, M. S. Characterization and pedogenesis of mangrove soils from Ilhéus-BA, Brazil. **Revista Ciência Agronômica**, v. 47, p. 599-608, 2016.

HAUSMANN, B.; KNORR, K.-H.; SCHRECK, K.; TRINGE, S. G.; GLAVINA DEL RIO, T.; LOY, A.; PESTER, M. Consortia of low-abundance bacteria drive sulfate reduction-dependent degradation of fermentation products in peat soil microcosms. **The ISME Journal**, v. 10, n. 10, p. 2365-2375, 2016.

HESTERBERG, D.; DUFF, M. C.; DIXON, J. B.; VEPRASKAS, M. J. X-ray Microspectroscopy and Chemical Reactions in Soil Microsites **Journal of Environmental Quality**, v. 40, n. 3, p. 667-678, 2011.

HOSSAIN, M. D.; NURUDDIN, A. A. Soil and Mangrove: A Review. **Journal of Environmental Science and Technology**, v. 9, n. 2, p. 198-207, 2016.

JACKSON, M. L.; SHERMAN, G. D.; NORMAN, A. G. Chemical Weathering of Minerals in Soils. In: (Ed.). **Advances in Agronomy**: Academic Press, 1953. v.5, p.219-318.

KINNIBURGH, D. G.; COOPER, D. M. **PhreePlot – Creating graphical output with PHREEQC**. Gwynedd, UK, 2011.

LEMONTE, J. J.; STUCKEY, J. W.; SANCHEZ, J. Z.; TAPPERO, R.; RINKLEBE, J. R.; SPARKS, D. L. Sea Level Rise Induced Arsenic Release from Historically Contaminated Coastal Soils. **Environmental Science & Technology**, v. 51, n. 11, p. 5913-5922, 2017.

LUOMA, S. N.; RAINBOW, P. S. Why Is Metal Bioaccumulation So Variable? Biodynamics as a Unifying Concept. **Environmental Science & Technology**, v. 39, n. 7, p. 1921-1931, 2005.

MADIGAN, M. T.; MARTINKO, J. M.; BENDER, K. S.; BUCKELEY, D. H.; STAHL, D. A. **Brock Biology of Microorganisms**. San Francisco: Pearson Benjamin-Cummings, 2015. 1006 p.

MISHANINA, T. V.; LIBIAD, M.; BANERJEE, R. Biogenesis of reactive sulfur species for signaling by hydrogen sulfide oxidation pathways. **Nature Chemical Biology**, v. 11, p. 457–464, 2015.

MORRIS, J. T. The salt and water balance of intertidal sediments: results from North Inlet, South Carolina. **Estuaries**, v. 18, n. 4, p. 556–567, 1995.

NEUBAUER, S. C.; GIVLER, K.; VALENTINE, S.; MEGONIGAL, J. P. Seasonal patterns and plant-mediated controls of subsurface wetland biogeochemistry. **Ecology**, v. 86, n. 12, p. 3334-3344, 2005.

PARKHURST, D. L.; APPELO, C. A. J. Description of input and examples for PHREEQC version 3 — A computer program for speciation, batch-reaction, one-dimensional transport, and inverse geochemical calculations
In: (Ed.). **U.S. Geological Survey Techniques and Methods**, 2013. v.6, p.497.

RAVEL, B.; NEWVILLE, M. ATHENA, ARTEMIS, HEPHAESTUS: data analysis for X-ray absorption spectroscopy using IFEFFIT. **Journal of Synchrotron Radiation**, v. 12, n. 4, p. 537-541, 2005.

RICKARD, D. **Sulfidic sediments and sedimentary rocks**. Amsterdam: Elsevier, 2012. 801 p.

RICKARD, D. T. The origin of framboids. **Lithos**, v. 3, n. 3, p. 269-293, 1970.

RICKARD, D. T. Kinetics and mechanism of pyrite formation at low temperatures. **American Journal of Science**, v. 275, n. 6, p. 636-652, 1975.

ROBERTSON, A. I.; ALONGI, D. M. **Tropical Mangrove Ecosystems**. Washington: American Geophysical Union, 1992, v.41 (Coastal and Estuarine Studies)

ROCHA, P. A. **Solos do manguezal da Baía de Guarapari – ES: mineralogia e fósforo como indicador de contaminação por esgoto doméstico**. Departamento de Solos, Universidade Federal de Viçosa, Viçosa, 2016. xi, 90p.

SAINT-PAUL, U.; SCHNEIDER, H. **Mangrove Dynamics and Management in North Brazil**. Berlin: Springer-Verlag Berlin Heidelberg, 2010, v.211 (Ecological Studies, Analysis and Synthesis)

SAWLOWICZ, Z. Pyrite framboids and their development: a new conceptual mechanism. **Geologische Rundschau**, v. 82, n. 1, p. 148-156, 1993.

SIX, J.; CONANT, R. T.; PAUL, E. A.; PAUSTIAN, K. Stabilization mechanisms of soil organic matter: Implications for C-saturation of soils. **Plant and Soil**, v. 241, n. 2, p. 155-176, 2002.

STILES, C. A.; MORA, C. I.; DRIESE, S. G. Pedogenic processes and domain boundaries in a Vertisol climosequence: evidence from titanium and zirconium distribution and morphology. **Geoderma**, v. 116, n. 3, p. 279-299, 2003.

TOBIAS, C.; NEUBAUER, S. C. Salt Marsh Biogeochemistry – An Overview. In: Perillo, G. M. E., Wolanski, E.*, et al* (Ed.). **Coastal wetlands: an integrated ecosystem approach**. Amsterdam: Elsevier B.V., 2009, p.445-492.

WERNER, F.; PRIETZEL, J. Standard Protocol and Quality Assessment of Soil Phosphorus Speciation by P K-Edge XANES Spectroscopy. **Environmental Science & Technology**, v. 49, n. 17, p. 10521-10528, 2015.

WERNER, F. LCF: Linear Combination Fitting R package. v. 1.7, 2017. Available in: <https://CRAN.R-project.org/package=LCF>. Accessed in: 01/10/2018.

WILKIN, R. T.; BARNES, H. L. Formation processes of framboidal pyrite. **Geochimica et Cosmochimica Acta**, v. 61, n. 2, p. 323-339, 1997.

WOODROFFE, C. D.; GRINDROD, J. Mangrove Biogeography: The Role of Quaternary Environmental and Sea-Level Change. **Journal of Biogeography**, v. 18, n. 5, p. 479-492, 1991.

ZHANG, M.; KONISHI, H.; XU, H.; SUN, X.; LU, H.; WU, D.; WU, N. Morphology and formation mechanism of pyrite induced by the anaerobic oxidation of methane from the continental slope of the NE South China Sea. **Journal of Asian Earth Sciences**, v. 92, n. Supplement C, p. 293-301, 2014.

2.8. Supporting Information for Chapter II

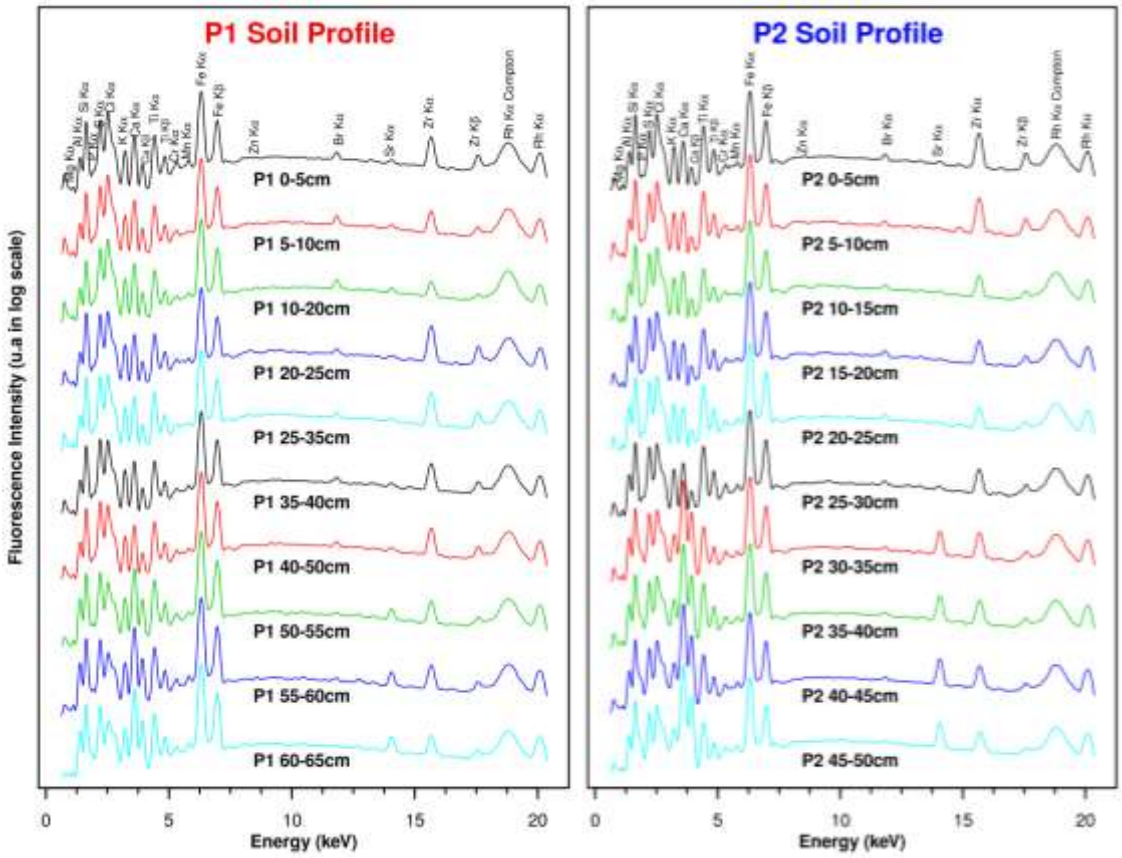

Figure S2.1. XRF spectra obtained from the ten layers of each soil profile sample collected in an undisturbed far from the beach area (P1, left) and in a near to the beach contaminated mangrove site (P2, right). X-ray fluorescence lines are indicated for those peaks with net intensity greater than $7\times\sqrt{\text{BG Intensity}}$.

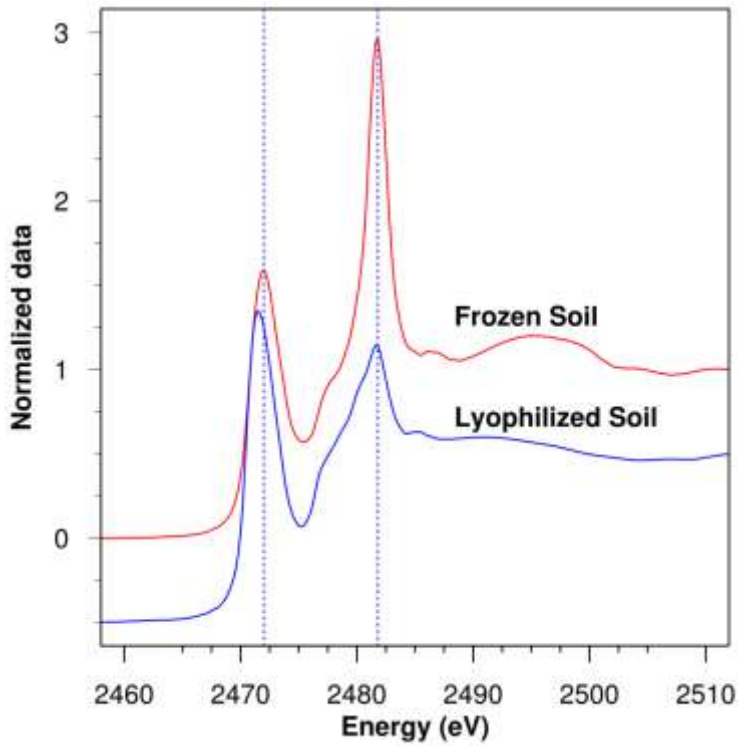

Figure S2.2. Results of the preliminary test performed before our soil sample analysis. S K-edge XANES of the same soil sample in two different conditions of sample preparation: Frozen (Red line) and Lyophilized Soil (Blue line) samples. The sample mounting process is described in Figure S2.3. The Frozen Soil showed a more intense S^{+6} peak than the Lyophilized Soil, meaning that this sample was oxidized during the sample preparation process. These results allowed us to choose the best way to prepare and to keep our samples in order to proceed with S speciation.

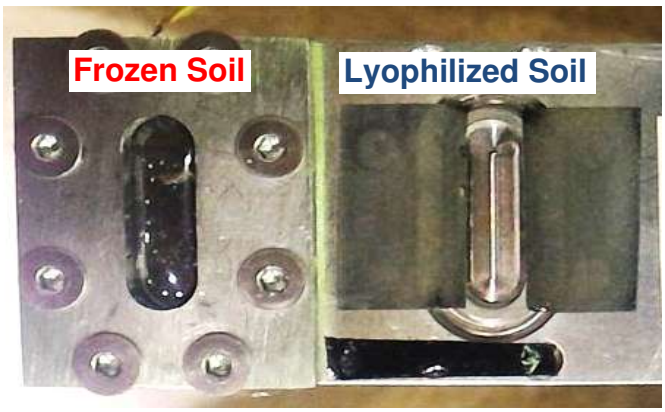

Figure S2.3. Soil samples mounted in the sample holder in our preliminary test: 1) Frozen Soil sample, that thawed at room temperature and was exposed to the atmospheric air for 15 min during the mounting process, and it was covered by 4 µm thin Ultralene® film. It is possible to see that Ultralene® film is inflated due to gas produced during the microorganisms oxidation process 2) Lyophilized Soil sample distributed on carbon S-free double face tape mounted to a stainless steel sample holder.

Table S2.1. Pearson correlation coefficient (below diagonal) and p-values (above diagonal) obtained between chemical elements content, determined by the XRF spectrometer in the mangrove soil profiles.

	S	Fe	Cl	Si	Al	Mg	P	Ca	K	Ti	Zr	Sr	Br
S	-	0.38	0.37	0.64	0.67	0.79	0.03	0.01	0.07	0.40	0.74	0.01	0.24
Fe	0.21	-	0.01	0.37	0.00	0.25	0.57	0.90	0.07	0.02	0.33	0.77	0.06
Cl	0.21	-0.60	-	0.86	0.00	0.01	0.64	0.03	0.22	0.62	0.07	0.02	0.00
Si	-0.11	0.21	0.042	-	0.10	0.12	0.16	0.75	0.01	0.00	0.00	0.74	0.38
Al	-0.10	0.89	-0.63	0.38	-	0.73	0.70	0.81	0.01	0.00	0.36	0.70	0.01
Mg	0.06	-0.27	0.54	0.36	-0.08	-	0.20	0.01	0.94	0.31	0.08	0.01	0.07
P	0.49	0.14	0.11	0.33	0.09	0.30	-	0.01	0.77	0.58	0.75	0.00	0.94
Ca	-0.60	0.03	-0.49	-0.08	0.06	-0.55	-0.56	-	0.02	0.88	0.46	0.00	0.05
K	-0.42	0.42	-0.29	0.58	0.56	-0.02	-0.07	0.5	-	0.00	0.76	0.02	0.13
Ti	-0.42	0.51	-0.12	0.63	0.62	0.24	0.13	-0.04	0.65	-	0.20	0.95	0.40
Zr	-0.20	-0.23	0.41	0.61	-0.21	0.40	0.08	-0.18	0.07	0.30	-	0.47	0.37
Sr	-0.58	0.07	-0.51	-0.08	0.09	-0.58	-0.61	0.99	0.50	-0.02	-0.17	-	0.04
Br	0.27	-0.43	0.92	-0.21	-0.54	0.42	0.02	-0.45	-0.35	-0.20	0.21	-0.46	-

In below diagonal, non-colored values means that the variables have not significant Pearson correlation ($p>0.1$); red and blue color means that the variables are inversely or directly correlated ($p<0.1$), respectively. In above diagonal, p-values less than 0.1 are in blue, meaning significant Pearson correlation coefficient.

Table S2.2. Linear Combination Fitting results of S K-edge XANES spectra from P1 and P2 soil profiles. Values in %.

P1 Soil Profile										
Standard	**00-05 cm**	**05-10 cm**	**10-20 cm**	**20-25 cm**	**25-35 cm**	**35-40 cm**	**45-50 cm**	**50-55 cm**	**55-60 cm**	**60-65 cm**
S^{+6} $ZnSO_4$	4 ± 1	8 ± 1	6 ± 0.4	3 ± 0.4	2 ± 0.3	3 ± 0.3	2 ± 1	1 ± 1	2 ± 1	1 ± 1
S^{+5} Anth Sulf Acid	5 ± 1	7 ± 1	6 ± 0.4	5 ± 0.4	4 ± 0.3	4 ± 0.3	3.7 ± 1	3 ± 1	3 ± 1	3 ± 1
S^{0} Elemental S	5 ± 4	10 ± 5	6 ± 4	8 ± 4	10 ± 3	6 ± 3	10 ± 6	0 ± 5	0 ± 5	0 ± 5
S^{-1} LCysteine	16 ± 1	17 ± 2	18 ± 1	14 ± 1	14 ± 0.9	15 ± 1	15 ± 2	9 ± 2	7 ± 1	3 ± 1
S^{-1} FeS_2 Pyrite	70 ± 4	59 ± 4	64 ± 3	70 ± 3	69 ± 2	72 ± 2.5	69 ± 5	87 ± 4	89 ± 4	93 ± 4
R.factor	0.00259	0.00234	0.00281	0.00237	0.00246	0.00258	0.00243	0.00329	0.00446	0.00567
pre.adj.1	-22	-22	-22	-22	-22	-22	-22	-22	-22	-22
pre.adj.2	-14	-14	-14	-14	-14	-14	-14	-14	-14	-14
post.adj.1	59	57	57	57	57	60	58	57	59	60
post.adj.2	68	69	67	78	66	68	67	76	71	92

P2 Soil Profile										
Standard	**00-05 cm**	**05-10 cm**	**10-15 cm**	**15-20 cm**	**20-25 cm**	**25-30 cm**	**30-35 cm**	**35-40 cm**	**40-45 cm**	**45-50 cm**
S^{+6} $ZnSO_4$	15 ± 1	11 ± 1	8 ± 1	8 ± 1	9 ± 1	9 ± 1	9 ± 1	10 ± 1	15 ± 1	19 ± 1
S^{+5} Anth Sulf Acid	7 ± 1	5 ± 1	4 ± 1	4 ± 1	2 ± 1	2 ± 1	2 ± 1	4 ± 1	4 ± 1	5 ± 1
S^{0} Elemental S	0 ± 5	0 ± 5	2 ± 5	6 ± 4	11 ± 4	10 ± 5	0 ± 4	0 ± 5	0 ± 6	0 ± 7
S^{-1} LCysteine	5 ± 1	5 ± 1	8 ± 2	7 ± 1	8 ± 1	6 ± 1	5 ± 1	5 ± 2	2 ± 2	1 ± 2
S^{-1} FeS_2 Pyrite	73 ± 4	79 ± 4	79 ± 4	76 ± 4	71 ± 4	73 ± 4	84 ± 4	81 ± 4	80 ± 5	75 ± 6
R.factor	0.00208	0.00293	0.00223	0.00166	0.00093	0.00107	0.00273	0.00334	0.0025	0.00258
pre.adj.1	-23	-22	-22	-23	-22	-22	-22	-22	-22	-22
pre.adj.2	-14	-16	-16	-14	-14	-14	-14	-14	-14	-14
post.adj.1	58	57	60	59	60	60	60	58	60	60
post.adj.2	68	76	91	71	92	88	68	68	69	67

P1: Well conserved, far from the sea, far from the urban area, and more clay soil. **P2**: Contaminated area with domestic sludge disposal, near to the sea, near to urban area, and more sand soil.

CHAPTER III

TENDER X-RAY SYNCHROTRON RADIATION DAMAGE IN ENVIRONMENTAL SAMPLES DURING SULFUR SPECIATION

3.1. Abstract

Radiation damage is a limiting factor during XANES studies, because the result obtained will not represent the natural condition of the sample. Thus, we evaluated the effect of tender X-ray radiation (2.4-2.6 keV) in the sulfur species present in environmental samples under cryo-temperature (115±5 K) to minimize the radiation-damage during S K-edge XANES analysis. We performed six sequential S K-edge XANES (2.4 to 2.6 keV) in pure standards (S_8 and $FeSO_4.7H_2O$), environmental samples (Pyrite, Frozen and Lyophilized Mangrove Soil), and a mixture of S_8 + Starch. Tender X-ray synchrotron radiation-damage resulted in the reduction of sulfur only in the carbon rich sample (S_8 + Starch). The cold finger at 115 K was effective in minimize the radiation-damage. Thus, it is recommended to use the cold finger during the S K-edge XANES data for those samples that are rich in organic carbon for environmental studies. Powder samples are recommended (as lyophilized soil) because they are simpler to mount, for obtain more homogenous sample, and to avoid analyze gaseous sulfur species, which is important when the objective is to study only the solid state phases in the sample.

3.2. Introduction

Synchrotron radiation has high photon flux, showing an excellent potential for application in environmental and biological analysis (MAJUMDAR et al., 2012; CASTILLO-MICHEL et al., 2016). However, the high photon flux can also promote radiation damage in the sample. Radiation damage refers to any alteration in the specimen due to ionizing radiation interaction, which can be associated to biological, physical or chemical process, as the mutations, mass

losses, and crystalline or speciation changes (BEETZ & JACOBSEN, 2003; MA et al., 2012; MAJUMDAR et al., 2012; JEFFRIES et al., 2015).

Several studies were performed to understand and mitigate radiation damage in macromolecular crystallography studies (GARMAN & NAVE, 2002; GARMAN & WEIK, 2017). Due to the importance of this topic the *Journal of Synchrotron Radiation* published eight special issues about radiation damage, between 2002 and 2017 (GARMAN & WEIK, 2017). With the evolution of the new fourth-generation synchrotron facilities, the synchrotron light will be more brightness, coherent, and focused. Thus, is expected that radiation damage process also increases, manly in biological or environmental studies.

Beyond crystallography, radiation damage must be avoided in X-Ray Absorption Near Edge Structure (XANES) studies, otherwise the XANES data will contain artifacts, and will not represent the natural condition of the sample. Castillo-Michel et al. (2016) highlighted studies in life sciences where organic S species were reduced by radiation damage. In these cases, mechanisms to avoid radiation damage must be applied, e.g. by changing the sample chamber atmosphere (He or vacuum) to avoid air-O_2 presence; by decreasing the income photon flux; or by sample cooling to cryogenic temperatures (~110 K) using liquid N_2, which have been used with success in some sample conditions (GARMAN & WEIK, 2015; CASTILLO-MICHEL et al., 2016; GARMAN & WEIK, 2017).

Thus, we aim to evaluate the tender X-ray synchrotron radiation damage in environmental samples at cryogenic and room temperatures, during S K-edge XANES spectroscopy (2.4-2.6 keV). We hypothesize that sulfur species are altered by reduction-oxidation (redox) reaction between the organic compounds of the sample induced by the X-ray beam and that cryo-temperatures minimize this radiation damage. Thus, our goal is to provide information for future tender X-ray synchrotron-based studies related to S speciation in environmental samples.

3.3. Materials and Methods

Sample selection and preparation: To evaluate the sulfur species stability in different kind of samples we selected two sulfur standards, two environmental samples, and one mixture of starch and elemental sulfur. The standards were elemental sulfur (S_8, Sigma-Aldrich, PA 99.5 %) and the ferrous sulfate heptahydrate ($FeSO_4.7H_2O$, Vetec, PA 99.9%). The first environmental sample was the pyrite which was extracted from geological collection at Federal University of Viçosa, Viçosa-MG, Brazil. The second environmental sample was a soil sample (S-rich) collected from the 60-65 cm soil layer depth in mangrove area (water-saturated and under reduction condition), located in Guarapari, Espírito Santo, Brazil. The soil sample was frozen in liquid nitrogen (77 K) during field sampling, to avoid its oxidation by microbiological process. The soil sample was kept frozen during transport and half part was lyophilized in a FreeZone Bulk Tray Dryer (model 7806031, Labconco, Kansas, MO) at laboratory.

The elemental S and starch were mixed in the 1:100 mass ratio. This mixture was performed to simulate sample with high carbon content (as plants, organic fraction of soils, and animal tissues) and with both oxidized and reduced sulfur species, where would possible to occur redox reactions between C and S species, mediated by the income synchrotron X-ray radiation.

The frozen soil sample was prepared into the inert gas sealed container (N_2 glovebox), and it was mounted into an eppendorf® cap with 50 mm of diameter covered with the 4 µm thick Ultralene® film. A plastic ring of the same eppendorf® vial was used to isolate the frozen soil and to fix the Ultralene® film.

S K-edge XANES spectroscopy: All samples were analyzed on the SXS beamline at Brazilian Synchrotron Light Laboratory (LNLS), Campinas city, São Paulo state, Brazil (ABBATE et al., 1999). The S K-edge XANES spectra were acquired in fluorescence mode (SuperFast SDD, AMPTEK, Bedford-MA, USA). The incident photon energy was selected by a Si(111) double-crystal monochromator with a 0.6 (H) x 1.2 mm (V) (FWHM) beam size. The monochromator energy calibration was performed by metallic Mo (Mo L_3-edge,

2520 eV) and calibration was checked each 12 h with pyrite sample, which was stable.

The powder samples (S_8, $FeSO_4.7H_2O$, Pyrite, Lyophilized Soil, and S_8+Starch) were distributed on carbon S-free double face tape mounted to a stainless steel sample holder. The previously prepared frozen soil system (soil in eppendorf® cap) was fixed on the sample holder with double face tape. The sample holder was fixed in a cryostage (cold finger). The cryostage was build with copper plate brazed to a stainless steel tube, where was possible to fill with liquid nitrogen, when necessary. The sample holder was fixed in the copper plate.

The samples were aligned at 45° incident angle from the incoming beam with the detector placed within the horizontal plane at 90° from the incoming beam to reduce the elastic scattering background (horizontal polarization from bending magnet). The measurements were performed under low-vacuum (~$5x10^{-7}$ mbar). Each XANES spectrum was constituted by 233 points collected the following energy ranges: 1) Pre-Edge = 2440 to 2467 eV, 1 eV step; 2) Edge = 2468 to 2486 eV, 0.2 eV step; 3) Post- Edge = 2487 to 2600 eV, 1 eV step. The dwell time by each point (energy) was 1 s (8 min whole spectra).

Each sample was analyzed six times sequentially to evaluate the tender X-ray synchrotron radiation damage. However, only in the S_8+Starch sample we had collected 20 spectra sequentially at room temperature. Each sample was analyzed at room temperature (298 K) and cryogenic temperature of 115±5 K. To analyze in cryogenic temperatures we utilized a cold finger device with liquid nitrogen (77 K) that was added into the tube of the sample holder. The temperature decreased by heat transfer between the tube wall and sample holder contact (cold finger). The temperature was monitored with a type K thermocouple connected to the sample holder. In average, each 1 h, the tube was refilled to keep at constant cryogenic temperature of 115±5 K. The photon flux at the sample position, considering the Si(111) monochromator crystals and 200 mA storage ring current, was about $2.4x10^{11}$ ph/s.

The self-absorption effect was observed in the spectra of standards (S_8, $FeSO_4.7H_2O$, and Pyrite). However this effect did not influenced our results,

because we have not used these spectra as standards in the Linear Combination Fitting. Also, the self-absorption effect was constant in the same kind of sample, not influencing our research objective about radiation damage effect.

XANES Spectra Processing: The collected spectra were initially processed in Athena from Demeter software package (RAVEL & NEWVILLE, 2005). In the Athena software, we determined the edge-step values and the E_0 (2471 or 2482 eV) of all raw spectra by the zero crossing of the second derivative. All spectra were examined visually to remove any glitches, drifts correction, and to check for general quality before exported as ".xmu" from Athena. All spectra were linearly baseline-corrected from −28 to −17 eV and normalized and flattened to an absorption (edge-step) from +22 to +75 eV (linear regression) with respect to E_0 in Athena. Further processing was performed using statistical software R 3.4.2 (CORE, 2017) with the "LCF v. 1.6-6" package (WERNER, 2017).

We followed the protocol described by Werner & Prietzel (2015) to perform the linear combination fitting (LCF) of S_8+Starch sample spectra. For those spectra, we performed the LCF, using the first (initial sample condition) and the 20th (more radiation-damaged) spectra as standards. The combination of all possible baseline correction and edge-step normalization parameters using R code resulted in 9660 baseline corrected and edge-step-normalized sample spectra. The parameter "param.float" in the LCF package was configured as: 1) First range of Pre-edge = -30 to -22, each 2 eV; 2) Second range of Pre-edge = -20 to -14, each 2 eV; 3) First range of Post-edge = 15 to 60, each 2 eV; 4) Second range of Post-edge = 60 to 100, each 2 eV.

The best-chosen fit from the LCF analysis was the one showing the lowest R factor (from 0.9 to 5.6 x 10^{-3}). All graphs and statistical analysis were performed in the R 3.4.2 (CORE, 2017), using the "Graphics" v. 3.4.2 (CORE, 2017) package.

3.4. Results

Standards: In the standards, S_8 and $FeSO_4.7H_2O$, we did not observe significant differences between the first and the sixth spectra collected sequentially, both at room or cryogenic temperature (Figure 3.1). In other words, the standards seem not to be affect by the incident radiation, not promoting radiation damage.

However, a small peak at 2472 eV was observed in the $FeSO_4.7H_2O$ sample analyzed at 115 K (Figure 3.1 A), but we believe that it was not formed due radiation damage, because we did not observe the same peak at room temperature condition, and the 2482 eV peak intensity did not decrease, between the 1st and 6th scan.

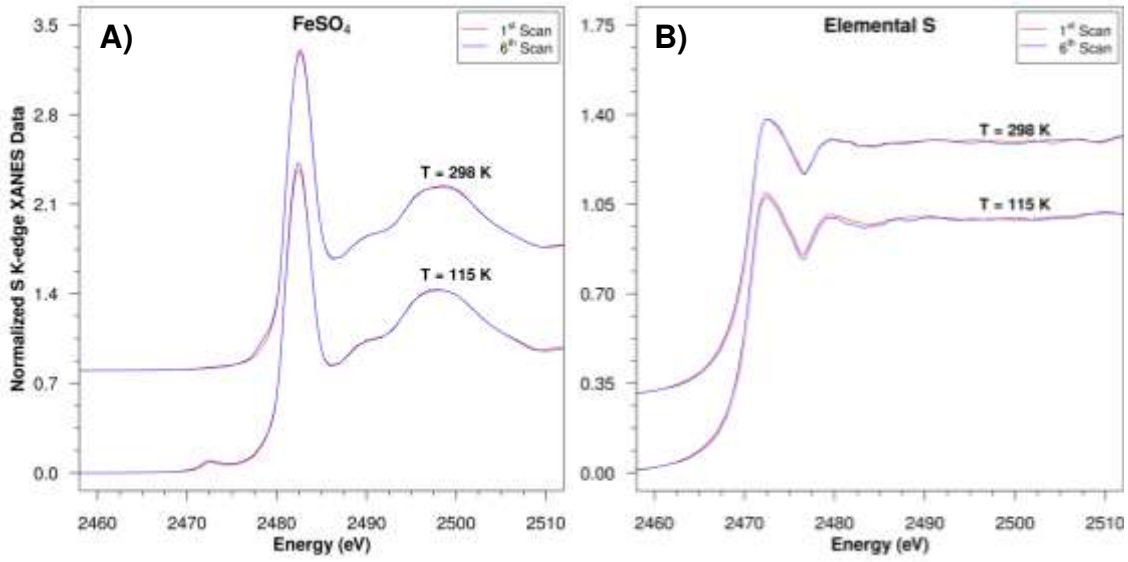

Figure 3.1. First (red line) and sixth (blue line) S K-edge XANES spectra of Ferrous Sulfate (A) and Elemental Sulfur (B) samples, analyzed at 298 K and 115 K.

Environmental Samples: We did not verify significant difference between the first and the sixth S K-edge XANES spectra of frozen soil, lyophilized soil, and pyrite samples, at both temperature conditions (Figure 3.2). Thus, we cannot clearly identify evidence of radiation damage. However, a more intensity peak at 2472 eV was verified in the frozen soil sample analyzed at cryogenic temperature compared to the soil sample analyzed at room temperature (Figure 3.2 A).

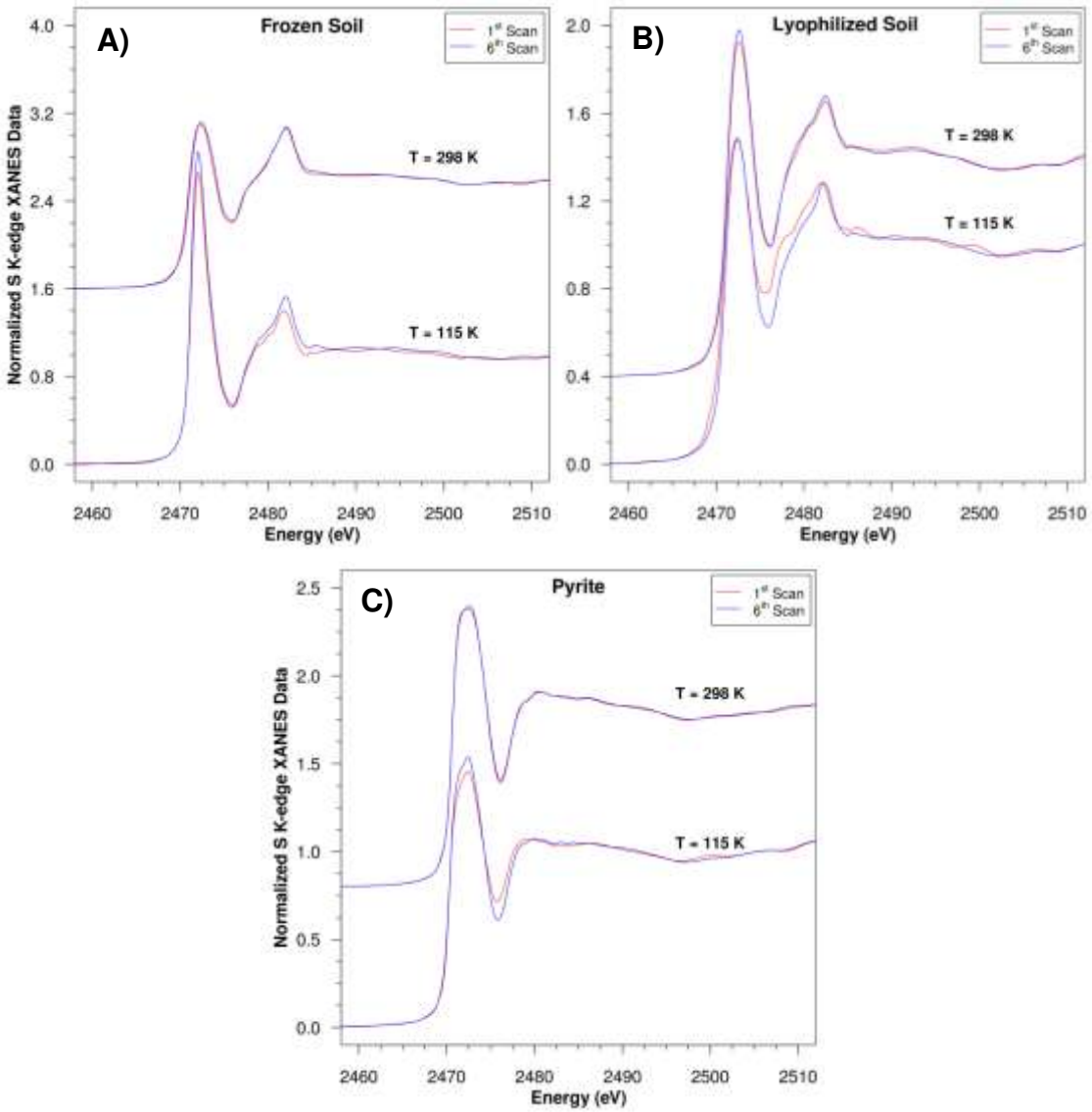

Figure 3.2. First (red line) and sixth (blue line) S K-edge XANES spectra of Frozen Soil (A), Lyophilized Soil (B), and Pyrite (C) samples, analyzed at 298 K and 115 K.

Elemental S + Starch: We did not verify difference between the first and the sixth spectra of Elemental S + Starch sample when the analysis was performed under cryogenic temperature (Figure 3.3). Therefore, when Elemental S + Starch sample was analyzed at room temperature, we verified that the first spectrum showed a higher peak at 2482 eV (S^{+6}) than the sixth S K-edge XANES spectra (Figure 3.3). The intensity of the peak at 2482 eV kept decreasing until the 20th spectra of the elemental S + Starch (Figure 3.4, Figure 3.6). The 3D plot shows the S K-edge XANES as function of scan number,

where is possible observe that the beam promote the reduction of the S in this carbon rich sample (Figure 3.4) until the 20th spectra collected sequentially.

The difference between the spectra obtained first and the sixth scans evidenced radiation damage in the sample, where was observed the sulfur reduction reaction due to income tender X-ray beam. The analysis performed at 115 K showed that the cryostage (cold finger) was effective to minimize the tender X-ray radiation damage in this sample. Furthermore, we observed a quadratic increment in the edge step of the non-normalized spectra of Elemental S + Starch analyzed 20 times under room temperature (Figure 3.5).

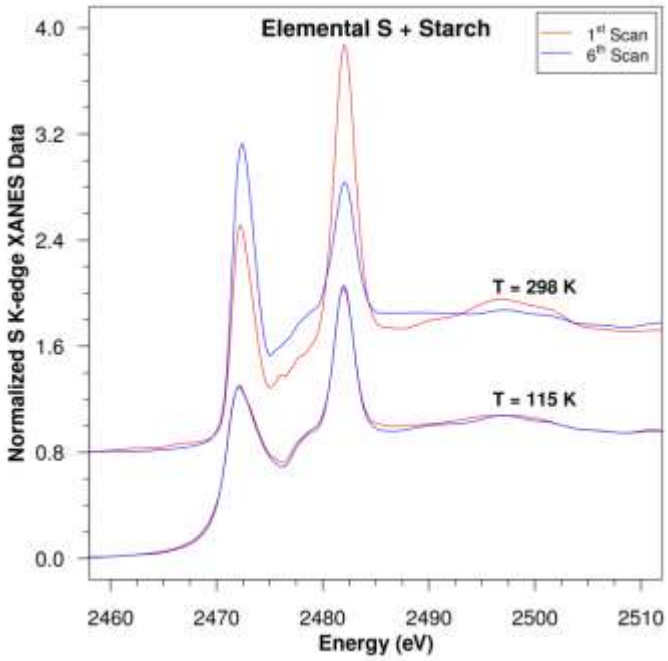

Figure 3.3. First (red line) and sixth (blue line) S K-edge XANES spectra of Elemental S + Starch sample analyzed at 298 K and 115 K.

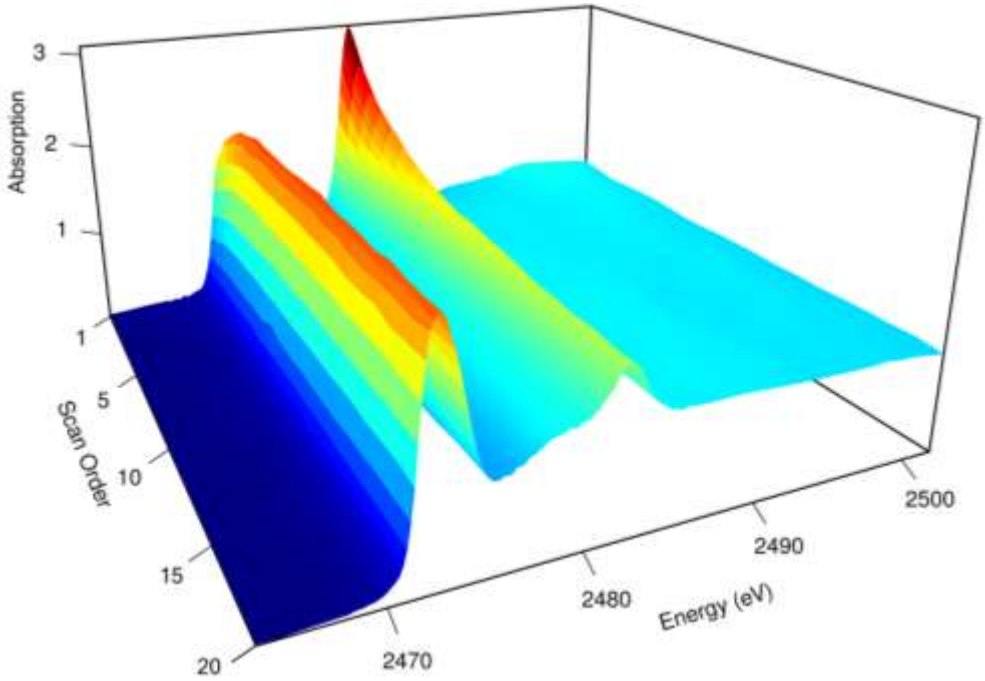

Figure 3.4. 3D plot of S K-edge XANES normalized spectra of the Elemental S + Starch sample analyzed 20 times sequentially at 298 K. Decreases in the 2482 eV peak from the 1st to the 20th scan means reduction o sulfate to more reduced sulfur species.

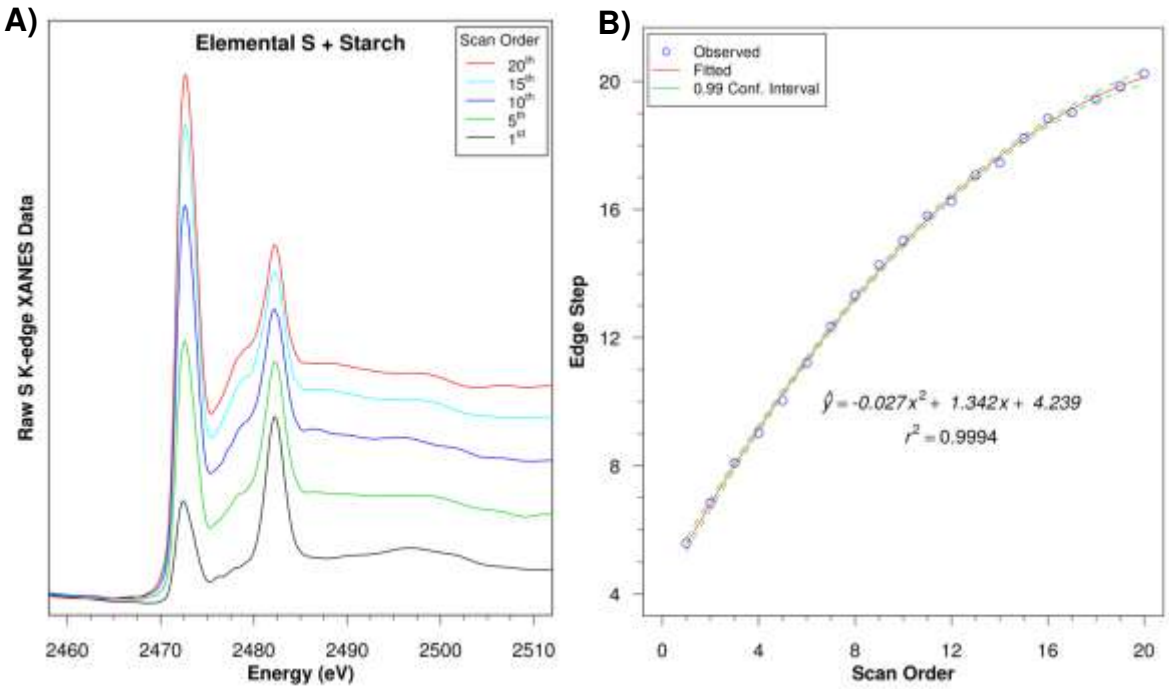

Figure 3.5. A) Raw S K-edge XANES spectra of Elemental S + Starch sample (only 1st, 5th, 10th, 15th, and 20th are presented) and B) Edge Step value of the spectra collected from the first to the 20th scan. Increasing edge step values indicates increases of S concentration in the sample due carbon losses.

The linear combination fitting result showed that the proportion of the first scan (first spectra obtained) decreased exponentially in function of the scan number from the first to the 20th scan (Figure 3.6). The exponential regression fitted in the LCF data (Figure 3.6, $\hat{y} = 1.226 \cdot e^{-0.2603 \cdot x}$) is related to the chemistry kinetic of the oxidoreduction reaction promoted by the income tender X-ray radiation in the S_8 + Starch sample.

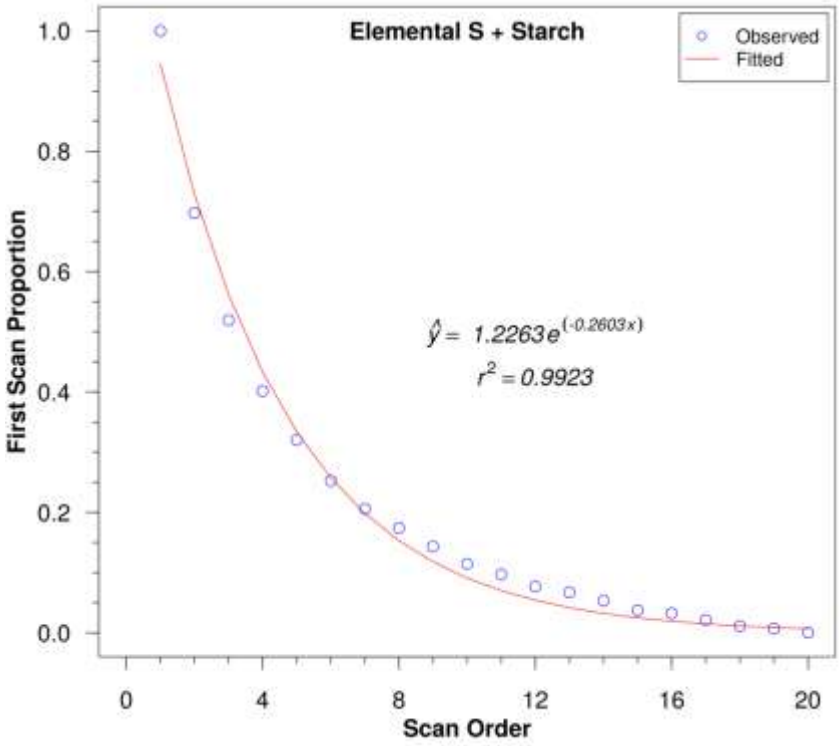

Figure 3.6. Proportion of first (vs. last) spectra fit to each of the 20 scans performed in the S_8 + Starch sample. This result is related the initial condition of the sample (1st scan) compared to the final condition (20th scan) due radiation damage. These data were resulted from Linear Combination Fitting using the 1st and the 20th scans as standards. Details in Table S1.

3.5. Discussion

Our results showed that sulfur present in inorganic standards (S_8, $FeSO_4.7H_2O$ and Pyrite) was not damaged by tender X-ray radiation. However, Wilke et al. (2008) observed the formation of S^{+4} species in silicate glasses due X-ray radiation damage in sulfur speciation study.

Our results indicated that carbon atoms of starch were electrons donor to sulfate present in the starch, promoting the S reduction. The starch is a glucose polymer which the constituent carbons have different oxidation states in the chain. The aldehyde terminal group has the C^{+1} and in the other chain end has C^{-1}, the others carbon atoms are C^0, and in the average, the starch molecule has C^0 (NELSON et al., 2008). The oxidation of C formed volatile gases (as CO or CO_2) that were removed by the vacuum system. Therefore, the S content increased relatively by the C losses in the analyzed area. This has been observed by the edge step increment with the scans (Figure 3.5). The edge step is related to the elemental concentration or the thickness of the sample (SITKO, 2005; 2009; SZCZERBOWSKA-BORUCHOWSKA, 2012; LERI & RAVEL, 2014; WRÓBEL et al., 2017). How we analyzed the same point in the sample, we expected that thickness did not increase, so the edge step increment is attributed by S concentration increases. Hackett et al. (2012) also observed the increment in the ~2470 eV peak during sulfur speciation in brain tissue, due to photoreduction of S^{+6}, result similar to our present study.

The more intense peak at 2472 eV in the frozen soil analyzed at 115 K than in the others soil samples (Figure 3.2 A and B) seem to be related to the following factors: 1) A more heterogeneous sample, due to sample preparation; and 2) The presence of condensed H_2S in the surface of sample, since the H_2S gas remained confined in the sample. The H_2S is naturally formed in mangrove soil due to natural reduction condition and sulfur content in the soil (RICKARD, 2012; BEHERA et al., 2014; GOMES et al., 2016; HOSSAIN & NURUDDIN, 2016). In temperatures lower than 187 K the H_2S is solid and greater than 213 K it is gas.

The mangrove soil has sulfide minerals that are formed by the microorganisms in anaerobic condition (FERREIRA et al., 2007; BEHERA et al.,

2014; HOSSAIN & NURUDDIN, 2016). The pyrite is the predominant mineral which has a specific morphology, denominated framboidal. The framboidal pyrite has variable sizes but they are found in the silt fraction in the soil with dimensions between 2 to 50 µm that can aggregate and concentrate in specific points of soil sample (RICKARD, 1970; ROBERTSON & ALONGI, 1992). The non homogenized frozen soil was analyzed in different regions, thus, these points may have different proportions of sulfate and sulfide mineral due to sample heterogenic characteristic, besides the H_2S surface condensation.

These results highlight the importance of sample preparation to perform the S K-edge XANES analysis in environmental studies. Working with frozen soil sample requires more steps to prepare and it is more complicate to homogenize than lyophilized soil. Besides, the frozen soil covered with thin film will keep the sulfur gaseous forms, which can interfere in the speciation results, when aim to study only the sulfur of solid state phases.

3.6. Conclusions

Tender X-ray synchrotron radiation-damage was observed only in a highly carbon enriched sample with oxidized sulfur species (SO_4^{2-}). The sample damage resulted in the reduction of sulfur and oxidation of carbon. The cold finger at 115 K was effective in minimize the radiation-damage. Thus, we recommend to use the cold finger during the S K-edge XANES data for those samples that are rich in organic carbon for environmental studies. Working with powder samples is recommended (as lyophilized soil), once that the sample mounting procedure is simple and a more homogenous sample is obtained. Besides, lyophilized samples avoid analyze gaseous sulfur species, which is important when the objective is to study only the solid state phases in sample.

3.7. References

ABBATE, M.; VICENTIN, F. C.; COMPAGNON-CAILHOL, V.; ROCHA, M. C.; TOLENTINO, H. The soft X-ray spectroscopy beamline at the LNLS: technical description and commissioning results. **Journal of Synchrotron Radiation**, v. 6, n. 5, p. 964-972, 1999.

BEETZ, T.; JACOBSEN, C. Soft X-ray radiation-damage studies in PMMA using a cryo-STXM. **Journal of Synchrotron Radiation**, v. 10, n. 3, p. 280-283, 2003.

BEHERA, B.; MISHRA, R.; DUTTA, S.; THATOI, H. Sulphur oxidising bacteria in mangrove ecosystem: A review. **African Journal of Biotechnology**, v. 13, n. 29, p. 2897-2907, 2014.

CASTILLO-MICHEL, H. A.; DIAZ-SANCHEZ, A. G.; MARTINEZ-MARTINEZ A; HESSE, B. Investigations of Sulfur Chemical Status with Synchrotron Micro Focused X-ray fluorescence and X-ray Absorption Spectroscopy. **Protein & Peptide Letters**, v. 23, n. 3, p. 291-299, 2016.

CORE, R. T. R: A Language and Environment for Statistical Computing. **R Foundation for Statistical Computing,** v. 3.4.2, 2017. Available in: <https://www.R-project.org/>. Accessed in: 10/10/2017.

FERREIRA, T. O.; OTERO, X. L.; VIDAL-TORRADO, P.; MACIAS, F. Redox processes in mangrove soils under *Rhizophora mangle* in relation to different environmental conditions. **Soil Science Society of America Journal**, v. 71, n. 2, p. 484-491, 2007.

GARMAN, E. F.; NAVE, C. Radiation damage to crystalline biological molecules: current view. **Journal of Synchrotron Radiation**, v. 9, n. 6, p. 327-328, 2002.

GARMAN, E. F.; WEIK, M. Radiation damage to macromolecules: kill or cure? **Journal of Synchrotron Radiation**, v. 22, p. 195-200, 2015.

GARMAN, E. F.; WEIK, M. X-ray radiation damage to biological macromolecules: further insights. **Journal of Synchrotron Radiation**, v. 24, p. 1-6, 2017.

GOMES, F. H.; KER, J. C.; FERREIRA, T. O.; MOREAU, A. M. S. S.; MOREAU, M. S. Characterization and pedogenesis of mangrove soils from Ilhéus-BA, Brazil. **Revista Ciência Agronômica**, v. 47, n. 4, p. 599-608, 2016.

HACKETT, M. J.; SMITH, S. E.; PATERSON, P. G.; NICHOL, H.; PICKERING, I. J.; GEORGE, G. N. X-ray Absorption Spectroscopy at the Sulfur K-Edge: A New Tool to Investigate the Biochemical Mechanisms of Neurodegeneration. **ACS Chemical Neuroscience**, v. 3, n. 3, p. 178-185, 2012.

HOSSAIN, M. D.; NURUDDIN, A. A. Soil and Mangrove: A Review. **Journal of Environmental Science and Technology**, v. 9, n. 2, p. 198-207, 2016.

JEFFRIES, C. M.; GRAEWERT, M. A.; SVERGUN, D. I.; BLANCHET, C. E. Limiting radiation damage for high-brilliance biological solution scattering: practical experience at the EMBL P12 beamline PETRAIII. **Journal of Synchrotron Radiation**, v. 22, n. 2, p. 273-279, 2015.

LERI, A. C.; RAVEL, B. Sample thickness and quantitative concentration measurements in Br K-edge XANES spectroscopy of organic materials. **Journal of Synchrotron Radiation**, v. 21, n. 3, p. 623-626, 2014.

MA, Y.; NIE, H.; SHENG, C.; CHEN, H.; WANG, B.; LIU, T.; SHAO, J.; HE, X.; ZHANG, T.; ZHENG, C.; XIA, W.; YING, W. Roles of oxidative stress in synchrotron radiation X-ray-induced testicular damage of rodents. **International Journal of Physiology, Pathophysiology and Pharmacology**, v. 4, n. 2, p. 108-114, 2012.

MAJUMDAR, S.; PERALTA-VIDEA, J. R.; CASTILLO-MICHEL, H.; HONG, J.; RICO, C. M.; GARDEA-TORRESDEY, J. L. Applications of synchrotron μ-XRF to study the distribution of biologically important elements in different environmental matrices: A review. **Analytica Chimica Acta**, v. 755, p. 1-16, 2012.

NELSON, D. L.; LEHNINGER, A. L.; COX, M. M. **Lehninger Principles of biochemistry**: Macmillan, 2008

RAVEL, B.; NEWVILLE, M. Athena, Artemis, Hephaestus: data analysis for X-ray absorption spectroscopy using IFEFFIT. **Journal of Synchrotron Radiation**, v. 12, n. 4, p. 537-541, 2005.

RICKARD, D. **Sulfidic Sediments and Sedimentary Rocks**. Amsterdam: Elsevier, 2012. 801 p.

RICKARD, D. T. The origin of framboids. **Lithos**, v. 3, n. 3, p. 269-293, 1970.

ROBERTSON, A. I.; ALONGI, D. M. **Tropical Mangrove Ecosystems**. Washington: American Geophysical Union, 1992, v.41 (Coastal and Estuarine Studies)

SITKO, R. Empirical coefficients models for x-ray fluorescence analysis of intermediate-thickness samples. **X-Ray Spectrometry**, v. 34, n. 1, p. 11-18, 2005.

SITKO, R. Quantitative X-ray fluorescence analysis of samples of less than 'infinite thickness': Difficulties and possibilities. **Spectrochimica Acta Part B-Atomic Spectroscopy**, v. 64, n. 11-12, p. 1161-1172, 2009.

SZCZERBOWSKA-BORUCHOWSKA, M. Sample thickness considerations for quantitative X-ray fluorescence analysis of the soft and skeletal tissues of the human body - theoretical evaluation and experimental validation. **X-Ray Spectrometry**, v. 41, n. 5, p. 328-337, 2012.

WERNER, F.; PRIETZEL, J. Standard Protocol and Quality Assessment of Soil Phosphorus Speciation by P K-Edge XANES Spectroscopy. **Environmental Science & Technology**, v. 49, n. 17, p. 10521-10528, 2015.

WERNER, F. LCF: Linear Combination Fitting R package. v. 1.7, 2017. Available in: <https://CRAN.R-project.org/package=LCF>. Accessed in: 01/10/2018.

WILKE, M.; JUGO, P. J.; KLIMM, K.; SUSINI, J.; BOTCHARNIKOV, R.; KOHN, S. C.; JANOUSCH, M. The origin of S^{4+} detected in silicate glasses by XANES. **American Mineralogist**, v. 93, n. 1, p. 235-240, 2008.

WRÓBEL, P. M.; BAŁA, S.; CZYZYCKI, M.; GOLASIK, M.; LIBROWSKI, T.; OSTACHOWICZ, B.; PIEKOSZEWSKI, W.; SURÓWKA, A.; LANKOSZ, M. Combined micro-XRF and TXRF methodology for quantitative elemental imaging of tissue samples. **Talanta**, v. 162, p. 654-659, 2017.

3.8. Supporting Information for Chapter III

Table S3.1. Linear Combination Fitting result of each 20 scans performed in the S_8 + Starch sample using the 1st and the 20th scans as standards. Values of R-factors and pre-edge and post-edge parameters used in the LCF are presented.

S_8 + Starch	Scan 1	Scan 20	R.fac	pre.adj.1	pre.adj.2	post.adj.1	post.adj.2
Scan 1	100%	0%	2.96E-07	-30	-16	21	76
Scan 2	70%	30%	0.000235	-26	-18	25	64
Scan 3	52%	48%	0.000389	-30	-18	25	62
Scan 4	40%	60%	0.000358	-22	-16	23	62
Scan 5	32%	68%	0.000427	-22	-16	23	62
Scan 6	25%	75%	0.000412	-22	-16	23	62
Scan 7	21%	79%	0.000367	-22	-16	23	60
Scan 8	17%	83%	0.000447	-22	-14	23	60
Scan 9	14%	86%	0.000334	-22	-14	21	62
Scan 10	11%	89%	0.000282	-22	-16	21	60
Scan 11	10%	90%	0.000248	-22	-18	21	62
Scan 12	8%	92%	0.000234	-22	-18	19	62
Scan 13	7%	93%	0.000192	-26	-18	21	60
Scan 14	5%	95%	0.000167	-22	-14	21	62
Scan 15	4%	96%	0.000146	-28	-16	35	94
Scan 16	3%	97%	0.000151	-30	-16	35	94
Scan 17	2%	98%	0.000132	-26	-20	21	76
Scan 18	1%	99%	0.000128	-26	-18	39	80
Scan 19	1%	99%	0.000115	-30	-18	43	74
Scan 20	0%	100%	1.10E-07	-30	-16	21	62

CHAPTER IV

X-RAY ABSORPTION AND FLUORESCENCE MICROSCOPY APPLIED TO TREE-RING CHEMICAL STUDY OF TROPICAL MANGROVE

4.1. Abstract

Dendrochemistry studies enable the prediction of preterit chemical environmental conditions related to soil, water, and air chemical quality. In the last years, the X-ray fluorescence microscopy (μXRF) methods have been highlighted in these studies due to high spatial resolution and to be a non-destructive technique. However, the X-ray absorption spectroscopy microprobe (e.g., μXANES) has not been applied in these studies. μXANES analysis has a potential application in dendrochemistry studies by provide information about chemical species into tree-rings. Thus, we aim assesses the Ca distribution and speciation into *Avicennia* mangrove tree, using μXRF and Ca K-edge μXANES analysis (5 μm beam size) combined with multivariate analysis during data process. Increment cores were extracted from the *Avicennia* mangrove at Concha D'Ostras Sustainable Development Reserve, Southeast Brazil, and were analyzed by XRF and XANES techniques at Stanford Synchrotron Radiation Laboratory. The Ca content was greater in internal part of wood (heartwood) than in the external part (sapwood) and showed a systematic distribution into tree-rings, being possible to use this data to identify "chemical-rings" in the sample. The PCA and Cluster multivariate analysis showed that Ca species are distinct in the sapwood (more calcium oxalate and carbonate) and heartwood (more calcium sulfate), which can be related to a Ca role in the plant, as structural (heartwood) or a labile form (sapwood). This study showed that multivariate analysis of Ca speciation data and the Ca distribution in the tree-ring, using a microprobe X-ray spectroscopy, provide valuable information about chemical records in the mangrove tropical tree-rings.

4.2. Introduction

Tree-rings are formed due to seasonality of environmental condition (e.g., rainfall, temperature, sunlight duration, flooding) during the tree growth and they are found in several woody species worldwide (DUNWIDDIE & LAMARCHE, 1980; WORBES, 1995). The chemical analysis of these tree-rings is namely dendrochemistry, a subdiscipline of dendrochronology science (BALOUET et al., 2009). Dendrochemistry studies enable the prediction of preterit chemical environmental conditions related to soil, water, and air chemical quality (BALOUET et al., 2009; SMITH et al., 2014). Natural and anthropogenic events as volcanic eruption or toxic chemical elements release, respectively, can be registered as chemical information inside tree-ring, being possible to access this information by dendrochemistry methodologies (SMITH et al., 2014).

Tree rings analysis has a high potential application to assess tropical mangrove trees and the estuarine ecosystems. The mangrove ecosystems are very dynamic and they are subject to tide fluctuations, being threaded by the sea level rinsing (CHURCH et al., 2008). Thus, this tool can be applied to investigate impacts of the sea level fluctuations in the recent years on the biogeochemical dynamics (LAMBECK & CHAPPELL, 2001).

Different analytical techniques can be used in dendrochemistry studies. In the last years, spectroscopy techniques, as the X-ray fluorescence microscopy (μXRF), have been highlighted in these studies due to high spatial resolution, fast results, simultaneously chemical elements analysis, and to be a non-destructive technique (SMITH et al., 2014). However, dendrochemistry studies using X-ray absorption spectroscopy microprobe (μXAS), like the X-ray absorption near edge structure microscopy (μXANES) are scant. Some these studies is relating a sulfur speciation in tree wood (BARRELET et al., 2008; STRUIS et al., 2008; FAIRCHILD et al., 2009; FORS et al., 2014) and Ca K-edge XANES have not been applied in dendrochemistry study. The μXANES analysis has a potential application in dendrochemistry studies by provide information about chemical species into tree-rings in high spatial resolution, being possible to assess the intra and inter-annual variations of chemical speciation (MAJUMDAR et al., 2012).

The μXRF and μXANES microscopy analyses applied to dendrochemistry studies provide a large datasets. Process these large datasets is usually difficult. However, multivariate statistical tools can be helpful to extract and to interpret main information (LEROTIC et al., 2004; THYREL et al., 2016). The principal components analysis (PCA) is a multivariate data analysis tool that can be used to extract information in a large multi-dimension dataset in fewer dimensions, namely principal components (PCs). The first obtained PCs explain most of the variance of the dataset (usually greater than 60%), and they are plotted with two or three dimensions to visualize the similarities between data (LEROTIC et al., 2004).

The cluster analysis method is also used to find similarities between data and to create dendrograms which show how the samples are clustered. The cluster analysis has the advantage for using all the variance in the dataset, while the three first PCs in PCA analysis contain usually less than 90% of the variance. However, cluster analysis loses relational information about the variables within each cluster (LEROTIC et al., 2004; XUE et al., 2011). Thus, PCA and cluster analysis are complementary tools that provides together more information than using either method alone (LEROTIC et al., 2004; XUE et al., 2011).

Thus, we aimed to assesses the Ca distribution and speciation into *Avicennia* Brazilian tropical mangrove tree, using μXRF and Ca K-edge μXANES analysis combined with PCA and cluster multivariate analysis during data process.

4.3. Materials and Methods

Study Area Characterization: Sampling was conducted in a mangrove forest located in the Concha D'Ostras Sustainable Development Reserve, Guarapari city, Espírito Santo state, Southeast region of Brazil (Figure 2.1). The climate according to Köppen classification is Aw, tropical hot and wet, characterized by a short dry season in the winter and a rainy summer (ALVARES et al., 2013). The average annual temperature is 24.4 °C, and the average annual precipitation is 1,084 mm. The Concha D'Ostras Reserve has

9.3 km^2 and the mangrove forest is composed by *Rhizophora, Avicennia* and *Langucularia* species (IEMA, 2004).

The sampled tree was located in the extreme border of the Reserve area (20° 39' 54.1" S, 40° 29' 56.5" W, sea level), situated near to the urban area and few meters from the river mouth to sea. The soil is sandy, and it is highly contaminated by domestic sludge disposal coming from the urban center (Figure 2.1).

Figure 4.1. Tropical Brazilian mangrove located in the Concha D'Ostras Sustainable Development Reserve, Guarapari city, Espírito Santo state, Brazil. Red point indicates the sampled area.

Wood Sampling and Preparation: On May 2015, two increment cores were extracted from the stem 1 m above the ground from living *Avicennia* tree with 0.5 m of diameter at breast height. The samples were air-dried as they were collected. Dried cores samples, with 80 x 5 mm dimension, were mounted

into grooved wooden blocks and surfaced with a graded series of silicon carbide sandpaper (60, 100, 300, and 600 grit cm^{-2}), and the surface was cleaned with air jet.

Energy Dispersive X-Ray Fluorescence Microscopy (µEDXRF): A core sample with flat-surface was analyzed by a benchtop µEDXRF spectrometer (model 1300, Shimadzu, Kyoto, Japan). This spectrometer has a X-ray tube of Rh anode, worked with 50 keV and 50 µA; a Si(Li) detector with 4096 channels, cooled with liquid nitrogen; and a polycapillary beam optic with 50 µm diameter and 1.5 mm work-distance from the sample surface.

Two transects was selected from the internal (heartwood) to external (sapwood) regions of the core sample, with 80 mm length. The X-ray fluorescence was measured in spots with diameter of 50 µm with step size of 100 µm between the spots, and 40 s of acquisition livetime (25% of dead time) by spot. A total of 800 spots were analyzed in ~11 h period.

Synchrotron X-Ray Fluorescence Microscopy (µSXRF): We used the results obtained from the µEDXRF analysis to plan and to obtain high resolution microchemical maps of the wood samples using the synchrotron radiation. The same flat core sample was analyzed on the 14-3b beamline at the Stanford Synchrotron Radiation Lightsource – SSRL, Stanford University, CA, USA. A External (sapwood, 23.2 x 2 mm) and an Internal (heartwood, 18.2 x 2 mm) sections of the core sample was selected and analyzed with synchrotron monochromatic X-ray beam of 4.1 keV (near Ca K-edge), and was obtained microchemical maps of S, Cl, P and Ca, in each wood sections. The µSXRF analysis was performed under helium atmosphere; at room temperature; with a 5 µm diameter incident monochromatic X-ray beam (4.1 keV); with 10 µm step size, and 50 ms of acquisition time per analyzed spot. A total of 800,000 spots in both wood sections spent 12 h to be analyzed.

X-Ray Absorption Near Edge Structure Microscopy (µXANES): We selected 40 points of interest in each µSXRF maps based on Ca Kα intensity and regions inside and outside tree-rings (Figure 4.4 and Figure 4.5). We collected one Ca K-edge µXANES spectra in each selected point (5 µm diameter). The µXANES spectra were collected randomly positions in the

sample wood. However, the point's numbers were renamed from 1 to 40 during data processing to make easier the association/visualization between spectra and points localization in the map.

The energy ranges used during μXANES spectra collection were: Pre-edge = 3950 to 4030 eV, 5 eV step; Edge = 4035 to 4080 eV, 0.25 eV step; Post-edge = 4081 to 4220 eV, 1 eV step. The acquisition time was 1 s per energy. A total of 80 μXANES spectra (3.95 to 4.22 keV) were obtained in both two wood sample sections.

μSXRF maps Processing: The μSXRF maps were processed in the software SMAK v. 1.4 (WEBB, 2011). During maps process, we identified spectral interferences of Ca Kα Escape in the P Kα lines, which overestimated the P abundance. Thus, we applied a mathematical method in SMAK software to minimize this artifact in the P Kα μSXRF maps.

μXANES data normalization: The Ca K-edge μXANES spectra were initially processed with the program Athena of the Demeter software package (RAVEL & NEWVILLE, 2005). In the Athena software, we determined the E_0 (~4048 eV) of all raw spectra by the zero crossing of the second derivative. All spectra of the same sample/standard were examined visually to remove any glitches, and to check for general quality.

The spectra were linearly baseline-corrected from −95 to −40 eV, normalized and flattened to an absorption (edge-step) of 1 from 20 to 150 eV with respect to E_0 ($\Delta E = E-E_0$). The spectra were exported as ".nor" file from Athena software to perform statistical multivariate analysis in the statistical software PAST v. 3.18 (HAMMER et al., 2001). The spectra also were exported as ".xmu" from Athena and further processing was performed using statistical software R 3.3.2 (CORE, 2017) with the "LCF v. 1.7[1]" package (WERNER, 2017).

[1] The last update made in the "LCF" package (v. 1.7) was suggested by Elton E. Novais Alves in contacted with the package author Dr. Florian Werner. The last update included the energy shift correction option, when necessary.

Statistical multivariate analysis: The normalized data of μXANES spectra were exported to software PAST v. 3.18 (HAMMER et al., 2001). We used the normalized absorption data in the 4025 to 4122 eV energy range (225 variables) to perform the PCA and Cluster multivariate analysis. The Cluster analysis was used to evaluate the similarities between the 80 spectra by tree diagram. No additional normalization or transformations were used to perform the multivariate analysis, because the data were previously normalized in Athena software. We selected visually six spectra from the PCA and Cluster analysis results. These spectra were denominated “Local Standards” (STD).

Linear combination fitting (LCF): The six spectra selected from the multivariate analysis (STDs) were exported to R software and we utilized the “LCF v. 1.7” package according to the protocol described by Werner & Prietzel (2015) to perform the linear combination fitting of the six STDs with six pure calcium standards. The pure standards selected in this step were Ca-Oxalate, $CaCl_2$, $CaSO_4$, Ca-carboxymethyl cellulose, $CaCO_3$, and Ca-Apatite. The spectra of these standards were obtained during sample collection, as described in previously section. After the LCF of the STDs, we used the six standards to also perform the LCF of the 80 Ca K-edge μXANES spectra. All the LCF was performed for the relative to E_0 energy range of -15 to 80 eV.

The μXANES spectra were initially linearly baseline-corrected from −95 to −40 eV and normalized and flattened to an absorption (edge-step) of 1 from 20 to 150 eV with respect to E_0. The combination of all possible baseline correction and edge-step normalization parameters using R code resulted in 1320 baseline corrected and edge-step-normalized sample spectra. The parameter “param.float” in the LCF package was configured as: 1) First range of Pre-edge = -95 to -85, each 5 eV; 2) Second range of Pre-edge = -60 to -40, each 5 eV; 3) First range of Post-edge = 0 to 70, each 10 eV; 4) Second range of Post-edge = 70 to 170, each 10 eV.

The LCF was performed to estimate the calcium species abundance in the tree-rings of wood sample. The results of the LCF were exported to PAST software, and we performed the PCA and Cluster analysis to evaluate the similarity between the Ca species abundance in different positions/age of the tropical mangrove (*Avicennia*) wood sample.

4.4. Results and Discussion

The *Avicennia* mangrove tree showed a total of 31 very distinct tree-rings (Figure 4.2), corresponding to 31 years old of the tree. Most of tree-rings studies (dendrochronology) are related to tree species located in temperate climate regions, where the seasons are well defined (DUNWIDDIE & LAMARCHE, 1980; WORBES, 1995). However, several researches have demonstrated that tropical trees species, including mangroves, also are able to form tree-rings (WORBES, 2002; MENEZES et al., 2003; VERHEYDEN et al., 2004a; VERHEYDEN et al., 2004b; VERHEYDEN et al., 2005; SOUZA et al., 2016).

The tree-rings presence indicates that the *Avicennia* tree was exposed to adverse environmental conditions during its annual growth, which limited its growth. These adverse environmental conditions are more accentuated during the winter, where there is lower sunlight plant exposure, lower average air temperature (chilling), lower precipitation, and increment of water salinity (CHEN et al., 2017).

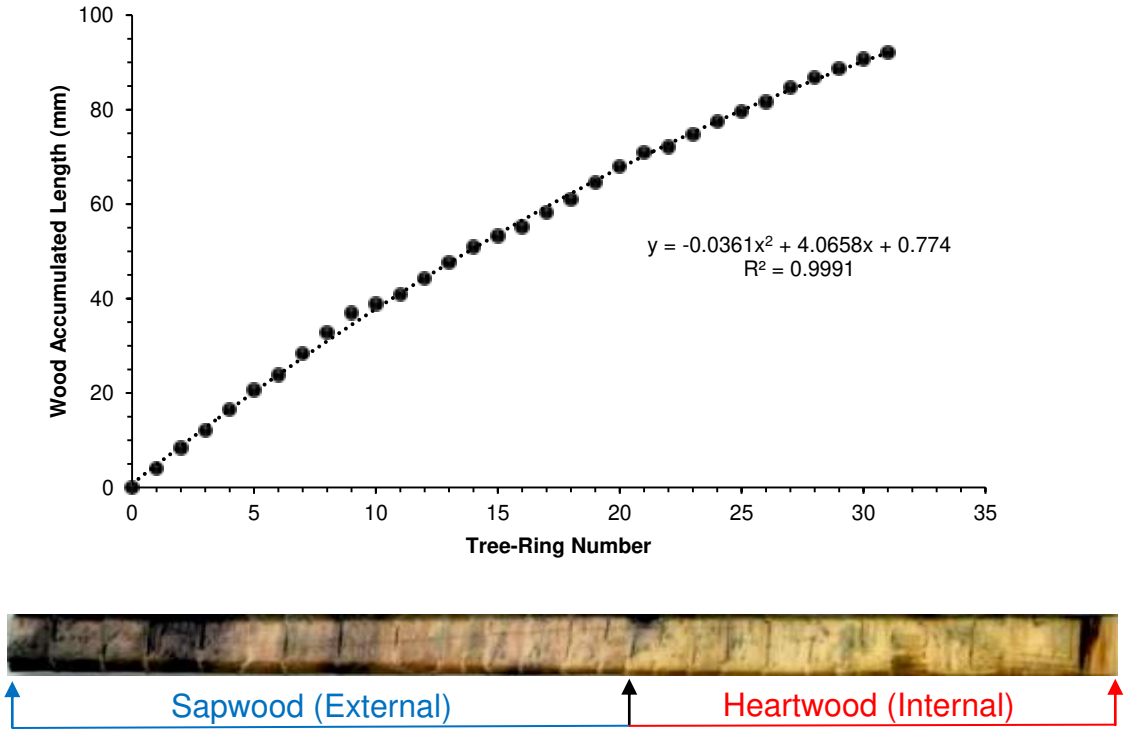

Figure 4.2. Photography of *Avicennia* wood sample with 9.2 cm length, 33 tree-rings/years old, and the accumulated tree-rings length

X-ray fluorescence analysis (µEDXRF and µSXRF): The Ca, K, S, and P were the major chemical elements identified by the µEDXRF analysis in the *Avicennia* wood (Figure 4.3). The high resolution microchemical maps generated by the µSXRF analysis of the chemical elements Ca, Cl, K, P, S are in Figure 4.4 (heartwood) and Figure 4.5 (sapwood).

The Ca Kα signal was more intense in the internal part (heartwood) than in the external part (sapwood) of the wood sample. Also, we observed a systematic distribution (peaks) of Ca profile in the tree-rings (Figure 4.3, Figure 4.4, Figure 4.5). These Ca peaks are related a high Ca content, and they were located close to the tree-ring formed on the wood formed at the end of wet season (latewood), as verified in Figure 4.4 and Figure 4.5.

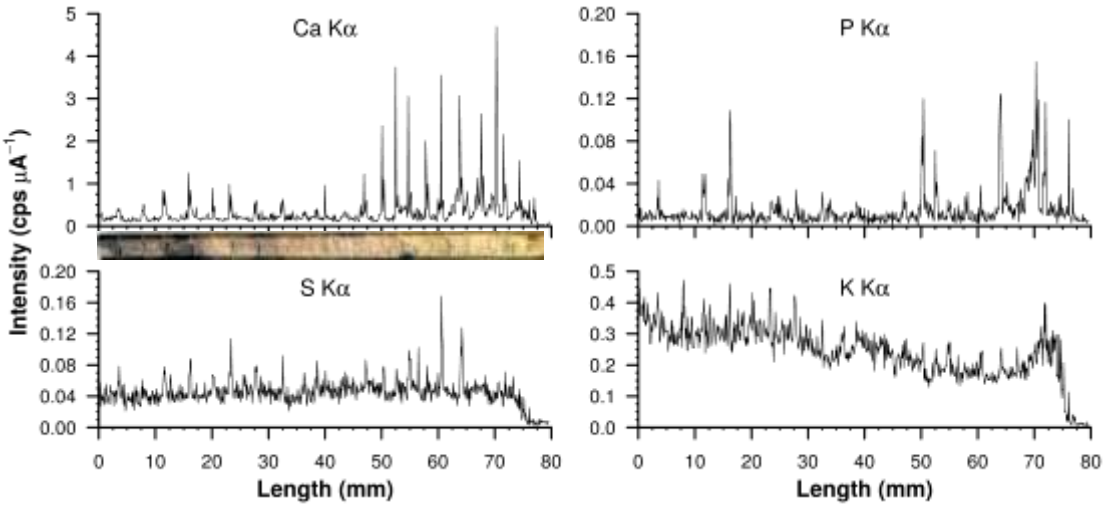

Figure 4.3. Fluorescence Kα lines of chemical elements detected in the tropical mangrove wood sample by µEDXRF analysis (benchtop spectrometer).

Smith et. al (2014) found evidences that the Ca and other cations accumulation are related to environmental and plant physiological factors. These same authors verified that heartwood and sapwood can be identified by the difference of the Ca content between these plant tissues, as we found in our research. Also, the K profile (Figure 4.3) and microchemical maps (Figure 4.4 and Figure 4.5) show that the K content is higher in the sapwood (active xylem) than in the heartwood, but we have not observed its systematic distribution as for Ca.

The phosphorous profile (Figure 4.3) showed high P peaks (content) in the wood sample in different ages. We observed high spots of P in the µSXRF P Kα map mainly in the heartwood (Figure 4.4). These high P content spots can be related to high phosphorus availability in the mangrove environmental that was absorbed by the plant and deposited in the wood. A possible P source in this mangrove site is the presence of *in natura* domestic sludge disposal. In biogeochemistry study of the same area, Rocha (2016) correlated the P content in the soil as a key chemical elemental to indentify contaminated mangrove sites.

The S content is more homogenous along the wood, with higher peaks in the heartwood (S Kα profile in Figure 4.3), being located in the latewood rings as the Ca (Figure 4.4 and Figure 4.5). The main S source is the seawater, and the S dynamics is governed by soil microorganisms under redox potential (RICKARD, 2012; BEHERA et al., 2014; FIKE et al., 2016) (see Chapter II). Thus, the S availability to tree is coupled to soil microorganisms activity and of the input sulfate rates of the seawater to the mangrove soil.

The Cl content was greater in the sapwood than in heartwood (Figure 4.4 and Figure 4.5), similar to K. However, we verify that the Cl have not accumulated in the latewood, as Ca and K. As S and K, the main source of Cl is the seawater. And this element is very mobile in the plant. Only in high concentrations, this element can precipitate with cations as Na, Ca and K in the wood (RANA & MARK, 2008).

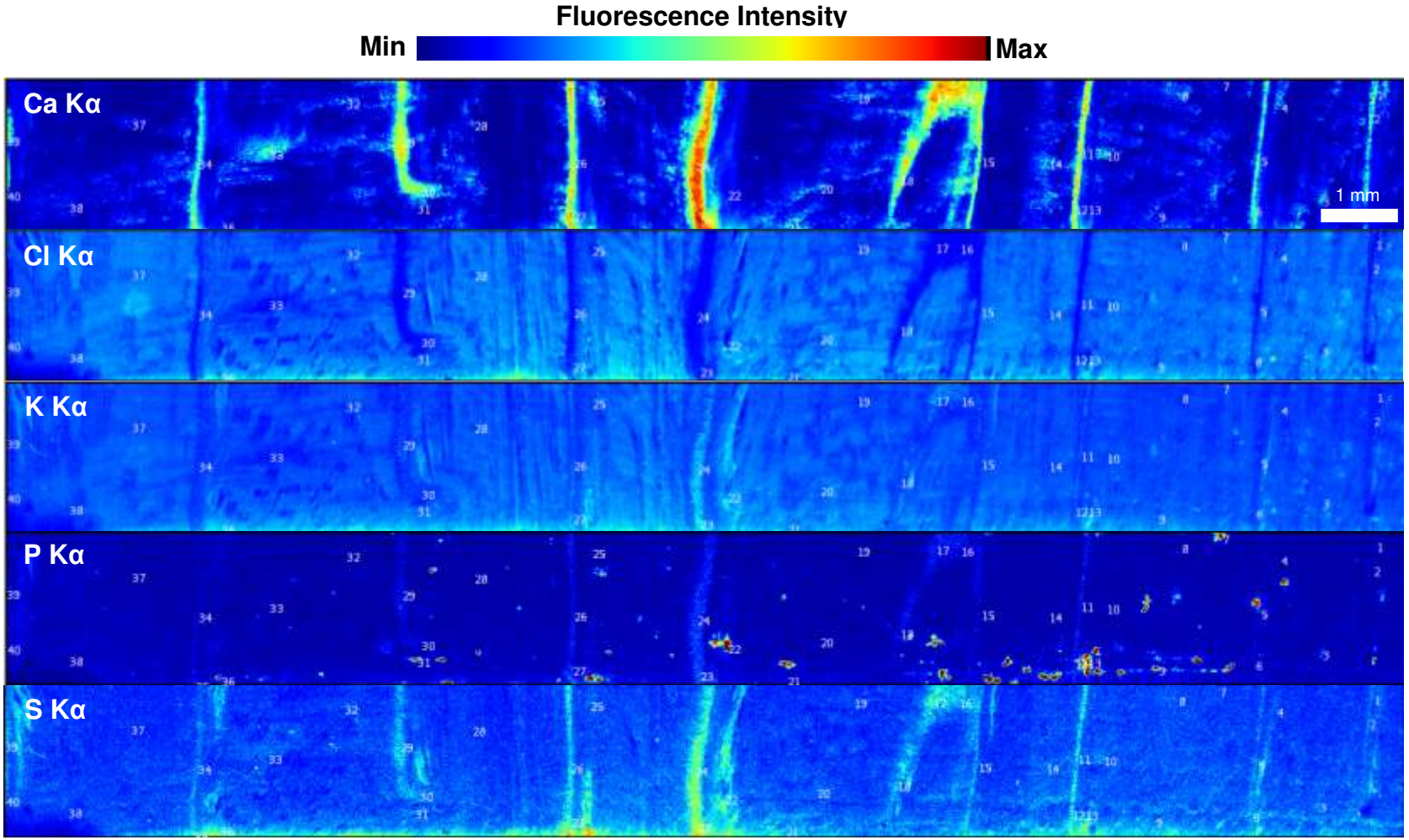

Figure 4.4. Results of μSXRF analysis. Maps of Kα fluorescence lines of chemical elements Ca, Cl, K, P, and S in the Internal (heartwood) part of *Avicennia* tropical mangrove tree. The right part of the map is the more internal part of tree (core). The numbers correspond to the μXANES analyzed points

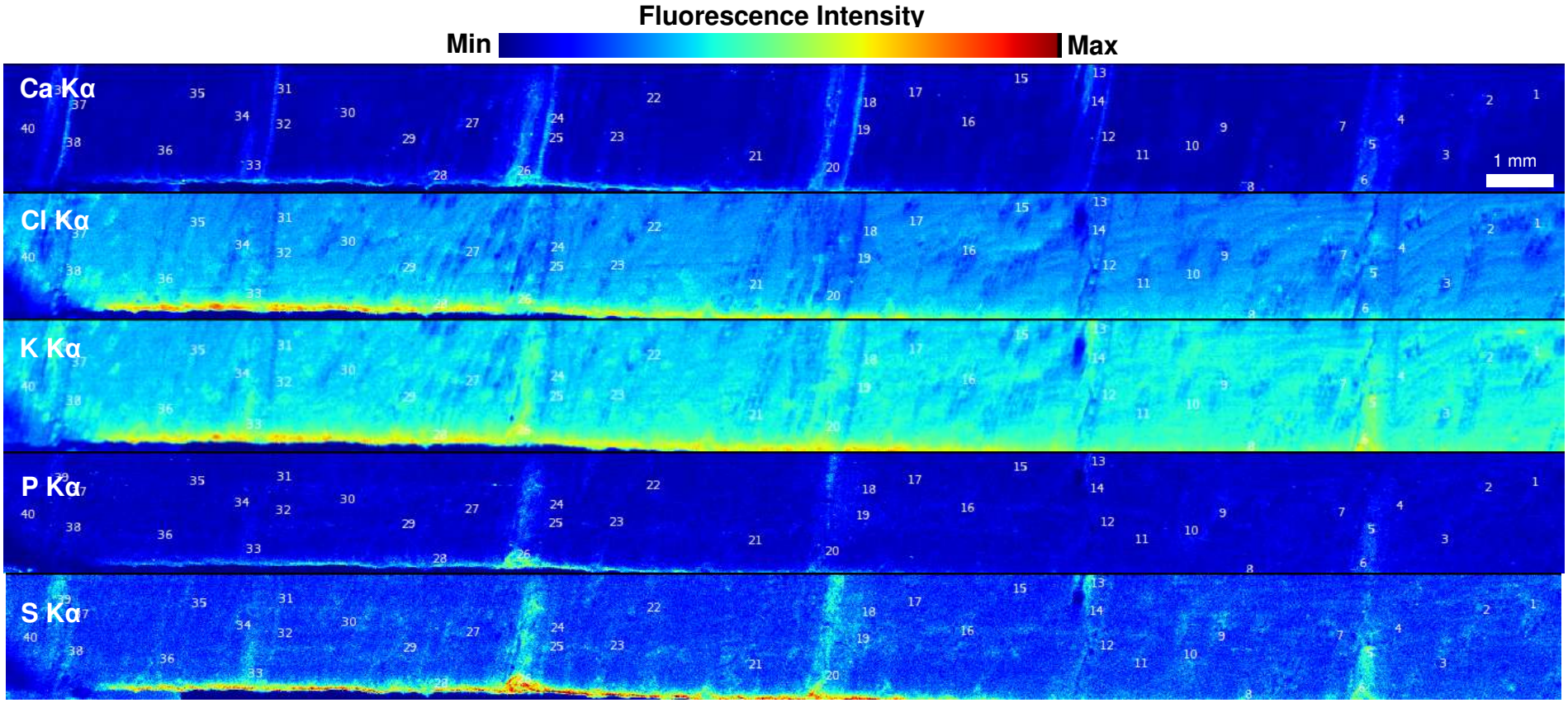

Figure 4.5. Results of μSXRF analysis. Maps of Kα fluorescence lines of chemical elements Ca, Cl, K, P, and S in the External (sapwood) part of *Avicennia* mangrove tree. The right part of the map is the more external part of tree (close to the bark). The numbers correspond to the μXANES analyzed points

Multivariate analysis of µXANES data: The first multivariate analysis performed from the 80 Ca K-edge µXANES normalized spectra showed that Ca species found in the sapwood are different from the heartwood (Figure 4.6). Calcium carbonate, sulfate and oxalate were the main Ca species found in LCF results of the six STDs with Ca standards (Figure 4.7).

Calcium is important plant nutrient and has several important roles in the plant. Calcium regulates the plants growth and development; plays a crucial role in determining the structural rigidity of the cell wall; it participates in the membrane structure and function; cell division; and as signaling in the plants cells, being found in several part of plant (HEPLER, 2005). Calcium oxalate and carbonate can accumulate in specialized cell into wood, as phytoliths (JANIN & CLÉMENT, 1972; FRANCESCHI & NAKATA, 2005). There are some discussions about the function of calcium accumulation as oxalate crystal. It can be used by plant as a Ca source reserve; as a structural function (mechanical support); to light gathering and reflection; or to alleviate toxic levels of Ca and others cations (SCHNEIDER, 1901; FRANCESCHI & NAKATA, 2005). Calcium sulfate accumulation into wood seems to be related to high availability of sulfate in the mangrove soil solution due seawater influence. The $CaSO_4$ was more abundant in the heartwood than in sapwood.

The second PCA and cluster analysis from the LCF results of the 80 µXANES with six pure Ca standards (Figure 4.8) showed that $CaCl_2$ and $CaSO_4$ is greater in the heartwood and $CaCO_3$ and Ca-Oxalate is greater in the sapwood. These results evidence that Ca species are formed differently in wood regions and those species can be linked to specific roles in the plant tissue. Environmental factors can also have influence in this Ca speciation. However, further data process and input (as climate, physiological, and soil data) is necessary to determine which factors have more influence in the Ca species accumulation into tree-rings.

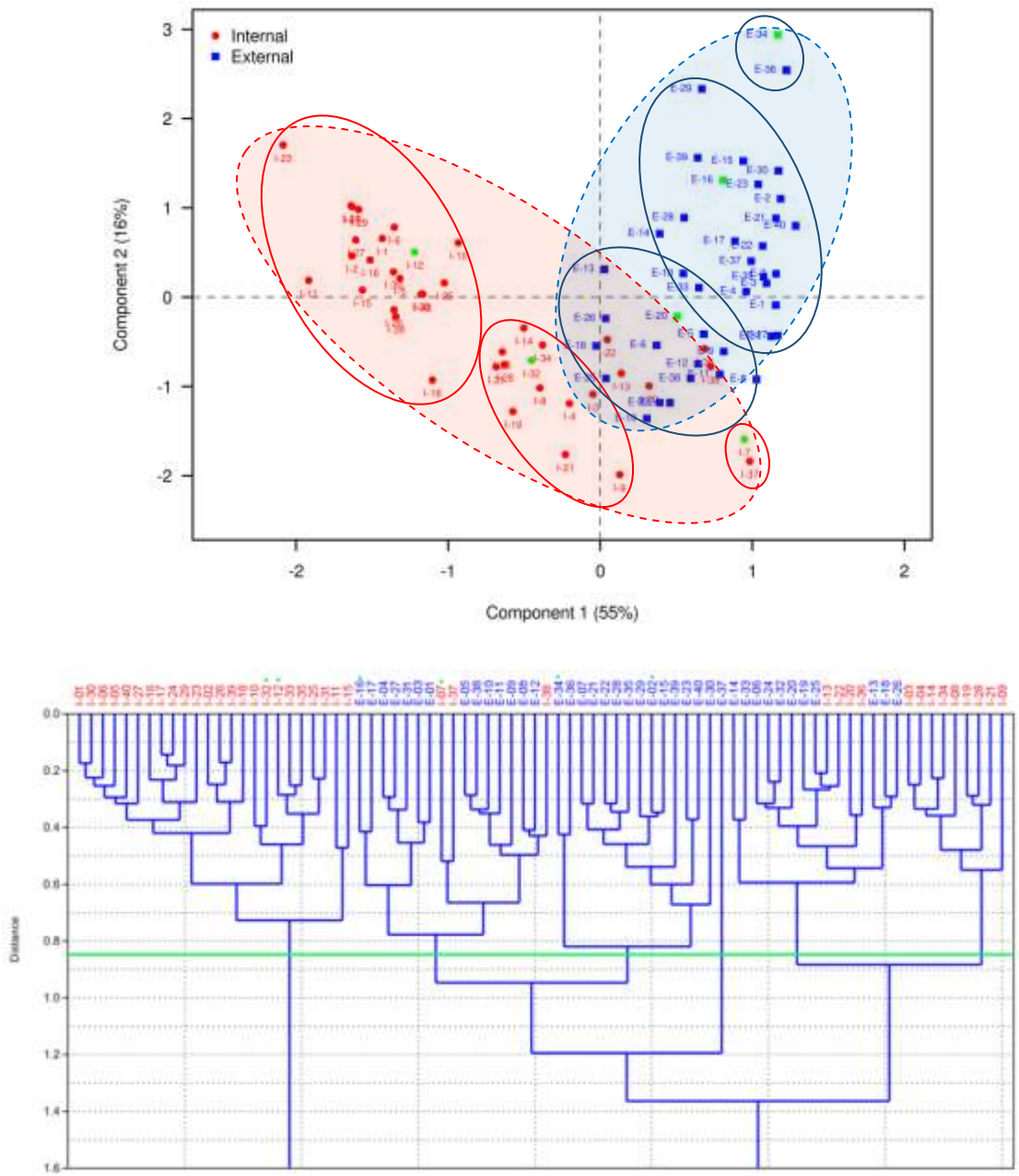

Figure 4.6. PCA and cluster results from 80 Ca K-edge µXANES spectra showed that Ca species are distinct of the sapwood (external) and heartwood (internal). The multivariate analyses were performed from the normalized spectra in the energy range from 4025 to 4122 eV (225 variables). We select six regions from the PCA biplot and, together with cluster dendrogram, we select six spectra as “local standards” (green color markers) to perform LCF with standards (Figure 4.7).

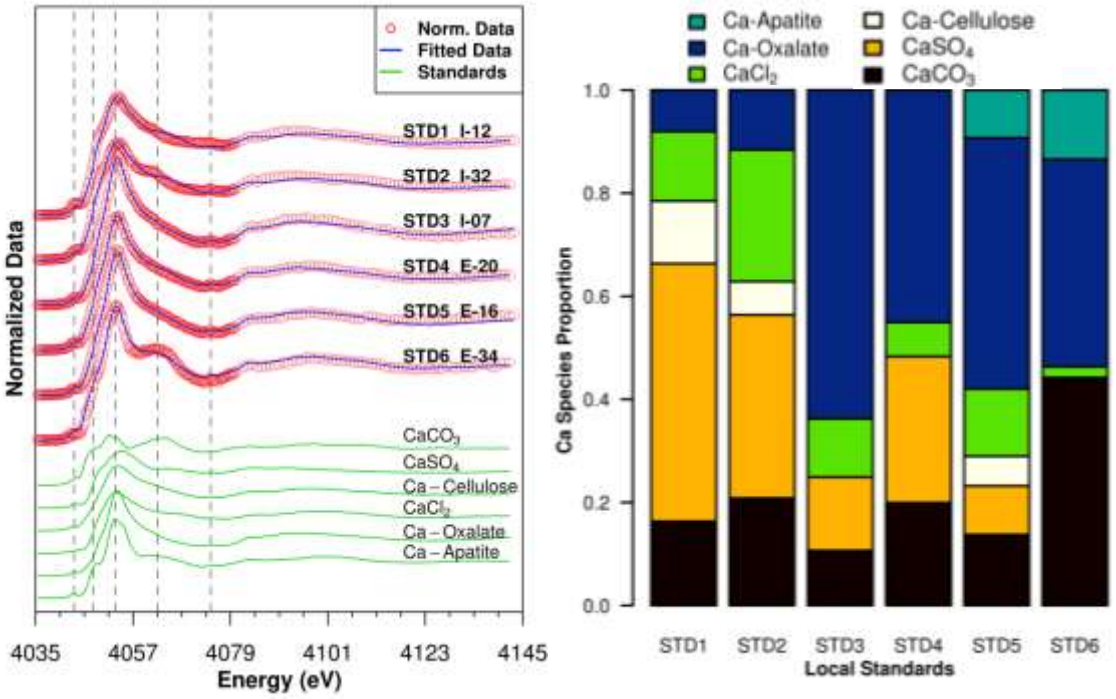

Figure 4.7. The six “local standards” (STD) normalized and stacked Ca K-edge μXANES spectra, which were selected from the PCA analysis. Vertical dashed lines highlight the specific shapes that are specific in the spectra. The barplot represents the LCF results. The Ca sulfate, carbonate and oxalate were the main species founded.

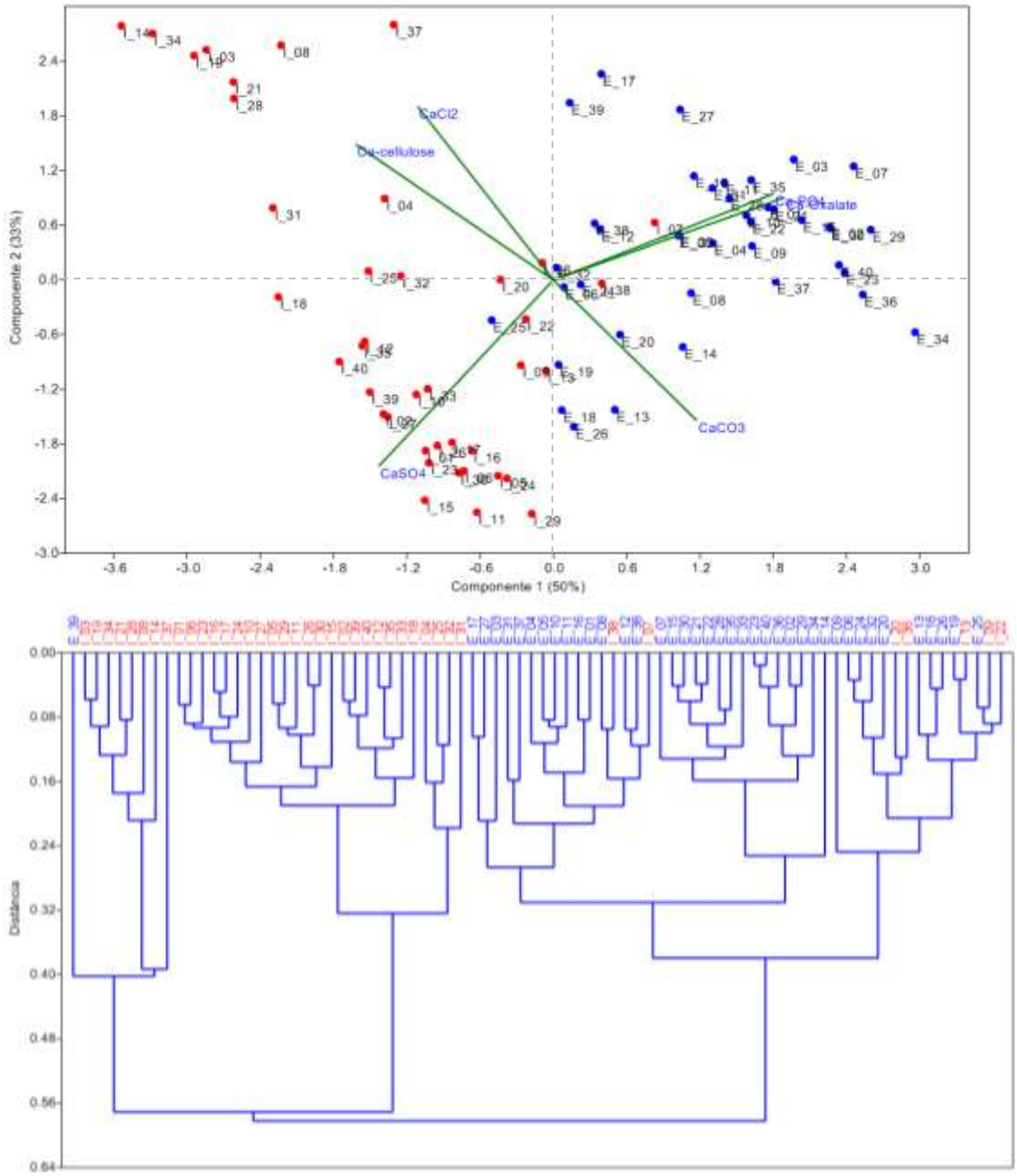

Figure 4.8. PCA and cluster analysis from the LCF results of the 80 µXANES with six pure Ca standards

4.5. Conclusions

In this dendrochemistry study, we evidenced calcium chemical rings in the Brazilian tropical mangrove *Avicennia* by X-ray fluorescence microscopy (μXRF). Chemical profiles of Ca and K are related the kind of wood tissue (sapwood and heartwood) and the P chemical profile showed potential application to identify domestic sludge contamination in mangrove area. Main calcium species found by X-ray absorption near edge structure microscopy (μXANES) were $CaCl_2$ and $CaSO_4$ in the heartwood and $CaCO_3$ and Ca-Oxalate in the sapwood.

Here we demonstrated how μXANES and μXRF can provide information about chemical composition, distribution and speciation to dendrochemistry studies. PCA and cluster analysis were important tools to process these dataset. However, further data process tools, as statistical multivariate analysis or neural networks with environmental data, are recommended to be applied to extract maximum of information that has been recorded into the chemical tree-rings. These chemical information have several potential applications as in environmental sciences, agronomy and forensic areas.

4.6. References

ALVARES, C. A.; STAPE, J. L.; SENTELHAS, P. C.; GONÇALVES, J. L. M.; SPAROVEK, G. Köppen's climate classification map for Brazil. **Meteorologische Zeitschrift**, v. 22, p. 711-728, 2013.

BALOUET, J. C.; SMITH, K. T.; VROBLESKY, D.; OUDIJK, G. Use of Dendrochronology and Dendrochemistry in Environmental Forensics: Does It Meet the Daubert Criteria? **Environmental Forensics**, v. 10, n. 4, p. 268-276, 2009.

BARRELET, T.; ULRICH, A.; RENNENBERG, H.; ZWICKY, C. N.; KRÄHENBÜHL, U. Assessing the suitability of Norway spruce wood as an environmental archive for sulphur. **Environmental Pollution**, v. 156, n. 3, p. 1007-1014, 2008.

BEHERA, B.; MISHRA, R.; DUTTA, S.; THATOI, H. Sulphur oxidising bacteria in mangrove ecosystem: A review. **African Journal of Biotechnology**, v. 13, n. 29, p. 2897-2907, 2014.

CHEN, L.; WANG, W.; LI, Q. Q.; ZHANG, Y.; YANG, S.; OSLAND, M. J.; HUANG, J.; PENG, C. C. E. Mangrove species' responses to winter air temperature extremes in China. **Ecosphere**, v. 8, n. 6, p. e01865-n/a, 2017.

CHURCH, J. A.; WHITE, N. J.; AARUP, T.; WILSON, W. S.; WOODWORTH, P. L.; DOMINGUES, C. M.; HUNTER, J. R.; LAMBECK, K. Understanding global sea levels: past, present and future. **Sustainability Science**, v. 3, n. 1, p. 9-22, 2008.

CORE, R. T. R: A Language and Environment for Statistical Computing. **R Foundation for Statistical Computing,** v. 3.4.2, 2017. Available in: <https://www.R-project.org/>. Accessed in: 10/10/2017.

DUNWIDDIE, P. W.; LAMARCHE, V. C. Dendrochronological characteristics of some native Australian trees. **Australian Forestry**, v. 43, n. 2, p. 124-135, 1980.

FAIRCHILD, I. J.; LOADER, N. J.; WYNN, P. M.; FRISIA, S.; THOMAS, P. A.; LAGEARD, J. G. A.; MOMI, A. D.; HARTLAND, A.; BORSATO, A.; PORTA, N. L.; SUSINI, J. Sulfur Fixation in Wood Mapped by Synchrotron X-ray Studies: Implications for Environmental Archives. **Environmental Science & Technology**, v. 43, n. 5, p. 1310-1315, 2009.

FIKE, D. A.; BRADLEY, A. S.; LEAVITT, W. D. Geomicrobiology of Sulfur. In: Ehrlich, H. L., Newman, D. K., *et al* (Ed.). **Ehrlich's Geomicrobiology**. Boca Raton: CRC Press 2016, p.479-515.

FORS, Y.; GRUDD, H.; RINDBY, A.; JALILEHVAND, F.; SANDSTRÖM, M.; CATO, I.; BORNMALM, L. Sulfur and iron accumulation in three marine-archaeological shipwrecks in the Baltic Sea: The Ghost, the Crown and the Sword. **Scientific Reports**, v. 4, n. 4222, p. 1-6, 2014.

FRANCESCHI, V. R.; NAKATA, P. A. Calcium Oxalate in Plants: Formation and Function. **Annual Review of Plant Biology**, v. 56, n. 1, p. 41-71, 2005.

HAMMER, Ø.; HARPER, D. A. T.; RYAN, P. D. PAST: Paleontological statistics software package for education and data analysis. **Palaeontologia Electronica**, v. 4, n. 1, p. 9, 2001.

HEPLER, P. K. Calcium: A Central Regulator of Plant Growth and Development. **The Plant Cell**, v. 17, n. 8, p. 2142-2155, 2005.

IEMA. **Concha D'Ostra (2) - Levantamento Das Informações Básicas. Relatório Parcial** Vitória, ES: Instituto Estadual de Meio Ambiente, 2004.

JANIN, G.; CLÉMENT, A. Mise en évidence de cristaux de carbonate de calcium dans le bois des peupliers. Conséquences sur la répartition des ions minéraux liée à la duraminisation. **Annales des Sciences Forestièsres**, v. 29, n. 1, p. 67-105, 1972.

LAMBECK, K.; CHAPPELL, J. Sea Level Change Through the Last Glacial Cycle. **Science**, v. 292, n. 5517, p. 679-686, 2001.

LEROTIC, M.; JACOBSEN, C.; SCHÄFER, T.; VOGT, S. Cluster analysis of soft X-ray spectromicroscopy data. **Ultramicroscopy**, v. 100, n. 1, p. 35-57, 2004.

MAJUMDAR, S.; PERALTA-VIDEA, J. R.; CASTILLO-MICHEL, H.; HONG, J.; RICO, C. M.; GARDEA-TORRESDEY, J. L. Applications of synchrotron μ-XRF to study the distribution of biologically important elements in different environmental matrices: A review. **Analytica Chimica Acta**, v. 755, p. 1-16, 2012.

MENEZES, M.; BERGER, U.; WORBES, M. Annual growth rings and long-term growth patterns of mangrove trees from the Bragança peninsula, North Brazil. **Wetlands Ecology and Management**, v. 11, p. 233–242, 2003.

RANA, M.; MARK, T. Mechanisms of Salinity Tolerance. **Annual Review of Plant Biology**, v. 59, n. 1, p. 651-681, 2008.

RAVEL, B.; NEWVILLE, M. Athena, Artemis, Hephaestus: data analysis for X-ray absorption spectroscopy using IFEFFIT. **Journal of Synchrotron Radiation**, v. 12, n. 4, p. 537-541, 2005.

RICKARD, D. **Sulfidic Sediments and Sedimentary Rocks**. Amsterdam: Elsevier, 2012. 801 p.

ROCHA, P. A. **Solos do manguezal da Baía de Guarapari – ES: mineralogia e fósforo como indicador de contaminação por esgoto doméstico**. Departamento de Solos, Universidade Federal de Viçosa, Viçosa, 2016. xi, 90 p.

SCHNEIDER, A. The Probable Function of Calcium Oxalate Crystals in Plants. **Botanical Gazette**, v. 32, n. 2, p. 142-144, 1901.

SMITH, K. T.; BALOUET, J. C.; SHORTLE, W. C.; CHALOT, M.; BEAUJARD, F.; GRUDD, H.; VROBLESKY, D. A.; BURKEN, J. G. Dendrochemical patterns of calcium, zinc, and potassium related to internal factors detected by energy dispersive X-ray fluorescence (EDXRF). **Chemosphere**, v. 95, p. 58–62, 2014.

SOUZA, B. T.; ESTRADA, G. C. D.; SOARES, M. L. G.; CALLADO, C. H. Occurrence of annual growth rings in Rhizophora mangle in a region with low climate seasonality. **Anais da Academia Brasileira de Ciências**, v. 88, n. 1, p. 517-525, 2016.

STRUIS, R. P. W. J.; LUDWIG, C.; BARRELET, T.; KRÄHENBÜHLC, U.; RENNENBERG, H. Studying sulfur functional groups in Norway spruce year rings using S L-edge total electron yield spectroscopy. **Science of The Total Environment**, v. 403, n. 1, p. 196-206, 2008.

THYREL, M.; BACKMAN, R.; THÅNELL, K.; KARUNAKARAN, C.; SKYLLBERG, U.; LESTANDER, T. R. A. Nanomapping and speciation of C and Ca in thermally treated lignocellulosic cell walls using scanning transmission X-ray microscopy and K-edge XANES. **Fuel**, v. 167, p. 149-157, 2016.

VERHEYDEN, A.; HELLE, G.; SCHLESER, G. H.; DEHAIRS, F.; BEECKMAN, H.; KOEDAM, N. Annual cyclicity in high-resolution stable carbon and oxygen isotope ratios in the wood of the mangrove tree Rhizophora mucronata. **Plant, Cell & Environment**, v. 27, n. 12, p. 1525-1536, 2004a.

VERHEYDEN, A.; KAIRO, J. G.; BEECKMAN, H.; KOEDAM, N. Growth Rings, Growth Ring Formation and Age Determination in the Mangrove Rhizophora mucronata. **Annals of Botany**, v. 94, n. 1, p. 59-66, 2004b.

VERHEYDEN, A.; ROGGEMAN, M.; BOUILLON, S.; ELSKENS, M.; BEECKMAN, H.; KOEDAM, N. Comparison between $\delta^{13}C$ of α-cellulose and bulk wood in the mangrove tree *Rhizophora mucronata*: Implications for dendrochemistry. **Chemical Geology**, v. 219, n. 1, p. 275-282, 2005.

WEBB, S. M. The MicroAnalysis Toolkit: X-ray Fluorescence Image Processing Software. **AIP Conference Proceedings**, v. 1365, n. 1, p. 196-199, 2011.

WERNER, F.; PRIETZEL, J. Standard Protocol and Quality Assessment of Soil Phosphorus Speciation by P K-Edge XANES Spectroscopy. **Environmental Science & Technology**, v. 49, n. 17, p. 10521-10528, 2015.

WERNER, F. LCF: Linear Combination Fitting R package. v. 1.7, 2017. Available in: <https://CRAN.R-project.org/package=LCF>. Accessed in: 01/10/2018.

WORBES, M. How to Measure Growth Dynamics in Tropical Trees a Review. **IAWA Journal**, v. 16, n. 4, p. 337-351, 1995.

WORBES, M. One hundred years of tree-ring research in the tropics - a brief history and an outlook to future challenges. **Dendrochronologia**, v. 20, n. 1, p. 217-231, 2002.

XUE, J.; LEE, C.; WAKEHAM, S. G.; ARMSTRONG, R. A. Using principal components analysis (PCA) with cluster analysis to study the organic geochemistry of sinking particles in the ocean. **Organic Geochemistry**, v. 42, n. 4, p. 356–367, 2011.

4.7. Supporting Information for Chapter IV

P Kα spectral interference correction procedure for µSXRF map

Initially, a $CaCO_3$ standard was mapped by µSXRF (4100 eV monochromatic income beam, 25 ms dwell time, 50 µm step size, 1 µm beam size) at 14-3 beamline of SSRL. The MCA (multi-channel analyzer) file was used to extract the average spectra from several pixels in the map (Figure S4.1).

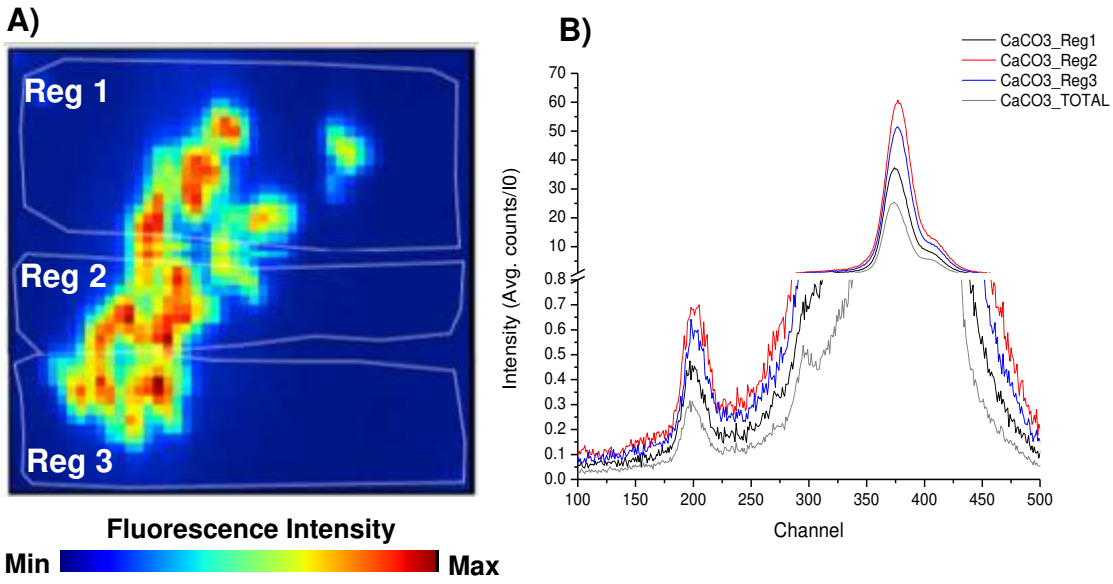

Figure S4.1. A) Ca Kα map of the $CaCO_3$ sample. The tree drawn white lines in A are the tree regions selected to extract MCA spectra. B) Spectra extracted from MCA file of $CaCO_3$ sample in total and three regions showed in A. The peak in channel 200 is Ca Kα-escape, and in channel 372 is Ca Kα peak.

Ca Kα Escape peak (1.95 keV) intensity was estimated by integration of peak in the region of interest (ROI) between 180 to 222 detector channels and Ca Kα intensity in the ROI between 350 to 400 detector channels. The ratio

Ca Kα/Ca Kα Escape of integrated range was calculated to estimate a correction factor.

Nine maps regions were selected based on Ca and P Kα (and overlapped Ca Kα Escape) intensities (Figure S4.2 A-B): 1) Low Ca and Low P (LCaLP); 2) High Ca and Low P (HCaLP); and 3) Low Ca and High P (LCaHP). We extract the average spectra from each one of those regions, where we verified Ca Kα Escape peak overlapping in P Kα peak (Figure S4.2C). In the Figure S4.2 C-D, the peak close to the channel 200 is the Ca Kα Escape, and in channel 372 is the Ca Kα peak. The peaks of green lines (LCaHP regions) refers to P Kα peak (2.01 keV), which was shifted in relation with blue and red lines (Ca Kα Escape overlap)

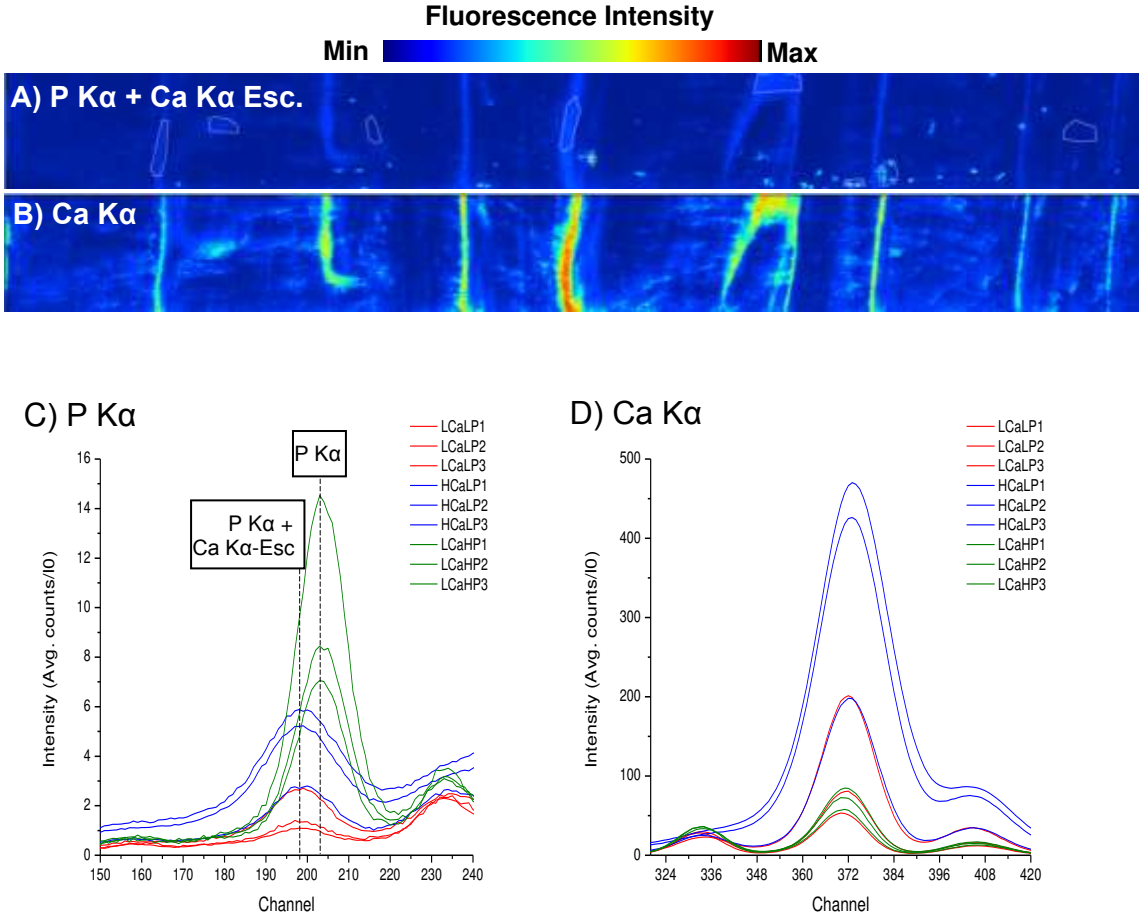

Figure S4.2. A) Original P Kα map of wood sample; B) Ca Kα map; C) and D) Spectra extracted from MCA file in the nine regions in the original P Kα map (A).

The Ca Kα and Ca Kα Escape intergraded peaks ratio (Figure S4.1) was 81 ± 2 for $CaCO_3$ sample, indicating that the proportion between intensities of the Ca Kα and Ca Kα Escape peaks is 81:1. After that, we created a Ca Kα Escape map, in the SMAK software, based on the Ca Kα map ($\frac{\text{Ca K}\alpha}{81}$). Thus, a new P Kα map (corrected) was created by subtracting the original P Kα map by the Ca Kα Escape map (Eq. 1).

$$P\ \text{K}\alpha_{\text{corr}} = \text{P K}\alpha - \frac{\text{Ca K}\alpha}{81} \quad (4)$$

In which,

$\text{P K}\alpha_{\text{corr}}$: is the new corrected P Kα map by estimated Ca Kα Escape;

$\text{P K}\alpha$: is the original P Kα map, normalized by I0 detector;

$\frac{\text{Ca K}\alpha}{81}$: is the estimated Ca Kα Escape map, from the original Ca map, normalized by I0 detector, divided by empirically estimated factor 81.

After using the Eq. 1, we created a new map (P Kα corrected) showed in Figure S4.3 A. The original P map (Figure S4.3 B) shows high P Kα intensity, manly in the tree-rings regions of wood sample. But, these regions also have high Ca concentration (Figure S4.2), what suggest that the occurrence of Ca Kα Escape peak spectral interference in P Kα peak. The new P map looks clearer and less dependent of Ca Kα, showing a more reliable P data.

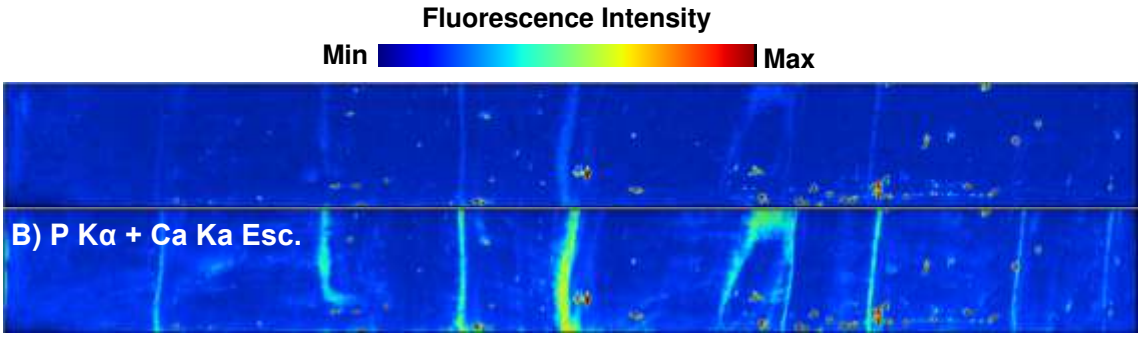

Figure S4.3. A) P Kα map after correction by Eq. 1. B) Original P Kα map, without correction. The P map in A shows the decrease of P intensity, mainly in areas with great amounts of Ca (showed in Figure S4.2 B). C) Ca map. All maps were normalized by I0 detector.

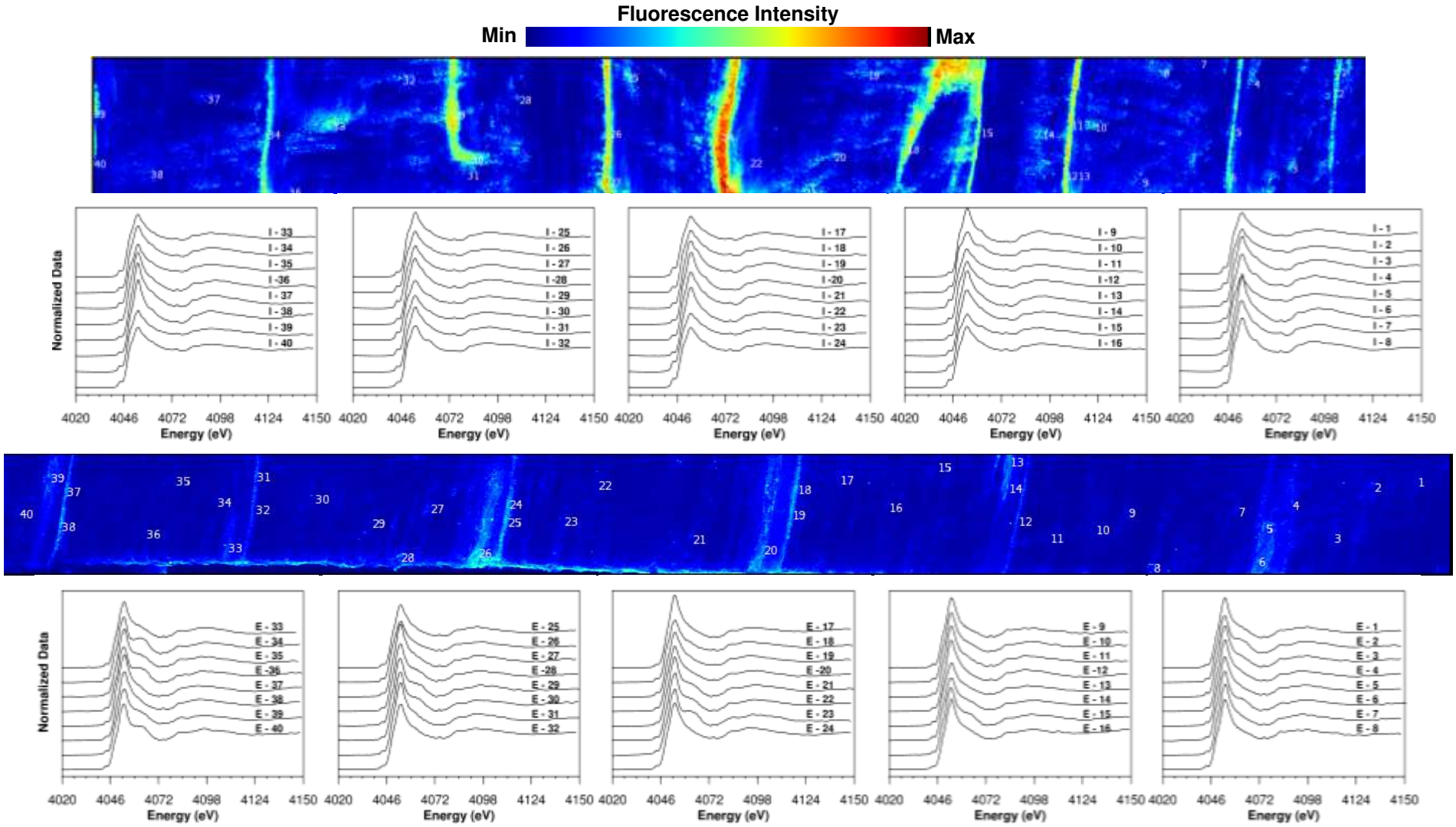

Figure S4.4. Below figure contain the Ca Kα maps (μSXRF analysis) of internal (upper map) and external (below map) parts of *Avicennia* mangrove tree. The numbers correspond to the Ca K-edge μXANES analyzed points that are showed in the referents spectra.

GENERAL CONCLUSIONS

The results obtained by XRF and XANES spectroscopy techniques provided valuable biogeochemical information about Concha D'Ostras Sustainable Development Reserve (CDSDR), contributing for a better understand of this environment. The methodology applied and developed in this research can be also applied in different wetland ecosystems for biogeochemical studies. Chemical elements content (Al, Br, Ca, Cl, Fe, K, S, Si, Sr, Ti, and Zr) in CDSDR mangrove soil profiles are influenced by site preservation state and seawater. Our results demonstrated that sulfur chemical species depend on mangrove position, condition, and soil depth, which influence the Eh-pH, carbon input, and microbiological activity. S K-edge XANES fitting results indicated that pyrite was the primary S specie in the soil and SO_4^{2-} presence in deeper soil layers is related the seawater influence, the main S source to this ecosystem. The higher content of organic forms of S and elemental S could be related to greater microbial activity in finer-textured, more organic-matter rich mangrove profile. The success of sulfur speciation in flooded environments was based sampling and analysis protocols that were intended to avoid sample oxidation by microorganism and the tender X-ray synchrotron radiation-damage.

The dendrochemistry study evidenced calcium chemical rings in the mangrove *Avicennia*. Heartwood and sapwood are chemically different, with different elemental content (Ca, P and K) and Ca species also are distinct. This is the first Ca K-edge XANES analysis applied in dendrochemistry study in tropical mangrove. Statistical multivariate analysis (PCA and cluster) are essential tools to process a large dataset of XANES and were very helpful to extract these chemical information. These chemical information have several potential applications as in environmental sciences, agronomy and forensic areas.

Further data process tools, as statistical multivariate analysis or neural networks with environmental data (e.g., climatic data), are recommended due to large dataset produced. Thus, we can have access to more information that has been recorded into the chemical tree-rings and in the mangrove soil layers.